SPACE TIME ADAPTIVE PROCESSING

FOR AIRBORNE RADAR

Thesis

Submitted to

The School of Engineering of the

UNIVERSITY OF DAYTON

In Partial Fulfillment of the Requirements for

The Degree

Master of Science in Electrical Engineering

By

Sreeveena Dontharaju

UNIVERSITY OF DAYTON

Dayton, Ohio

May, 2001

SPACE TIME ADAPTIVE PROCESSING FOR AIRBORNE RADAR.

APPROVED BY:

ABSTRACT

SPACE TIME ADAPTIVE PROCESSING FOR AIRBORNE RADAR.

Name: Dontharaju, Sreeveena
University of Dayton, 2001

Advisor: Dr. Krishna M. Pasala

The theory of STAP has been developed to a sufficient extent that we can now look into look into implementing these processors for real time target detection. The optimal theoretical performance may not be met due to a variety of in-homogeneities present in the secondary data used to calculate the interference covariance matrix. Two such in-homogeneities, the internal clutter motion and the presence of a mover have been investigated in this report. The effect of the received signal having a finite bandwidth has also been investigated. It is seen that there is degradation in filter performance due to a loss in SINR leading to an increased MDV and an increase in the interference sub-space. These factors must be a kept in mind when the processor is implemented.

This work is dedicated to
My Bullimama and Usha Aunty.

ACKNOWLEDGEMENTS

I cannot find words enough to thank my advisor Dr. Krishna Pasala, for his guidance and the time he has invested in this Thesis. Without his help this work would not have come to a conclusion. Dr. Pasala, thank you for having the patience in going through it 'all' over and over again with me. I am grateful to Dr. Gary Thiele and Dr Robert Penno for agreeing to be on my committee and scheduling the defense at such short notice.

I would like to express special thanks to the Pasalatrio' and the Yerubandis'- Swapna, Prasanthi, Kavitha, Sheela, Venu, little Sanjana and Nanamma for enveloping me into their fold and making me part of 'The Gang'. Without the support of you guys, I would have quit long ago. Usha Aunty, thank you so much for letting me make your home my home. I also would like to take this opportunity to thank my father Mallikarjuna Rao, mother Sujatha and sister Radhika. Your love, trust and guidance have brought me to this point in life.

Last but not the least, Raj my dear piya, I appreciate your being there for me through the long nights and the even longer days. You were my running buddy, source of strength and anchor.

TABLE OF CONTENTS

LIST OF ILLUSTRATIONS

Chapter I

INTRODUCTION

1.1: Purpose

The purpose of the present study is to examine Space Time Adaptive Processing (STAP) in the context of Airborne radar for the detection of both airborne and ground moving targets. The detection of these targets is complicated by the presence of clutter and also jammers in addition to the usual receiver noise. Typically, the power of the clutter and jamming signals are much higher than that of the target signals. Of late, there is a considerable interest in space-based radar to monitor targets on the ground. The geometry of the space-based radar is such that vast swaths of land are illuminated giving rise to a very large clutter signal power. One way to reduce this clutter power is to increase the range resolution of the radar by increasing the signal bandwidth. Also, there has been a considerable interest in airborne radars that are capable of target identification. These radars also require high range resolution and hence signal bandwidth. Extensive studies conducted so far have clearly demonstrated that STAP filters have great potential for suppressing clutter and jamming signals and provide significant sub clutter visibility making it possible to detect even slow ground moving targets. However, much of this research has been carried out using idealized models. For example, clutter environment is assumed to be homogeneous. The secondary clutter data vectors used to estimate the

interference covariance matrix are obtained from this assumed homogeneous clutter environment. In practice, though, the clutter is more often inhomogeneous than homogeneous. Also, the STAP modeling is based on the assumption that the signal is narrowband. Thus, the actual performance obtained from STAP may fall short of the predicted theoretical optimums. In the present study, we consider the effect of two different kinds of inhomogeneity of clutter that is often present in practice. These are the inhomogeneity due to internal clutter motion and the presence of a "mover" in secondary data. In addition, the effect of bandwidth is also considered. It is shown that even when signal bandwidth is less than 1%, there is a significant effect on the performance of the STAP filter.

1.2: Background

Before STAP came into vogue, clutter filters based on temporal filtering were used in both stationary and airborne pulse Doppler MTI radar [1]. The pulse Doppler radar exploited the difference between the target and the clutter velocities and the corresponding Doppler shifts to detect moving targets. These filters operating on a pulse-to-pulse basis provide a notch at zero Doppler frequency. Low Doppler targets, that are targets with low relative radial velocity, are buried in the clutter bandwidth and are cancelled by the filter along with the clutter and are hard to detect. These filters are exclusively temporal in nature and hence are helpless in the presence of jamming. The concept of adaptive antenna arrays has been developed to detect signals in the presence of jamming both in the context of radar and communication systems. The theory of adaptive antenna arrays is now well developed and the books by Widrow [2], Monzingo and

Miller [3], Hudson [4], and Compton[5] are excellent sources. Adaptive arrays achieve the suppression of the jammer by carrying out *spatial filtering* rather than temporal filtering. One of the first approaches to space-time filtering was the displaced phase center antenna (DPCA) concept [6]. The DPCA is a side looking arrangement and is non adaptive in nature. Space time adaptive processing combines both temporal and spatial filtering to achieve the suppression of both clutter and jamming signals. In addition, STAP makes possible sub-clutter visibility. The first significant work detailing the theory of STAP was reported by Brennan and Reed [7]. Klemm [8]-[11] carried out a number of investigations in this area and much of his work is now summarized in his book [12]. A number of authors have made significant contributions [13]-[18] developing the concept of STAP to the point where STAP based radars have become practical. Ward [19] presents a comprehensive account of various STAP algorithms including the partially adaptive algorithms. Under practical operating conditions, it may not be possible to realize the theoretical optimum performance predicted for STAP. Barile et al [20] have examined some of these limitations. More recently, research in the area of STAP is concentrating on overcoming the issues that make its practical realization difficult [16]. Paucity of sufficient sample support [21], inhomogeneity of the data [22], effect of mutual coupling between antenna elements [23] etc., are examples of difficulties to be overcome before STAP realizes its full potential.

1.3: Overview

The following investigation seeks to assess the performance of STAP filters in the presence of heterogeneous clutter such as internal clutter motion. Most models of STAP have ignored the effect of signal bandwidth. In the present investigation the clutter covariance matrix is modified to account for finite non-zero bandwidth and is used to compute the optimum weight vector and also the signal to interference noise ratio.

Chapter-2 develops the signal models for the target, clutter, jamming and thermal noise signals and also the STAP architecture. Only fully adaptive architecture is considered here. Chapter-3 considers performance of STAP in the presence of non-homogeneous clutter. The losses in SINR due to ICM and the presence of movers in the secondary data are presented here. Chapter-4 presents the effect of bandwidth. It is shown that even for bandwidths less than 1%, the clutter notch is significantly widened resulting in the increase of the minimum detectable velocity.

CHAPTER II

THEORY OF STAP

2.1: Introduction

In this chapter a model is developed for the signals received by airborne pulsed-Doppler radar. The received signals will contain a component due to receiver noise and may contain components due to both the desired targets and undesired interference. This interference could be jamming, clutter or both. Also developed is the general architecture and assumptions behind the theory of Space Time Adaptive Processing (STAP) with specific attention devoted to the 'Fully Adaptive STAP' case. The concept of signal-to-interference-plus-noise ratio is presented and developed for the fully adaptive STAP model. Finally a frequency domain analysis achieved by unitary transformations is carried out.

2.2: Signal Model

The radar utilizes an array antenna with an independent receiver channel behind each element. The received signals have interference components due to both jamming and clutter. The clutter is the most complicated of the signal components.

2.2.1: Radar System Description

The specific structure of the signals received by the radar depends upon the geometry used and is described here. The radar is carried by airborne platform at the height h_a above ground and is moving with a speed $\vec{v}_a$. The coordinate system is shown in Figure 1. Note that the co-ordinate system shown is not the standard spherical coordinate system. A unit vector pointing in the direction (ϕ, θ) is given by

$$\hat{k}(\phi,\theta) = k_x\hat{x} + k_y\hat{y} + k_z\hat{z} \qquad = cos\theta\, sin\phi\ \hat{x} + cos\theta\, cos\phi + sin\theta\ \hat{z} \tag{2.1}$$

A plane wave traveling in the direction $\hat{k}$ given by,

$$u(\phi,\theta,t) = u_0 e^{-j\hat{k}\cdot\vec{r}} e^{j\omega t}$$

$$= u_0 e^{-jk_x x} e^{-jk_y y} e^{-jk_z z} e^{j\omega t} \tag{2.2}$$

We will limit ourselves to the case of a uniformly spaced linear array consisting of N elements. The array is taken to lie along the x-axis and the position of the n^{th} element is given by,

$\vec{r}_n = nd\hat{x}$, where d is the inter-element spacing.

The radar may be forward looking or side looking according to whether $\vec{v}_a$ is perpendicular to the array axis or parallel to the array axis.

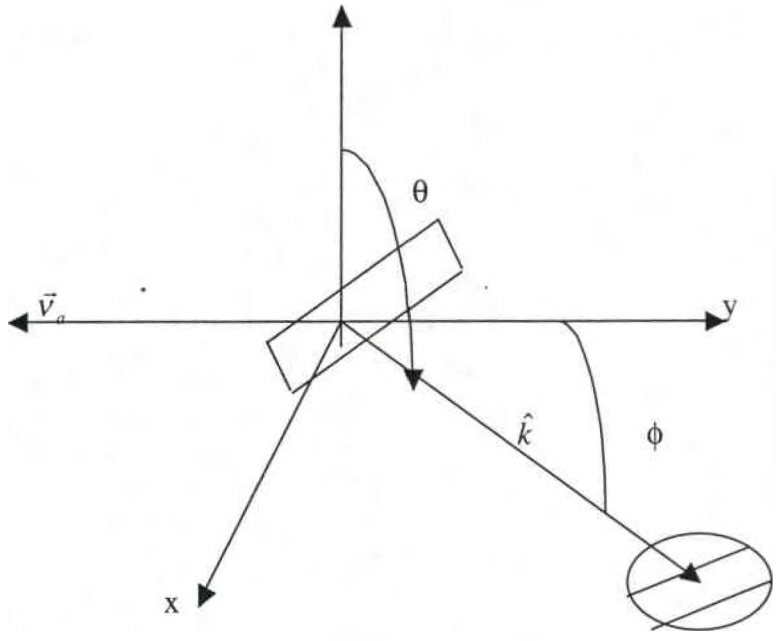

Figure 1. (a) Platform Geometry.

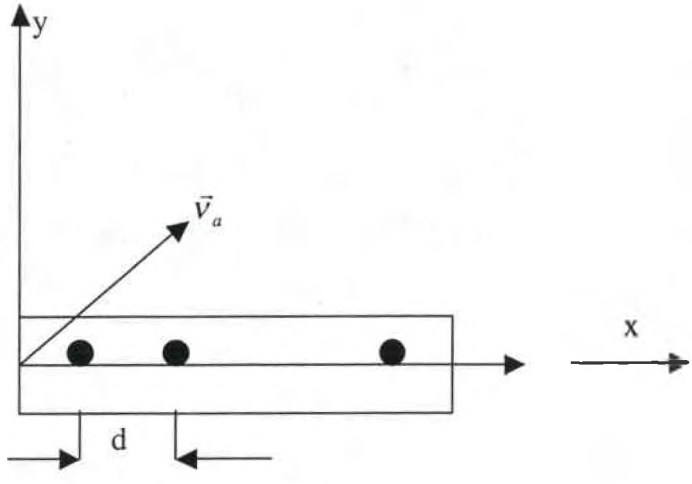

Figure 1. (b) Top View.

2.2.1.1: The data cube

The radar transmits a coherent burst of M pulses at a constant PRF, f_r. A pulse of duration T_p corresponding to a bandwidth of B is assumed. A down converter, matched filter and A/D converters follow each of the elements as shown in Figure 2.

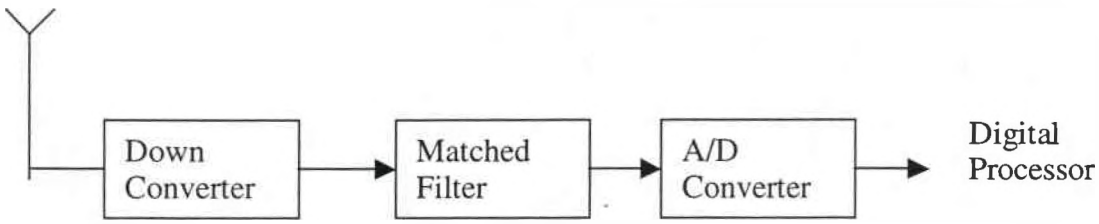

Figure 2. Processing for each array element channel

For each PRI, L time samples are collected. Each time sample corresponds to a particular range. Thus, during each coherent pulse interval (CPI) the data collected consists of MNL complex base band samples. This 'data cube' may be visualized as shown in Figure 3.

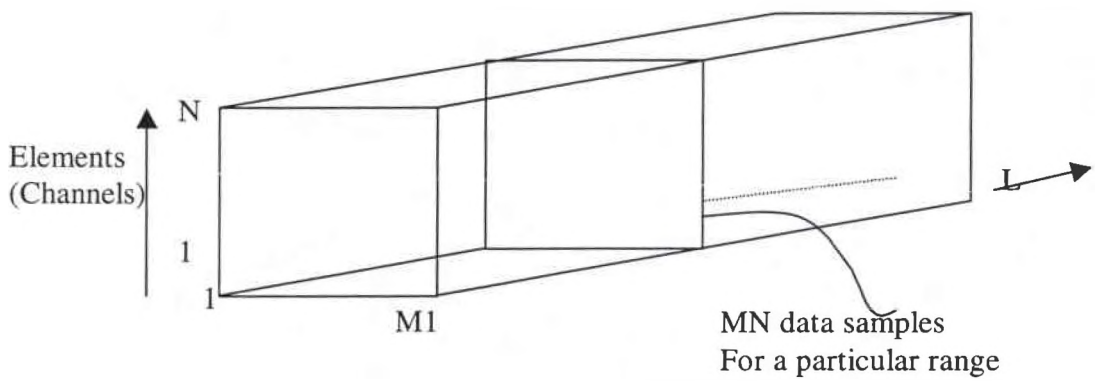

Figure 3. The Radar CPI Data Cube

Let m, n and l be indices corresponding to element, pulse and range. Let $\vec{x}_{m,l}$ be the spatial snapshot corresponding to the m^{th} pulse and the l^{th} range. Then the data corresponding to the l^{th} range gate may be arranged in the form of a (N x M) matrix as,

$$x_l = [\vec{x}_{0,l}, \vec{x}_{1,l}, ..., \vec{x}_{M-1,l}]$$

This data also may be arranged in the form of a vector

$$\vec{\psi}_l = vec(x_l) = [\vec{x}_{0,l}, \vec{x}_{1,l}, ..., \vec{x}_{M-1,l}] \tag{2.3}$$

2.2.1.2: The detection problem

Let $\vec{\psi}_u$ represent the data vector at any specific range in the absence of target at that range. Let $\vec{v}_t$ represent the known response of an unit amplitude target. Let $\vec{\psi}$ represent the observed space-time snapshot at the range of interest. This observed signal vector corresponds to one of the two hypotheses, viz.

$$\vec{\psi} = \vec{\psi}_u \qquad H_o\text{: Target absent}$$

$$= \alpha_t \vec{v}_t + \vec{\psi}_u \qquad H_1\text{: Target present} \tag{2.4}$$

Detection consists of making a decision between one of these two hypotheses.

2.2.2: Target Signal:

A target can be defined as a moving point scatterer that has to be detected. The target is modeled as a point target with the co-ordinates, R_t, the target range, ϕ_t, the azimuth and, θ_t, the elevation moving with a relative radial velocity v_t. The transmitted waveform is given by

$$\tilde{s}(t) = a_t e^{j\psi} u(t) e^{j\omega_0 t}$$

Where $u(t) = \sum_{m=0}^{M-1} u_p(t - mT_r)$ (2.5)

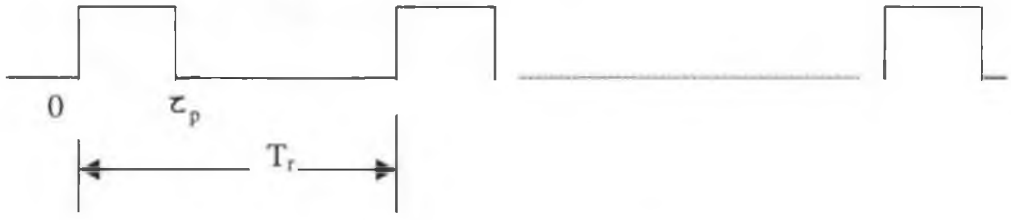

Figure 4. Pulse waveform.

The pulses are taken to be of unit energy, i.e.,

$$\int_0^{\tau_p} |u_p(t)|^2 \, dt = 1 \quad (2.6)$$

The energy in the transmitted waveform is given by $M.|\alpha_t|^2$

2.2.2.1: The received signal

The output of the n[th] element is a scaled and delayed version of the transmitted waveform and is given by,

$$\tilde{s}_n(t) = a_r e^{j\psi} u(t - \tau_n) e^{j2\pi(f_0 + f_t)(t - \tau_n)}$$

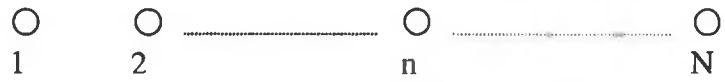

Figure 5. Antenna Array Elements.

Note that the frequency of the received signal is different from the transmitted signal due to Doppler shift and is given by $f_0 + f_t$ where $f_t = \frac{2v_t}{\lambda_0}$

The time delay τ_n is given by,

$$\tau_n = \frac{R_t + R_{t,n}}{c}$$

$$
\begin{aligned}
R_{t,n} &= R_t - \hat{k}(\phi_t,\theta_t).\vec{r}_n \\
\therefore \tau_n &= \frac{R_t + R_t - \hat{k}(\phi_t,\theta_t).\vec{r}_n}{c} \\
&= \frac{2R}{c} + \frac{-\hat{k}(\phi_t,\theta_t).\vec{r}_n}{c} \\
&= \tau_t + \tau_n'
\end{aligned}
\tag{2.7}
$$

$\tau_n' = \dfrac{-\hat{k}(\phi_t,\theta_t).\vec{r}_n}{c}$ is the relative delay measured from the phase reference to the nth element. For the present geometry,

$$
\tau_n' = \frac{-\hat{k}(\phi_t,\theta_t).nd\hat{x}}{c} = -\frac{nd}{c}\cos\theta_t \sin\phi_t \tag{2.8}
$$

Note that $\tau_t >> \tau_n'$ and $u(t-\tau_n) \approx u(t-\tau_t)$ with this approximation,

$$
\begin{aligned}
\tilde{s}_n(t) &= a_r e^{j\psi} u(t-\tau_t) e^{j2\pi f_0(t-\tau_t)} e^{j2\pi f_t(t-\tau_t)} \\
&= a_r e^{j\psi} u(t-\tau_t) e^{j2\pi f_0 t} e^{j2\pi f_t t} e^{-j2\pi f_0\tau_n} e^{-j2\pi f_t\tau_n} \\
&= a_r e^{j\psi} u(t-\tau_t) e^{j2\pi f_0 t} e^{j2\pi f_t t} e^{-j2\pi f_0\tau_t} e^{-j2\pi f_0\tau_n'} e^{-j2\pi f_t\tau_t} e^{-j2\pi f_t\tau_n'} \\
&= a_r e^{j\psi} (e^{-j2\pi f_0\tau_t} e^{-j2\pi f_t\tau_t}) u(t-\tau_t) e^{j2\pi f_0 t} e^{j2\pi f_t t} e^{-j2\pi f_0\tau_n'} e^{-j2\pi f_t\tau_n'}
\end{aligned}
$$

Since $f_0\tau_n' >> f_t\tau_n', e^{j2\pi f_t\tau_n'}$ may be neglected.

Also, $-2\pi f_0\tau_n' = 2\pi f_0 \dfrac{nd}{c}\cos\theta_t \sin\phi_t = 2\pi \dfrac{nd}{\lambda_0}\cos\theta_t \sin\phi_t$

Defining $\dfrac{d}{\lambda_0}\cos\theta_t \sin\phi_t = \vartheta_t$, the spatial frequency, $-2\pi f_0\tau_n' = n2\pi\vartheta_t$.

The received signal is now given by

$$
\tilde{s}_n(t) = a_r e^{j2\psi_1} u(t-\tau_t) e^{j2\pi f_0 t} e^{j2\pi f_t t} e^{jn2\pi\vartheta_t} \tag{2.9}
$$

After down shifting

$$
\begin{aligned}
s_n(t) &= \tilde{s}_n(t) e^{j2\pi f_0 t} \\
&= a_r e^{j\psi_1} u(t-\tau_t) e^{j2\pi f_t t} e^{jn2\pi\vartheta_t}
\end{aligned}
\tag{2.10}
$$

2.2.2.2: Output of matched filter

The impulse response of the matched filter is given by $h(t) = u_p^*(-t)$. Then the output of the matched filter is given by $s_n(t) * u_p^*(-t)$. The matched filter output

$$x_n(t) = s_n(t) * u_p^*(-t)$$

$$= \int_{-\infty}^{\infty} s_n(v) u_p^*(v-t) dv$$

$$= \int_{-\infty}^{\infty} a_r e^{j\psi_1} [\sum_{m=0}^{M-1} u_p(v - m\tau_r - \tau_t)] . e^{j2\pi f_t v} e^{j2n\pi\vartheta_t} u_p^*(v-t) dv$$

$$= \sum_{m=0}^{M-1} a_r e^{j\psi_1} e^{j2n\pi\vartheta_t} \int_{-\infty}^{\infty} u_p(v - m\tau_r - \tau_t) . u_p^*(v-t) e^{j2\pi f_t v} dv.$$

Consider the integral

$$\int_{-\infty}^{\infty} u_p(v - m\tau_r - \tau_t) u_p^*(v-t) e^{j2\pi f_t v} dv.$$

With the substitution $v' = v - m\tau_r - \tau_t$, the integral becomes

$$e^{j2\pi f_t (m\tau_r + \tau_t)} \int_{-\infty}^{\infty} u_p(v') u_p^*(v - \{t - m\tau_r - \tau_t\}) e^{j2\pi f_t v'} dv$$

$$= e^{j2\pi f_t (m\tau_r)} e^{j2\pi f_t \tau_t} . \chi(t - m\tau_r - \tau_t, f_t)$$

Where $\chi(\tau, f) = \int_{-\infty}^{\infty} u_p(v') u_p^*(v - \{t - m\tau_r - \tau_t\}) e^{j2\pi f_t v'} dv$

$\chi(\tau, f)$ is the ambiguity function. Note that $\chi\ (0,0) = 1$

$$x_n(t) = a e^{j\psi_1} e^{j2\pi f_t \tau_t} \sum_{m=0}^{M-1} e^{jn2\pi\vartheta_t} e^{jm2\pi f_t \tau_r} . \chi(t - m\tau_r - \tau_t, f_t) \qquad (2.11)$$

Now considering only the samples corresponding to the range gate whose delay is τ_t, for the mth pulse.

Figure 6. Samples, in the range gate of interest

$$t_m = \tau_t + m\tau_r, m = 0,1,.....M-1$$

$$x_n(t_m) = a_r e^{j\psi_2} e^{jn2\pi\vartheta_t} e^{jm2\pi f_t \tau_r} \chi(0, f_t)$$

Since $f_t << \frac{1}{\tau_p}, \chi(0, f_t) \approx 1$, and

$$x_{nm} = x_n(t_m) = a_r e^{j\psi_2} e^{jn2\pi\vartheta_t} e^{jm2\pi f_t \tau_r}$$

Defining the normalized Doppler, $\varpi_t = f_t \tau_r$,

$$x_{nm} = \alpha_t e^{jn2\pi\vartheta_t} . e^{jm2\pi\varpi_t}$$

The general form of the signal received is given by

$$x_{nm} = \alpha_t e^{jn2\pi\vartheta_t} . e^{jm2\pi\varpi_t} \qquad n = 0,1,2,.....N-1 \qquad (2.12)$$

$$m = 0,1,2,.....M-1$$

The amplitude α_t is related to the SNR and can be deduced from it using the radar equation. The SNR per element, per pulse is given by

$$\xi_t = \frac{P_t G_t \tau_p g \lambda_0^2 \sigma_t}{(4\pi)^3 N_0 L_s R_t^4} \qquad (2.13)$$

Where N_o is the noise power per unit BW. The average target power is now given by,

$$\text{Avg\_target\_power} = E(|\alpha_t|^2) = \sigma^2 \xi_t \qquad (2.14)$$

2.2.2.3: Expression for $\vec{\chi}_t$

$$\vec{\chi}_t = \begin{bmatrix} \vec{x}_0 \\ \vec{x}_1 \\ .. \\ . \\ \vec{x}_{M-1} \end{bmatrix}$$

where $\vec{x}_m$ is the spatial snapshot for the mth pulse.

$$\vec{x}_m = \begin{bmatrix} x_{0,m} \\ x_{1,m} \\ . \\ . \\ . \\ x_{N-1,m} \end{bmatrix} = \begin{bmatrix} \alpha_t e^{jm2\pi\varpi_t}.1 \\ \alpha_t e^{jm2\pi\varpi_t}.e^{j\pi 2\vartheta_t} \\ . \\ \alpha_t e^{jm2\pi\varpi_t}.e^{j\pi 2n\vartheta_t} \\ . \\ \alpha_t e^{jm2\pi\varpi_t}.e^{j\pi 2(N-1)\vartheta_t} \end{bmatrix}$$

$$\vec{x}_m = \alpha_t . e^{jm2\pi\varpi_t} . \vec{a}(\vartheta_t) \tag{2.15}$$

Where $\vec{a}(\vartheta_t) = [1, e^{j\pi 2\vartheta_t}, ...e^{j\pi 2(N-1)\vartheta_t}]$ is the spatial steering vector Thus,

$$\begin{aligned} \vec{\chi}_t &= [\vec{x}_0; \vec{x}_1; .....; \vec{x}_{M-1}] \\ &= \alpha_t [\vec{a}(\vartheta_t); e^{j\pi 2\varpi_t}\vec{a}(\vartheta_t); .....; e^{j\pi 2(M-1)\varpi_t}\vec{a}(\vartheta_t)] \\ &= \alpha_t [1; e^{j\pi 2\varpi_t}; e^{j\pi 2.2\varpi_t}; .....; e^{j\pi 2(M-1)\varpi_t}] \otimes [\vec{a}(\vartheta_t)] \end{aligned}$$

By the definition of Kronecker product

$$\begin{aligned} A \otimes B &= [a(m,n) \times B] \\ \vec{\chi}_t &= \alpha_t \vec{b}(\varpi_t) \otimes \vec{a}(\vartheta_t) = \alpha_t \vec{v}_t \end{aligned} \tag{2.16}$$

Where

$$\vec{b}(\varpi_t) = [1; e^{j2\pi\varpi_t}; e^{j4\pi\varpi_t}; .....; e^{j2(M-1)\pi\varpi_t}] \tag{2.17}$$

and $\vec{v}_t = \vec{b}(\varpi_t) \otimes \vec{a}(\vartheta_t)$

$\vec{v}_t(\varpi_t, \vartheta_t)$ is called the steering vector.

2.2.3: Noise

The noise that we consider here is the internally generated noise and not the external sky noise. The following assumptions are made about this noise signal:

- The noise is independent from channel to channel.
- The correlation time of the noise signal is much less than the pulse repetition interval (PRI). Thus noise signal is de-correlated from pulse to pulse.

These two assumptions result in:

$$E\left[x_{n1,m}x^{*}{}_{n2,m}\right]=\sigma^{2}\delta_{n1,n2}$$

$$E\left[x_{n,m1}x^{*}{}_{n,m2}\right]=\sigma^{2}\delta_{m1,m2}$$

Hence σ^{2} is the average noise power.

Thus, the noise signal at any element and sampled during a pulse is correlated with itself and de-correlated with the noise signal at any other pulse or element. The correlation matrix corresponding to the noise signal is therefore,

$$R_{n}=\sigma^{2}I_{MN}=\sigma^{2}I_{M}\otimes I_{N} \tag{2.18}$$

2.2.4: Jamming

In this section, expressions are derived for the jamming contribution to a space-time snapshot vector and its co-variance matrix. Only the barrage noise jammers are considered for the analysis.

2.2.4.1: Assumptions

The following assumptions are made about the jamming signal.

- The jammer is on at all times. Hence jamming signal is present in all range bins.
- The correlation time of the jamming signal is taken to be much greater than the time it takes the signal to propagate across the array. Thus, the jamming signal at the two (spatial) extremes of the array, are not de-correlated. Such is the case with the target signal or indeed any narrow band signal. Note that, as the bandwidth of the signal is increased, the correlation time is decreased and becomes comparable to the transit time of the signal across the array. Thus the assumption implies that the jamming signal is "narrow band".

2.2.4.2: Expression for $\vec{\chi}_j$

We can define a spatial steering vector $\vec{a}_j$ corresponding to a jammer arriving from (θ_j, ϕ_j). The correlation time of the signal is taken to be much smaller than the PRI. As a result, the jamming signal is de-correlated from pulse to pulse, much like a thermal noise signal. Thus, the barrage noise signal is like a narrowband (target like) signal spatially and wideband (noise like) signal temporally.

Let $\vec{a}_j$ be the spatial steering vector corresponding to (θ_j, ϕ_j).

Then $\vec{\chi}_j = [\alpha_0 \vec{a}_j; \alpha_1 \vec{a}_j; .....; \alpha_m \vec{a}_j; .....; \alpha_m \vec{a}_j]$

where, $\vec{\alpha}_j = [\alpha_0; \alpha_1; .....\alpha_m; .....; \alpha_{M-1}]$ is a (random) vector, containing jammer amplitudes from pulse to pulse.

$\therefore E[\alpha_{m1}\alpha^{*}_{m2}] = \sigma^2\xi_j\delta_{m1,m2}$ and $E[\vec{\alpha}_j\vec{\alpha}_j{}^H] = \sigma^2\xi_j I_M$, ξ_j being the JNR.

From the structure of $\vec{\chi}_j$, we can express it as,

$$\vec{\chi}_j = \vec{\alpha}_j \otimes \vec{a}_j \tag{2.19}$$

2.2.4.3: Expression for $\vec{R}_j$

The jammer space-time covariance matrix is then,

$$\begin{aligned} R_j &= E[\vec{\chi}_j\vec{\chi}_j{}^H] \\ &= E[(\vec{\alpha}_j \otimes \vec{a}_j)(\vec{\alpha}_j \otimes \vec{a}_j)^H] \\ &= E[(\vec{\alpha}_j \otimes \vec{a}_j)(\vec{\alpha}_j{}^H \otimes \vec{a}_j{}^H)] \\ &= E[(\vec{\alpha}_j\vec{\alpha}_j{}^H) \otimes (\vec{a}_j\vec{a}_j{}^H)] \\ &= E[\vec{\alpha}_j\vec{\alpha}_j{}^H] \otimes [\vec{a}_j\vec{a}_j{}^H] \\ &= \sigma^2\xi_j I_M \otimes (\vec{a}_j\vec{a}_j{}^H) \\ &= I_M \otimes \sigma^2\xi_j(\vec{a}_j\vec{a}_j{}^H) \\ &= I_M \otimes \Phi_j \end{aligned} \tag{2.20}$$

where $\Phi_j = \sigma^2\xi_j(\vec{a}_j\vec{a}_j{}^H)$ is the jammer spatial covariance matrix.

In the case of multiple jamming signals,

$$\begin{aligned} \Phi_j &= \Phi_{j1} + \Phi_{j2} + ... + \Phi_{jJ} \\ &= \sigma^2\xi_{j1}\vec{a}_{j1}\vec{a}_{j1}{}^H + \sigma^2\xi_{j2}\vec{a}_{j2}\vec{a}_{j2}{}^H + ... + \sigma^2\xi_{jJ}\vec{a}_{jJ}\vec{a}_{jJ}{}^H \\ &= A_j \sum \mathrm{j} A_j^H \end{aligned} \tag{2.21}$$

Where $A_j = [\vec{a}_{j1}, \vec{a}_{j2}, ..., \vec{a}_{jJ}]$ and

$\sum \mathrm{j} = diag[\sigma^2\xi_{j1}, \sigma^2\xi_{j2}, ..., \sigma^2\xi_{jJ}]$ for jammers that are completely independent of each other. Else $\sum \mathrm{j}$ represents the source covariance matrix of the j jammers.

If rank $(\sum \mathrm{j}) = \mathrm{J}$, corresponding to the case when no two jammers are coherent,

$$rank(R_j) = rank(I_M \otimes \Phi_J) = M \times rank(\Phi_J) = MJ \tag{2.22}$$

Note that, even though the size of R_j is MN x MN, its rank equals MJ, which can be much smaller than MN.

2.2.5: Clutter

2.2.5.1: Clutter Model

We discuss here a simple clutter model. Our goal is to understand the distribution of clutter in range, angle and time or equivalently in range, spatially frequency and Doppler. Consider the model as shown in Figure 7.

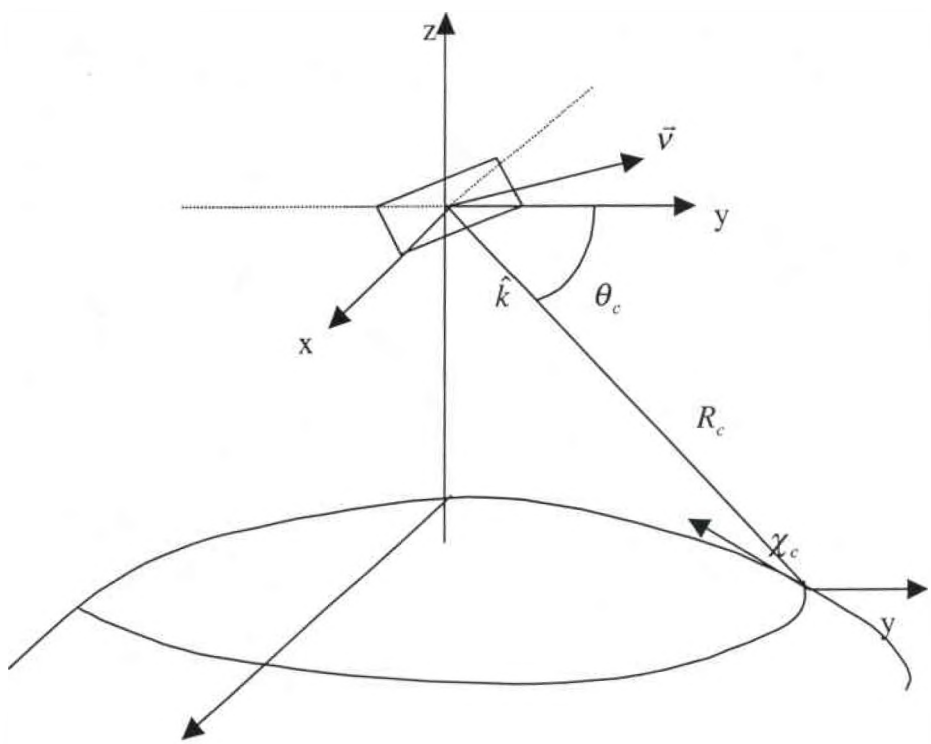

Figure 7: Clutter Model

Corresponding to a depression angle, θ_c there is a range R_c that defines a clutter ring on the ground. The entire signal scattered by the ground in this ring maps to a single range bin corresponding to the range R_c. When the maximum un-ambiguous range, $R_u = \frac{c}{2f_r}$ is greater than the range to horizon, there is only one clutter ring on the ground corresponding to each range. If not, (that is if the distance to horizon is less than R_u), then the clutter is range ambiguous and in any range bin, clutter may be due to more than one clutter ring.

Let there be N_r clutter rings.

Let $R_i = R_c + (i-1)R_u$ be the range corresponding to the i^{th} ambiguous range.

Let $\theta_i = \theta_c(R_i)$ be the depression angle corresponding to R_i and χ_i be the grazing angle.

Then,

$$\theta_c = -Sin^{-1}\left[\frac{R_c^{\,2} + h_a(h_a + 2a_e)}{2R_c(a_e + h_a)}\right] = -Sin^{-1}\left(\frac{R_c}{2a_e} + \frac{h_a}{2a_e}\right)$$
$$\chi_c = -Sin^{-1}\left[\frac{R_c^{\,2} - h_a(h_a + 2a_e)}{2R_c a_e}\right] = -Sin^{-1}\left(\frac{R_c}{2a_e} - \frac{h_a}{2a_e}\right) \qquad (2.23)$$

With $a_e = \frac{4}{3}r_e$, r_e being the earth's radius.

Let R_h be the range to horizon. Then,

$$R_h = \sqrt{2a_e h_a + h_a^2} \approx \sqrt{2a_e h_a} \qquad (2.25)$$

2.2.5.2: Expression for $\vec{\chi}_c$

The clutter signal from each clutter ring is modeled as the superposition of a sufficiently large number, N_c, of independent clutter sources distributed evenly in azimuth. Let the azimuth associated with the k^{th} cell of the i^{th} ring be ϕ_{ik}.

Then the normalized spatial frequency associated with this clutter patch is given by

$$\vartheta_{ik} = \frac{\hat{k}(\theta_i, \phi_{ik}).\vec{d}}{\lambda_0} = \frac{d}{\lambda_0}\cos\theta_i \sin\phi_{ik} \tag{2.26}$$

The Doppler frequency corresponding to this clutter patch is given by,

$$f_{ik} = \frac{2\hat{k}(\theta_i, \phi_{ik}).\vec{v}_a}{\lambda_0} \tag{2.27}$$

For $\vec{v}_a = v_a\hat{x}$, $\quad f_c = \frac{2v_a}{\lambda_0}\cos\theta_i \sin\phi_{ik}$

The normalized Doppler frequency is given by,

$$\varpi_{ik} = f_{ik}\tau_r = \frac{2v_a\tau_r}{\lambda_0}\cos\theta_i \sin\phi_{ik} \tag{2.28}$$

Then space-time steering vector is defined by,

$$v_{ik} = \vec{b}(\varpi_{ik}) \otimes \vec{a}(\vartheta_{ik}) \tag{2.29}$$

Then, the space-time signal vector $\vec{\chi}_{c,ik}$ from this clutter patch may be obtained by treating it as a point scatterer (akin to the target we dealt with) and is given by,

$$\vec{\chi}_{c,ik} = \alpha_{ik}\vec{v}_{ik}(\theta_i, \phi_{ik}) \tag{2.30}$$

The signal vector from the whole clutter ring is given by,

$$\vec{\chi}_{c,i} = \sum_{k=1}^{N_c} \alpha_{ik}\vec{v}_{ik}(\theta_i, \phi_{ik}) \tag{2.31}$$

The clutter from all the ambiguous ranges is given by

$$\vec{\chi}_c = \sum_{i=1}^{N_r} \vec{\chi}_{c,i} = \sum_{i=1}^{N_r} \sum_{k=1}^{N_c} \alpha_{ik} \vec{v}_{ik}(\theta_i, \phi_{ik}) \tag{2.32}$$

$\alpha_{i,k}$ is the random amplitude of the signal from the ikth patch. We assume that the clutter is Gaussian distributed and the clutter in patch (ik) is independent of clutter from patch (jl). That is,

$$E[\alpha_{ik}\alpha_{jl}^{*}] = P_{c,ik}\delta_{i-j}\delta_{k-l}$$

The amplitudes α_{ik} depend upon the reflectivity model of the area under consideration and is given by,

$$\sigma_{ik} = \sigma_0(\theta_i, \phi_k) \times patcharea$$
$$patcharea = (R_i \cdot \Delta\phi)(\Delta R Sec\chi_i)$$

One simple model for the ground reflectivity is the constant gamma model. According to this model,

$$\sigma_0 = \Gamma Sin\psi_c$$

Where Γ depends upon the terrain. The clutter to noise ratio is given by,

$$\xi_{ik} = \frac{P_t \tau_p G_t(\theta_i, \phi_{ik}) g(\theta_i, \phi_{ik}) \lambda_0^2 \sigma_{ik}}{(4\pi)^3 N_0 L_s R_i^4} \tag{2.33}$$

And the clutter from each patch is given by,

$$E(|\alpha_{ik}|^2) = \sigma^2 \xi_{ik}$$

2.2.5.3: Expression for R_c :

$$\begin{aligned} R_c &= E[\vec{\chi}_c \vec{\chi}_c^H] \\ &= E[(\sum_I \sum_k \alpha_{ik} \vec{v}_{ik})(\sum_j \sum_l \alpha_{jl}^* \vec{v}_{jl}^H)] \\ &= \sum_i \sum_k \sum_j \sum_l E(\alpha_{ik} \alpha_{jl}^*) \vec{v}_{ik} \vec{v}_{jl}^H \end{aligned} \tag{2.34}$$

Since $E(\alpha_{ik}\alpha_{jl}^*) = \sigma^2 \xi_{ik}\, \delta_{i-j} \delta_{k-l}$

Let us consider again the expression,

$$\begin{aligned} R_c &= \sum_i \sum_k \sigma^2 \xi_{ik} \vec{v}_{ik} \vec{v}_{ik}^H \\ &= \sum_i \sum_k \sigma^2 \xi_{ik} [\vec{b}(\varpi_{ik}) \otimes \vec{a}(\nu_{ik})][\vec{b}(\varpi_{ik}) \otimes \vec{a}(\nu_{ik})]^H \\ &= \sum_i \sum_k \sigma^2 \xi_{ik} [\vec{b}(\varpi_{ik}) \vec{b}(\varpi_{ik})^H] \otimes [\vec{a}(\nu_{ik}) \vec{a}(\nu_{ik})^H] \end{aligned} \tag{2.35}$$

Let us consider the expression again. R_c is the weighted sum of the outer products $\vec{v}_{ik} \vec{v}_{ik}^H$.

There are N_c x N_r patches. R_c may be expressed as

$$R_C = [V_C][\sum_C][V_C]^H \tag{2.36}$$

Where, $[V_C] = [\vec{V}_{11}, \vec{V}_{22}, ...\vec{V}_{1Nc}, \vec{V}_{21}, \vec{V}_{22}, ...\vec{V}_{2Nc}, ...\vec{V}_{Nr,1}, ...\vec{V}_{Nr,Nc}]$ is a (MN) x (N_rN_c) matrix and $[\sum_c]$ is a diagonal matrix corresponding to the clutter power from N_cN_r patches. That is,

$$[\sum_c] = \sigma^2 diag([\xi_{11}, \xi_{12}, ...\xi_{1Nc}, ...\xi_{Nr1}, ...\xi_{NrNc}])$$

2.2.5.4: Clutter Ridges

Consider the disposition of clutter in angle-Doppler space for a given range in relation to the signals from a target and jammer. The signal from the target is not

distributed in range and is a single point in the angle-Doppler space. The jamming signal is distributed in range occurring at all ranges but in the angle-Doppler space is limited to a line corresponding to a particular angle but distributed in Doppler. Clutter is distributed in range and for a given range distributed in both angle and Doppler. However, clutter is not smeared over the entire angle-Doppler space but limited to regions called clutter ridges. The geometry of those ridges depends upon the configuration of the radar. It is this mapping of jamming and clutter to distinct and separate regions in angle-Doppler space that leads to successful interference suppression via two-dimensional filtering. We will consider the configuration of the side looking radar.

The normalized spatial frequency is given by

$$\nu = \frac{\hat{k}(\theta_c,\phi_c).\vec{d}}{\lambda_0} = \frac{d}{\lambda_0}\cos\theta_c \sin\phi_c$$

The normalized Doppler frequency is given by

$$\begin{aligned}\varpi_c &= (2\frac{\hat{k}(\theta_c,\phi_c).\vec{v}_a}{\lambda_0}).T_r \\ &= (2\frac{\hat{k}(\theta_c,\phi_c).v_a\hat{x}}{\lambda_0}).T_r \\ &= \frac{2v_a}{\lambda_0}T_r\cos\theta_c\sin\phi_c \\ &= \frac{2v_aT_r}{d}.\vartheta_c = \beta\vartheta_c\end{aligned} \tag{2.37}$$

where $\beta = \frac{2v_aT_r}{d} = \frac{v_aT_r}{d/2}$ = no of inter element spacing traveled by radar in one PRI.

In the ϑ_c *vs* ϖ_c plane, the relationship $\varpi_c = \beta\vartheta_c$ is a straight line with slope = β. We will consider this for several values of β. Note that the highest spatial frequency is equal to

$\frac{1}{\lambda_0}$. Hence the minimum spatial frequency must be $2.\frac{1}{\lambda_0}$. The corresponding sampling period, the inter element spacing is $\frac{\lambda_0}{2}$. Thus we will take the spacing $d = \frac{\lambda_0}{2}$. Then

$$\beta = \frac{2v_a T_r}{d} = \frac{4v_a T_r}{\lambda_0} \tag{2.38}$$

Also note that the largest Doppler frequency is $\frac{2v_a}{\lambda_0}$. Thus the sampling frequency must be at least $\frac{4v_a}{\lambda_0}$.

$$\therefore f_r \geq \frac{4v_a}{\lambda_0}$$

$$T_r \leq \frac{\lambda_0}{4v_a}$$

$$\therefore \frac{4v_a T_r}{\lambda_0} \leq 1$$

Figures 8a, 8b and 8c show the clutter ridges obtained for different values of β. For β = 1, the Doppler is just full and there is no Doppler ambiguity. β=2.67 corresponds to under sampling leading to Doppler ambiguity. PRF is not high enough. A typical 3-D sketch of clutter is shown in the Figure 9. The main beam is steered to $\varphi = 90^0$. The extent of clutter in the spatial frequency, Doppler frequency space also depends upon the range. Note that each depression angle corresponds to a specific range; $\theta \approx 0$ corresponds to a large range and $\theta \approx \frac{\pi}{2}$ corresponds to shorter ranges.

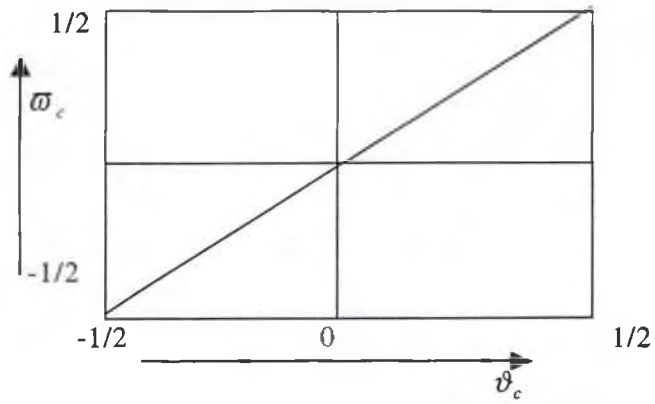

Figure 8a. Clutter Ridge, β=1

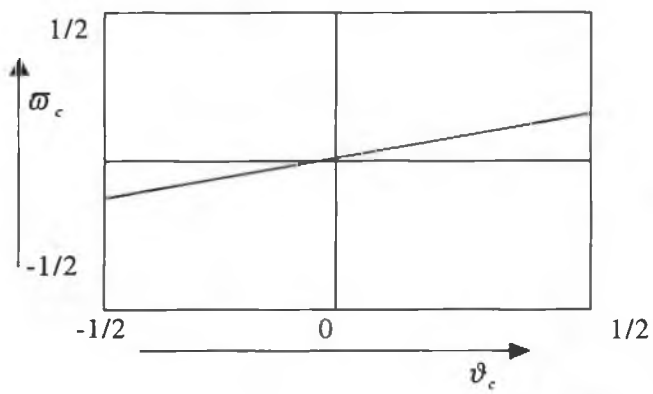

Figure 8b. Clutter Ridge, β=0.5

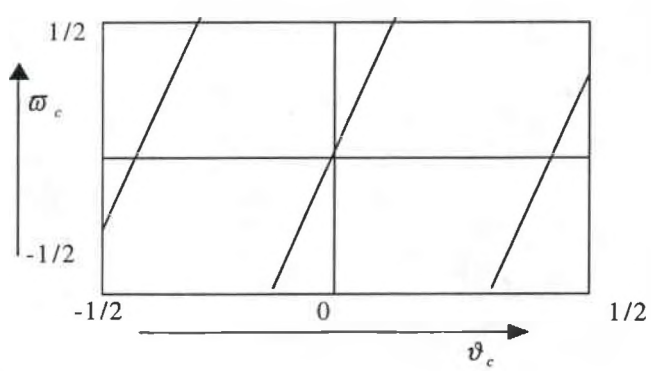

Figure 8c. Clutter Ridge, β=2.67

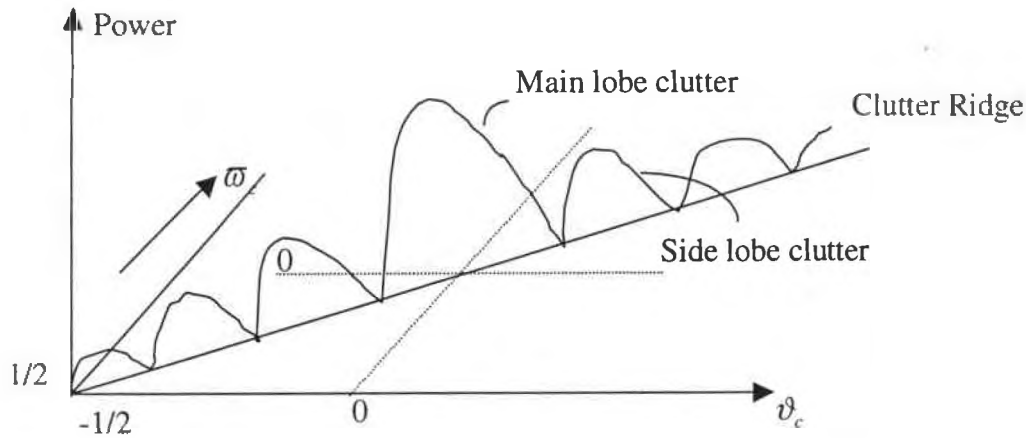

Figure 9. 3-D view of clutter

For $d = \frac{\lambda_0}{2}, \vartheta_c = \frac{1}{2}\cos\theta_c \sin\varphi_c$

Hence for larger ranges, $\theta_c \approx 0, \vartheta_c = \frac{1}{2}\sin\varphi_c$ clutter fills the entire ridge. But for shorter ranges $\theta_c \approx 0$, clutter fills only part of the ridge.

2.2.5.3: Structure and Rank of the clutter covariance matrix

The clutter covariance matrix is defined by

$R_c = E[\vec{\chi}_c \vec{\chi}_c^H]$

$\vec{\chi}_c = [\vec{x}_0^T, \vec{x}_1^T, ...\vec{x}_{M-1}^T]^T$

$\vec{x}_p$ is the spatial snapshot corresponding to the pth pulse. Therefore,

$$R_c = E\{\begin{bmatrix} \vec{x}_0 \\ \vec{x}_1 \\ . \\ . \\ \vec{x}_{M-1} \end{bmatrix} [\vec{x}_0^H, \vec{x}_1^H, ...\vec{x}_{M-1}^H]\} \quad (2.39)$$

$$R_c = \begin{bmatrix} R_c(0) & R_c(1).....R_c(M-1) \\ R_c(-1) & R_c(0).....R_c(M-2) \\ . & \\ . & \\ R_c(-(M-1)0) & ..... \quad R_c(0) \end{bmatrix}$$

$R_c(p) = E[\vec{x}_m \vec{x}_{m+p}^H]$ is the cross-convergence of two spatial snapshots in time by pT_r. Thus R_c is an MxM block matrix with each block being NxN. The pq^{th} elements of this matrix corresponds to correlation between two signals corresponding to [n(p),m(p)] and [n(q),m(q)], where

$$n(p) = \text{modulo}(p,N), \quad n(q) = \text{modulo}(q,N)$$

and $$m(p) = \text{floor}(\frac{p}{n}), \qquad m(q) = \text{floor}(\frac{q}{n})$$

The clutter signal from patch ik sampled at n(p) and m(p) is given by,

$$\alpha_{ik} e^{jn(p)2\pi\vartheta_{ik}} . e^{jm(p)2\pi\varpi_{ik}}$$

Similarly the clutter signal from the same patch ik but sampled at n(q) and m(q) is given by

$$\alpha_{ik} e^{jn(q)2\pi\vartheta_{ik}} . e^{jm(q)2\pi\varpi_{ik}}$$

The correlation between these two samples is given by

$$E[\alpha_{ik}\alpha_{ik}^* e^{j[n(p)-n(q)]2\pi\vartheta_{ik}} e^{j[m(p)-m(q)]2\pi\varpi_{ik}}]$$

This term gives the correlation between these two different samples form a single patch. The total correlation is obtained by summing the contributions from all the patches. That is

$$[R_c]_{p,q} = \sum_{i=1}^{N_r}\sum_{k=1}^{N_c} \sigma^2 \xi_{ik} e^{j2\pi[n(p)-n(q))\vartheta_{ik}} e^{j2\pi[m(p)-m(q)]\varpi_{ik}} \qquad (2.40)$$

Note that each of the blocks of matrices Rc(p) is Toeplitz and in addition, the matrix Rc itself is block Toeplitz.

Under certain conditions, the clutter covariance matrix has an especially simple structure and its rank is much less than the size of the matrix. Let us consider the flowing special code.

- The radar is a side looking array
- $\beta = \frac{2v_a\tau_r}{d} = 1,\ \text{with}\ d = \frac{\lambda}{2} and\ \tau_r = \frac{\lambda}{4v_a}$
- The clutter ridge is defined by $\varpi_c = \theta_c$

The general structure of Rc is given by

$$R_c = \begin{bmatrix} R_c(0) & R_c(1).....R_c(M-1) \\ R_c(-1) & R_c(0).....R_c(M-1) \\ . & \\ . & \\ R_c(-(M-1).....R_c(0) \end{bmatrix} \text{ and}$$

$$R_c(0) = \begin{bmatrix} \alpha_0 & \alpha_1.....\alpha_{N-1} \\ \alpha_{-1} & \alpha_0.....\alpha_{N-2} \\ . & \\ \alpha_{-N-1}.....\alpha_0 \end{bmatrix}$$

$$\alpha_i = E[x(p,l)x^*(p+i,l)]$$

$$\text{where} \quad = E[(\sum_i \sum_k \alpha_{ik} e^{jp2\pi\vartheta_{ik}} e^{jl2\pi\vartheta_{ik}})(\sum_i \sum_k \alpha^*_{ik} e^{j(p+i)2\pi\vartheta_{ik}} .e^{-jl2\pi\vartheta_{ik}}) \qquad (2.41)$$

$$= \sum_i \sum_k \sigma^2 \xi_{ik} e^{-j(i)\vartheta_{ik}} \quad i = 0,1,2....N-1$$

α_i are the correlations at tap l between the array elements. To be specific, let us consider the example of N=3 and M=3

$$R_c(1) = E[\bar{x}(0)\bar{x}(1)^H]$$

$$= E\{\begin{bmatrix} x_o(0) \\ x_1(0) \\ x_2(0) \end{bmatrix}[x_0^*(1)x_1^*(1)x_2^*(1)]\}$$

$R_c(0)$ contains elements $E[x(p,0)x^*(p+i),0)]$for $i = 0,1,...N-1$

Let us consider $E[x(p,0)x^*(p+i),1)]$

$$= E[(\sum_i \sum_k \alpha_{ik} e^{jp2\pi\vartheta_{ik}} e^{j2\pi\vartheta_{ik}})(\sum_i \sum_k \alpha^*_{ik} e^{j(p)2\pi\vartheta_{ik}} .e^{-ji2\pi\vartheta_{ik}})$$

$$= \sum_i \sum_k \sigma^2 \xi_{ik} e^{-j2\pi(i-1)\vartheta_{ik}} \quad i = 0,1,2....N-1$$

$$= \alpha_{i-1}$$

Similarly $E[x(p,0)x^*(p+i),2)] = \alpha_{i-2}$

Putting the entire Rc together,

On observation it can be noted that, Row 1,5 and 9 are identical. Rows 2 and 6 are identical and Row 4 and 8 are identical. Thus the rank is 5 even though the size of the matrix is 9x9.

More generally the rank is equal to **N+M-1**.

$$R_c = \begin{bmatrix} R_c(0) & R_c(1) & R_c(2) \\ R_c^H(1) & R_c(0) & R_c(1) \\ R_c^H(2) & R_c^H(1) & R_c(0) \end{bmatrix}$$

$$
= \begin{bmatrix}
\begin{bmatrix} \alpha_0 & \alpha_1 & \alpha_2 \\ \alpha_{-1} & \alpha_0 & \alpha_1 \\ \alpha_{-2} & \alpha_{-1} & \alpha_0 \end{bmatrix} & \begin{bmatrix} \alpha_{-1} & \alpha_0 & \alpha_1 \\ \alpha_{-2} & \alpha_{-1} & \alpha_0 \\ \alpha_{-3} & \alpha_{-2} & \alpha_{-1} \end{bmatrix} & \begin{bmatrix} \alpha_{-2} & \alpha_{-1} & \alpha_0 \\ \alpha_{-3} & \alpha_{-2} & \alpha_{-1} \\ \alpha_{-4} & \alpha_{-3} & \alpha_{-2} \end{bmatrix} \\
\begin{bmatrix} \alpha_1 & \alpha_2 & \alpha_3 \\ \alpha_0 & \alpha_1 & \alpha_2 \\ \alpha_{-1} & \alpha_0 & \alpha_1 \end{bmatrix} & \begin{bmatrix} \alpha_0 & \alpha_1 & \alpha_2 \\ \alpha_{-1} & \alpha_0 & \alpha_1 \\ \alpha_{-2} & \alpha_{-1} & \alpha_0 \end{bmatrix} & \begin{bmatrix} \alpha_{-1} & \alpha_0 & \alpha_1 \\ \alpha_{-2} & \alpha_{-1} & \alpha_0 \\ \alpha_{-3} & \alpha_{-2} & \alpha_{-1} \end{bmatrix} \\
\begin{bmatrix} \alpha_2 & \alpha_3 & \alpha_4 \\ \alpha_1 & \alpha_2 & \alpha_3 \\ \alpha_0 & \alpha_1 & \alpha_2 \end{bmatrix} & \begin{bmatrix} \alpha_1 & \alpha_2 & \alpha_3 \\ \alpha_0 & \alpha_1 & \alpha_2 \\ \alpha_{-1} & \alpha_0 & \alpha_1 \end{bmatrix} & \begin{bmatrix} \alpha_0 & \alpha_1 & \alpha_2 \\ \alpha_{-1} & \alpha_0 & \alpha_1 \\ \alpha_{-2} & \alpha_{-1} & \alpha_0 \end{bmatrix}
\end{bmatrix}
$$

2.3: Space Time Processing

In the presence of strong clutter and interference environment, it is difficult to detect weak moving targets. Typically ground based radars separate the signal returned by the target from the clutter by making use of the Doppler frequency shift induced by virtue of the motion of the target. In the case of airborne radar, the echoes from the target are a function of both angle and frequency.

A space-time processor provides temporal filtering of the radar return at each (spatial) element of the antenna array. The received data can thus be resolved into an angular spectrum, which is a function of Doppler frequency. For clutter with no relative motion with respect to the ground, the return is proportional to the Doppler shift induced by the motion of the radar platform. The Doppler spectrum of all the clutter signals from a range ring will lie on single clutter ridge in the angle Doppler domain. Since moving targets have no defined relationship between their Doppler returns and direction relative to the radar, the target contributions will lie away from this clutter ridge and can be distinguished from the clutter.

To implement STAP, requires sampling the radar returns at each element over several pulse repetition intervals. The output of this processor is a linear combination or weighted sum of the input samples. These weights are computed to reflect the signal interference environment. In the subsequent sections, the STAP algorithm (method of forming these weights) is explained and the fully adaptive STAP is introduced. Finally SINR, which is used as a performance metric, is explained.

2.3.1 General STAP architecture

As explained in section 2.2.1.1, with the radar geometry we have used, the data available to the space-time processor is in the form of a data cube with data from M pulses over N elements and L range gates. The processor generates an output for each range gate by combining the returns from the MN samples. A general block diagram of the space-time processor is shown in Figure 10. The processor can be described as an MxN weight vector whose output is computed as the inner product of this weight and the radar return for that range of interest.

$$z = w^H \chi \tag{2.42}$$

These weights have to be formed such that there is a gain on the target data, but nulls are formed for the interference data. Since both the target and interference signals (clutter, jammers etc) are not known before hand, these weights have to be formed on the basis of the data we get from the radar returns.

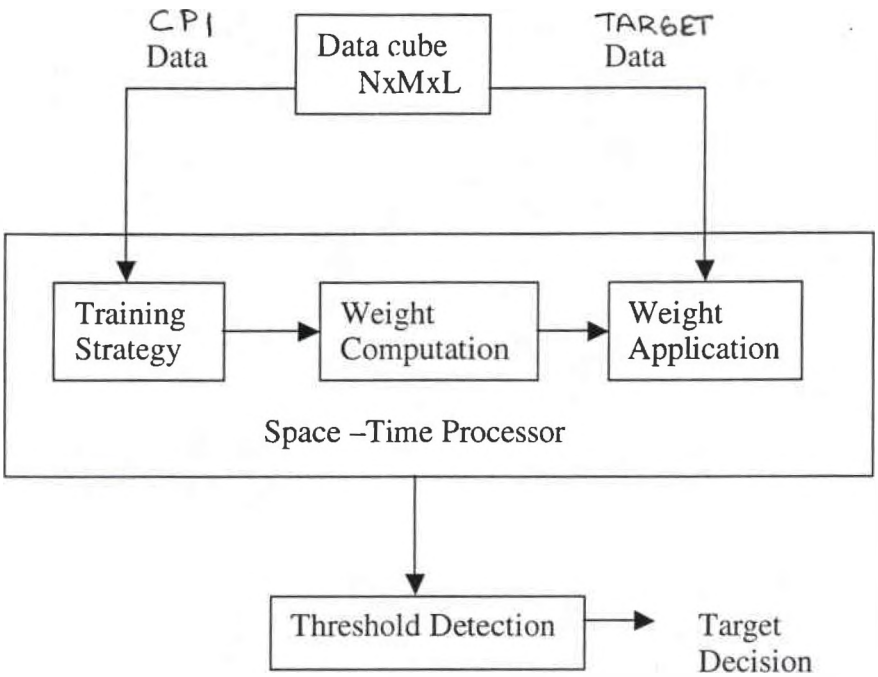

Figure 10: General block diagram of a STAP processor.

In the figure, the data from the range gate of interest is termed the target data. This is the data from the different pulses at each of the array elements. The processor can be divided into 3 sub-components as described below.

1. *Training strategy*: Here an estimate of the interference is formed on the basis of the CPI data. The data from several range bins adjacent to the one of interest is used. The PRI and instantaneous bandwidth are also taken into consideration. The output of this stage is a training data, which is then used for weight computation. Since the interference scenario is changing constantly, the training data has to be constantly updated.
2. *Weight computation*: A set of algorithms is applied to the training data from the output of the previous stage to get the weight vectors. This is the most computationally intensive part of the algorithm. New weight vectors have to be

computed for each set of training data. The first set of algorithms termed the '*simple matrix inversion*' are used to compute the weight vector from the inverse of the data co-variance matrix or more generally by performing an inverse transform by Q-R decomposition of the training data co-variance matrix. The next set is termed '*subspace projection*'. Here an estimate of the interference subspace is obtained by Eigen analysis or simple value de-composition of the training data. This is then projected orthogonal to the desired response to calculate the weights. This causes the interference to be nulled by the weight vector.

3. *Weight application*: is the place where the output is computed by the computation of the inner product of the data and the weight vector from the previous stage. Each set of weights is applied to a particular training data from the different range gates. Here again the PRF and instantaneous bandwidth, which determine the computational complexity.

The processor output is compared to a threshold level for the detection of a target. The ability of constant false alarm rate (CFAR) is usually incorporated into the weight computations.

2.3.2: Fully Adaptive STAP:

Here the output is computed by the application of a separate weight for each element and pulse. Therefore the size of the weight vector is MN. Let ϑ_t, ϖ_t and α_t represent the target angle, Doppler and amplitude.

$$\chi = \alpha_t v_t + \chi_U \text{ where } \chi_U = \chi_c + \chi_j + \chi_n \text{ the interference.} \quad (2.43)$$

An optimum space-time filter can be computed as

$$w = R_U^{-1} v_t \tag{2.44}$$

where RU is the correlation matrix formed by $R_U = E[\chi_U \chi_U{}^H]$. This weight vector has the characteristics of

- Maximum SINR (explained in the next section)
- Maximum probability of detection
- High side lobes in both Doppler and angle for detection of side lobe targets.

The block diagram for fully adaptive STAP is shown in Figure 11. Fully adaptive STAP requires the solution of an MN dimensional system of equations, which in turn is dependant on array length and the CPI. Because of this, real time computation is not possible. This helps as a baseline against which other methods can be computed.

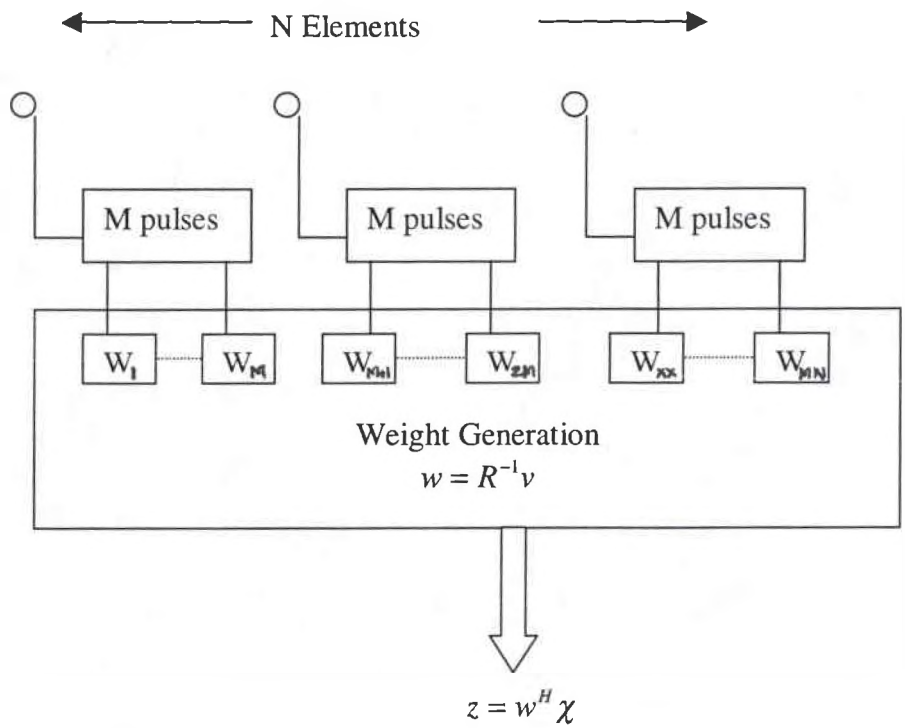

Figure 11. Fully Adaptive STAP

2.3.3 STAP Performance Metrics

Developed below are two performance metrics, which are used to compare STAP algorithms.

2.3.3.1: Adapted Patterns

The response of the weight vector as a function of angle and Doppler is called the adapted pattern which is computed as

$$P_w(\vartheta,\varpi) = \mid w^H v(\vartheta,\varpi) \mid^2 \tag{2.45}$$

This is usually computed as the Fourier transform of the weight vector if the PRI is a constant. This pattern shows nulls in the direction of interference and high gain at the target Doppler and angle. Figure 12 shows the adapted pattern for fully optimum STAP which was developed previously. The vertical grooves show the nulls at jammer azimuths and the diagonal null represents the clutter ridge.

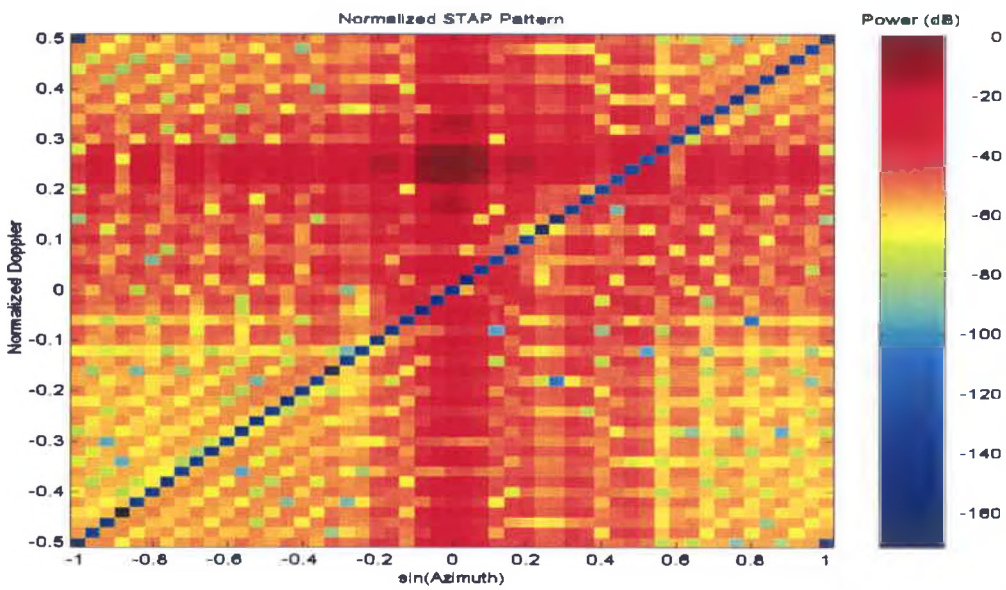

Figure 12. Pattern Output for fully adaptive STAP

2.3.3.2: Signal to Interference plus Noise ratio (SINR):

The signal component in the output can be expressed as

$z_t = \alpha_t w^H v_t$, and the noise component as

$$z_u = w^H \chi_u \tag{2.46}$$

The SINR is computed as the ratio of the powers of these two components.

$$\text{SINR} = \frac{P_t}{P_u} = \frac{E[|z_t|^2]}{E[|z_u|^2]} = \frac{\sigma^2 \xi_t |w^H v_t|^2}{w^H R_u w}$$

Substituting the optimum weight vector as $w = R_u^{-1} v_t$

$$\text{SINR} = \frac{\sigma^2 \xi_t |(R_u^{-1} v_t)^H v_t|^2}{(R_u^{-1} v_t)^H R_u (R_u^{-1} v_t)}, \text{ Simplifying}$$

SINR at a single angle and Doppler is $\sigma^2 \xi_t v_t R_u^{-1} v_t^H$

Computing $v_t(\varpi)$ as a function of target Doppler, the optimum SINR is given by

$$SINR_o = \sigma^2 \xi_t v_t(\varpi) R_u^{-1} v_t(\varpi) \tag{2.47}$$

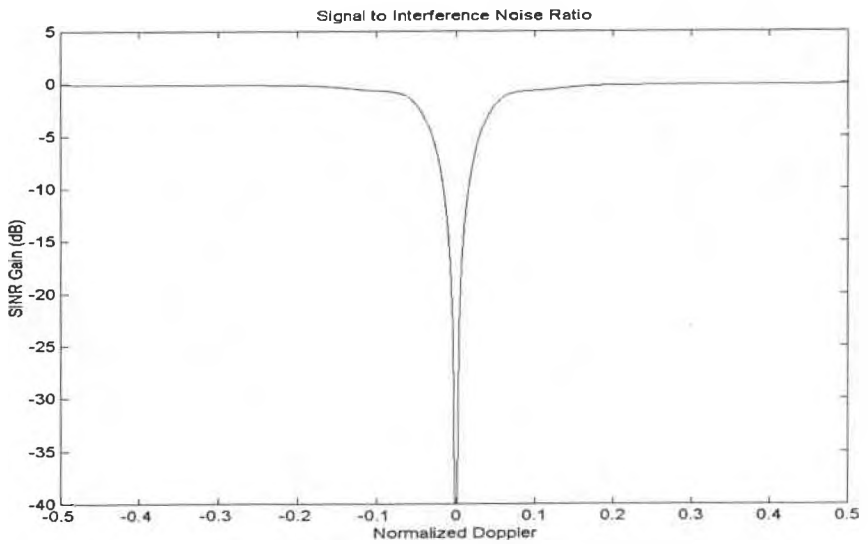

Figure 13. SINR for fully adaptive STAP

2.4 Frequency domain analysis

2.4.1 Unitary transformations

Let F be the unitary transformation. The signal vector in the range bin of interest, $\bar{\chi}$ is given by

$$\bar{\chi} = \alpha_t \bar{v}_t + \bar{\chi}_u$$

After transformation, the signal vector becomes,

$$\tilde{\chi} = F\bar{\chi} = \alpha_t F\bar{v}_t + F\bar{\chi}_u$$

The optimum weight vector is given by $\tilde{w}_{opt} = \tilde{R}_u^{-1}\tilde{v}_t$ where $\tilde{v}_t = F\bar{v}_t$ and

$$\begin{aligned}
&\tilde{R}_u = E[\tilde{\chi}_u \tilde{\chi}_u^H] \\
&\quad = E[F\bar{\chi}_u \bar{\chi}_u^H F^H] = FR_u F^H \\
&\therefore \tilde{w}_{opt} = (FR_u F^H)^{-1} F\bar{v}_t = FR_u^{-1} F^H F\bar{v}_t = FR_u^{-1}\bar{v}_t \\
&\tilde{w}_{opt} = F\bar{w}_{opt}
\end{aligned} \tag{2.48}$$

2.4.1.1 Filter output

$$\begin{aligned}
&y = \tilde{w}^H \tilde{\chi} = \alpha_t \tilde{w}^H \tilde{\chi}_t + \tilde{w}^H \tilde{\chi}_u \\
&y_s = \alpha_t \tilde{w}^H \tilde{v}_t \\
&y_u = \tilde{w}^H \tilde{\chi}_u \\
&P_s = E[|\, y_s\,|^2] = E[|\,\alpha_t\,|^2].|\,\tilde{w}^H \tilde{v}_t\,|^2 = P_t\,|\,\tilde{w}^H \tilde{v}_t\,|^2 = \sigma^2 \xi_t\,|\,\tilde{w}^H \tilde{v}_t\,|^2 \\
&P_u = E[|\, y_u\,|^2] = E[\tilde{w}^H \tilde{\chi}_u \tilde{\chi}_u^H \tilde{w}] = \tilde{w}^H \tilde{R}_u \tilde{w} \\
&SINR = \frac{\sigma^2 \xi_t\,|\,\tilde{w}^H \tilde{v}_t\,|^2}{\tilde{w}^H \tilde{R}_u \tilde{w}}
\end{aligned}$$

Noting that $\tilde{w} = F\bar{w}, \tilde{v}_t = F\bar{v}_t and \tilde{R}_u = FR_u F^H$,

$$SINR = \frac{\sigma^2 \xi_t\,|\,\bar{w}^H F^H F\bar{v}_t\,|^2}{\bar{w}^H F^H (FR_u F^H) F\bar{w}} \tag{2.49}$$

Since $F^H F = I$,

$$SINR = \frac{\sigma^2 \xi_t \mid \bar{w}^H \bar{v}_t \mid^2}{\bar{w}^H R_u \bar{w}} \tag{2.50}$$

But $\frac{\sigma^2 \xi_t \mid \bar{w}^H \bar{v}_t \mid^2}{\bar{w}^H R_u \bar{w}}$ is the expression for SINR computed in the space-time domain. *Thus SINR is invariant to unitary transformation.*

2.4.1.2 Computational Aspects of SINR

Since we are interested in computing SINR as a function of Doppler, $\tilde{v}_t$ must be computed for several values of the Doppler.

Let $\tilde{v}_{t,mat} = [\tilde{v}_{t,1}\tilde{v}_{t,2}.....\tilde{v}_{t,L}]$

$$\tilde{w}_{smi} = A^{-1}\tilde{v}_{t,mat} = A^{-1}[\tilde{v}_{t,1}\tilde{v}_{t,2}.....\tilde{v}_{t,L}] = [A^{-1}\tilde{v}_{t,1}A^{-1}\tilde{v}_{t,2}.....A^{-1}\tilde{v}_{t,L}]$$

Consider $\tilde{w}_{smi}^H \tilde{v}_{t,mat} = [A^{-1}\tilde{v}_{t,1}A^{-1}\tilde{v}_{t,2}.....A^{-1}\tilde{v}_{t,L}]\tilde{v}_{t,mat}$

$$= \begin{bmatrix} \tilde{v}_{t,1}^H A^{-1} \\ \tilde{v}_{t,2}^H A^{-1} \\ . \\ . \\ \tilde{v}_{t,L}^H A^{-1} \end{bmatrix} \left[\tilde{v}_{t,1}, \tilde{v}_{t,2}, ...\tilde{v}_{t,L}\right]$$

$$= \begin{bmatrix} \tilde{v}_{t,1}^H A^{-1}\tilde{v}_{t,1}, \tilde{v}_{t,1}^H A^{-1}\tilde{v}_{t,2}, ...\tilde{v}_{t,1}^H A^{-1}\tilde{v}_{t,L} \\ \tilde{v}_{t,2}^H A^{-1}\tilde{v}_{t,1}, \tilde{v}_{t,2}^H A^{-1}\tilde{v}_{t,2}, ...\tilde{v}_{t,2}^H A^{-1}\tilde{v}_{t,L} \\ . \\ . \\ \tilde{v}_{t,L}^H A^{-1}\tilde{v}_{t,1}, \tilde{v}_{t,L}^H A^{-1}\tilde{v}_{t,2}, ...\tilde{v}_{t,L}^H A^{-1}\tilde{v}_{t,L} \end{bmatrix}$$

Now examine the diagonal term, say the p[th] term $\tilde{V}_{t,p}^{H} A^{-1} \tilde{V}_{t,p}$. The signal power corresponding to the p[th] term is given by

$$\sigma^2 \xi_t \mid \tilde{w}^H \tilde{V}_{t,p} \mid^2 = \sigma^2 \xi_t \mid (A^{-1}\tilde{V}_{t,p})^H \tilde{V}_{t,p} \mid^2$$
$$= \sigma^2 \xi_t \mid \tilde{V}_{t,p}^H A^{-1} \tilde{V}_{t,p} \mid^2$$

Thus the diagonal terms can be used to compute the numerator of the SINR. That is

$$neum\_f = psit * (diag(\tilde{w}_{smi}^{'} * \tilde{V}_{t,mat}) .* diag(\tilde{w}_{smi}^{'} * \tilde{V}_{t,mat})) \tag{2.51}$$

Let us consider $\tilde{w}_{smi}^H \tilde{R} \tilde{w}_{smi}$

$$\begin{bmatrix} \tilde{V}_{t,1}^H A^{-1} \\ \tilde{V}_{t,2}^H A^{-1} \\ . \\ . \\ \tilde{V}_{t,L}^H A^{-1} \end{bmatrix} \tilde{R}_u [A^{-1}\tilde{V}_{t,1}, A^{-1}\tilde{V}_{t,2}, \ldots\ldots A^{-1}\tilde{V}_{t,L}]$$

$$\begin{bmatrix} \tilde{V}_{t,1}^H A^{-1} \tilde{R}_u A^{-1} \tilde{V}_{t,1}, & x & , & , & x \\ x & , \tilde{V}_{t,1}^H A^{-1} \tilde{R}_u A^{-1} \tilde{V}_{t,1}, & , & x & \\ . & & & & \\ & , & x & , & , \tilde{V}_{t,1}^H A^{-1} \tilde{R}_u A^{-1} \tilde{V}_{t,1} \end{bmatrix}$$

As before, it is the diagonal term of the product $\tilde{w}_{smi}^H \tilde{R}_u \tilde{w}_{smi}$ that is of interest. Note that, $\tilde{R}_u$ must be the true theoretical expression.

$$i.e. \tilde{R}_u = F R_u F^H \tag{2.52}$$

Let the two dimensional unitary transformation between V (k, l) and U (m, n) i.e, $V(k,l) \Leftrightarrow U(m,n)$ be defined as

$$0 \le k \le M-1$$

$$0 \le l \le N-1$$

$$0 \le m \le M-1$$

$$0 \le n \le N-1$$

$$V(k,l) = \frac{1}{\sqrt{M}} \cdot \frac{1}{\sqrt{N}} \cdot \sum_{m=0}^{M-1} \sum_{n=0}^{N-1} u(m,n) W_M^{km} W_N^{ln}$$

$$U(m,n) = \frac{1}{\sqrt{M}} \cdot \frac{1}{\sqrt{N}} \cdot \sum_{m=0}^{M-1} \sum_{n=0}^{N-1} v(k,l) W_M^{-km} W_N^{-ln} \qquad (2.53)$$

$$W_M = e^{-j\frac{2\pi}{M}}; W_N = e^{-j\frac{2\pi}{N}}$$

Define the following matrices

$$\mathbf{V} = V(k,l), k = 0,1,.....M-1; l = 0,1,.....N-1$$

$$\mathbf{U} = U(m,n), m = 0,1,.....M-1; n = 0,1,.....N-1$$

$$F_M = F_M(k,m) = \frac{1}{\sqrt{M}} W_M^{km} \qquad 0 \le k \le M-1$$

$$F_N = F_N(l,n) = \frac{1}{\sqrt{N}} W_N^{ln} \qquad 0 \le l \le N-1 \qquad (2.54)$$

$$0 \le m \le M-1$$

$$0 \le n \le N-1$$

V (k, l) may be expressed as

$$V(k,l) = \sum_{m=0}^{M-1} \frac{1}{\sqrt{M}} W_M^{km} \sum_{n=0}^{N-1} u(m,n) \frac{1}{\sqrt{N}} W_N^{ln}$$

Let $\overline{U}(m,l) = \sum_{n=0}^{N-1} u(m,n) \frac{1}{\sqrt{N}} W_N^{ln}$

Since F_N is symmetric, $F_N(l,n) = F_N(n,l)$

$$\overline{U}(m,l) = \sum_{n=0}^{N-1} u(m,n) F_N(n,l)$$

$$\overline{U}(m,l) = UF_N$$

$$V(k,l) = \sum_{m=0}^{M-1} \frac{1}{\sqrt{M}} W_M^{km} \overline{U}(m,l) = F_M \overline{U} = F_M U F_N$$

$$\mathbf{V} = F_M U F_N$$

Pre-multiplying by F_M^H and post multiplying by F_N^H,

$$F_M^H V F_N^H = F_M^H F_M U F_N F_N^H = I_M U I_N = U$$

Therefore the forward and inverse transforms are given by

$$\mathbf{V} = F_M U F_N \tag{2.55}$$

$$\mathbf{U} = F_M^H V F_N^H \tag{2.56}$$

If the matrices are column ordered into vectors,

$\vec{v} = F\vec{u}$ and $\vec{u} = F^H v$, where $F = F_N \otimes F_M$

If the matrices are row ordered into vectors,

$\vec{v} = F\vec{u}$ and $\vec{u} = F^H v$, where $F = F_M \otimes F_N$

2.4.1.4: Results

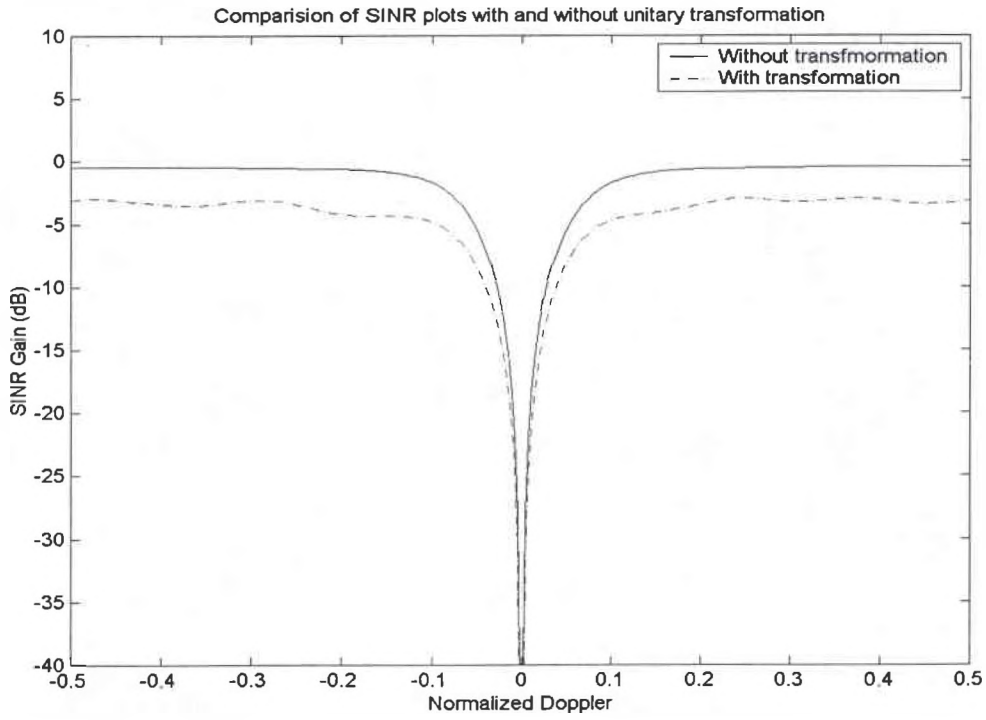

Figure14: SINR plots with and without Unitary Transformation.

CHAPTER III

Heterogeneity of Sample Support

3.1: Introduction

It is demonstrated in the last section that, significant suppression of the clutter and jamming interferences can be obtained by the two-dimensional filtering, effected by STAP. These results are, however, derived under the assumption that there is sufficient sample support available to accurately estimate the interference covariance matrix. Brennan and Reed [7] have shown that twice as many secondary data vectors as the size of the correlation matrix are needed to limit the estimation losses to about 3 dB. The secondary data vectors are derived from the range bins adjacent to the range bin under test with the implicit assumption that this interference is statistically similar to the interference present in the range bin where the target is present. That is, it is assumed that the clutter is homogeneously distributed in range. This may, often, not be the case. In a recent publication [11] Melvin has presented an asymptotic analysis of the loss in SINR due to a variety of factors that are responsible for the inhomogeneity of the secondary data. While this analysis provides a bound on the loss in performance, it does not suggest any means to ameliorate the problem. One possible way to minimize the loss in performance is to minimize the number of the secondary data vectors required. It has been demonstrated that it is possible to obtain near ideal performance with the number of

secondary vectors being no more than twice the dimension of the interference subspace rather than twice the number of the correlation matrix size. It is far easier to assume that the clutter is homogeneous over a smaller region than a larger region. Thus, eigen analysis of the interference covariance matrix is important in the performance of STAP.

In this chapter we carry out simulation studies to study two different kinds of inhomogeneity. These are the intrinsic clutter motion and the presence of a target like "mover" in the secondary data used to estimate the interference covariance matrix.

3.2: Intrinsic Clutter Motion

In the clutter model presented in the last chapter, it is assumed that the clutter signal from each patch is correlated from pulse to pulse. It is this pulse-to-pulse correlation that makes it possible to effect its cancellation. However, there are many practical situations where a certain amount of de-correlation from pulse to pulse of the clutter signal from each patch takes place. Ocean waves are a good example of this phenomenon. From pulse to pulse, each patch of the ocean is not exactly the same, especially so on a windy day. Cutter from a grassy field on a windy day also exhibits significant " Internal Clutter Motion" (ICM). In the absence of the internal clutter motion, the correlation width of the clutter signal is large and its temporal bandwidth is narrow. Thus, the width of the clutter ridge in the angle-Doppler space is small when there is no ICM present. When there is ICM present, the clutter interference spreads over into the rest of the angle-Doppler space from the normally narrow clutter ridge. This phenomenon of broadening Doppler spectrum makes the clutter cancellation considerably more difficult.

The effect of ICM may be summarized as follows:

- Because of the Doppler broadening, the clutter notch widens. As a result, the minimum detectable velocity increases. This is the most significant consequence of ICM
- The dimension of the interference subspace increases significantly as a result of ICM.

3.2.1: Theory

In the absence of ICM, the amplitude of clutter from each patch is taken to be invariant from pulse to pulse, in effect giving rise to zero Doppler bandwidth. That is, the Doppler from each clutter patch is induced by the platform motion and the disposition of the clutter patch with respect to the platform. To account for ICM, these amplitudes are no longer consider invariant but fluctuate with a given auto correlation function. This auto correlation function is typically taken to be a Gaussian function parameterized by the " spectral standard deviation" which in turn is related to the "velocity standard deviation" associated with the ICM. The details of the theoretical development follow:

From Equation (2.30) the echo from the k^{th} clutter patch is

$$\chi_c = \alpha_k(\vec{b}(\varpi_k) \otimes \vec{a}(v_k)) \tag{3.1}$$

A vector $\vec{\alpha}_k$ can represent the fluctuations as depicted below instead of a single scalar, where the term $\alpha_{k,m}$ represents amplitude from the k^{th} scatterer for m^{th} PRI.

$$\vec{\alpha}_k = [\alpha_{k,0}; \alpha_{k,1}; \ldots\ldots\ldots; \alpha_{k,M-1}]$$

Therefore the clutter echo now becomes

$$\chi_c = (\bar{\alpha}_k \circ \bar{b}_k(\varpi_k) \otimes \bar{a}(v_k)) \tag{3.2}$$

The temporal autocorrelation of the fluctuations is Gaussian using the assumption that the Doppler spectrum is Gaussian and can be modeled as

$$\gamma(m) \cong E\{\alpha_{l+m}\alpha_l^*\} = \sigma^2 \xi_k \exp\{-\frac{\kappa_c^2 T_r^2}{2} m^2\} \tag{3.3}$$

where ξ_k is the clutter CNR from Eqn xx and κ_c is the spectral standard deviation which can be expressed as

$$\kappa_c = \frac{\sigma_v 4\pi}{\lambda_0} \text{ where } \sigma_v \text{ is the velocity standard deviation.} \tag{3.4}$$

$$\begin{aligned} \Gamma_k &= E\{\alpha_k \alpha_k^H\} \\ &= \text{Toeplitz}(\gamma_c(0);.....;\gamma_c(M-1)\} \end{aligned} \tag{3.5}$$

is the covariance matrix of the fluctuations for the kth patch. The space-time co-variance matrix for a single clutter patch including ICM now is

$$R_c = \xi_k (\Gamma_k \circ b_k b_k^H) \otimes a_k a_k^H$$

For Nc clutter sources, now

$$R_c = \sum_{k=1}^{N_c} \xi_k (\Gamma_k \circ b_k b_k^H) \otimes a_k a_k^H \tag{3.6}$$

3.2.2: Results

The velocity standard deviation is changed over a range of values from 0.01 to 0.3. Using the model described above, the clutter covariance matrix and the corresponding weight vector are determined and used to SINR, filter pattern and the filter output. The distribution of the Eigen values are also computed in each case. The increase in the interference subspace size is clearly indicated (see figure-15). Associated with the change

in the Eigen distribution is the widening of the clutter notch (see figure-16) that results in the increase of the minimum detectable velocity.

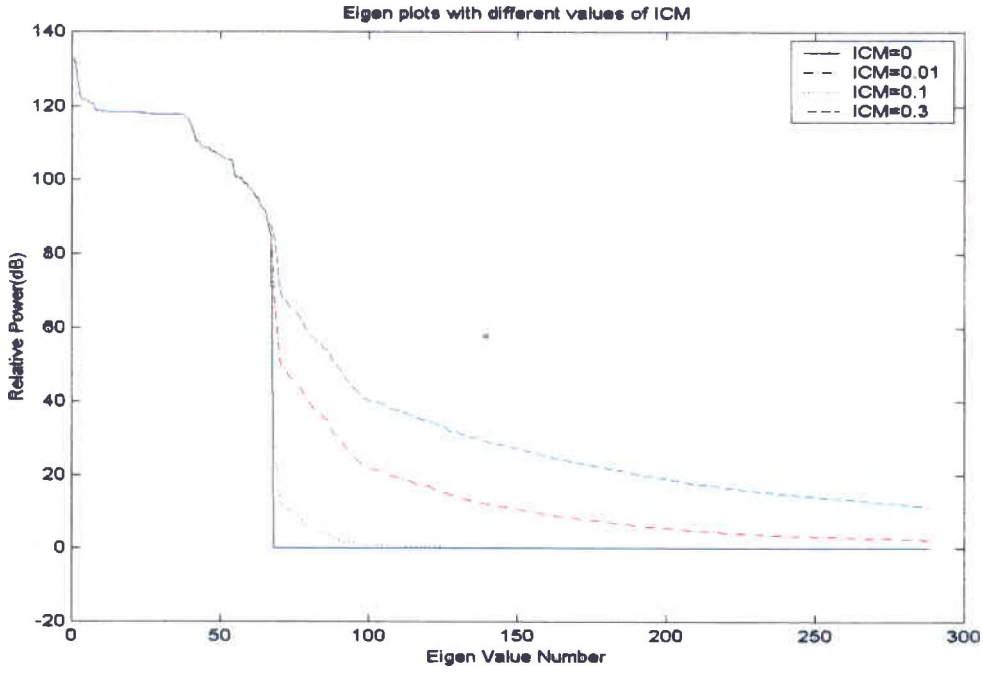

Figure15: Eigen plots with different values of ICM

Figure 17 and Figure 18 show the filter output and the filter pattern for different levels of ICM. While the filter patterns do not change substantially with the level of ICM, the filter output changes significantly, showing the spreading of clutter interference into the angle-Doppler space. It is this spreading that is responsible for the adverse effects of the ICM.

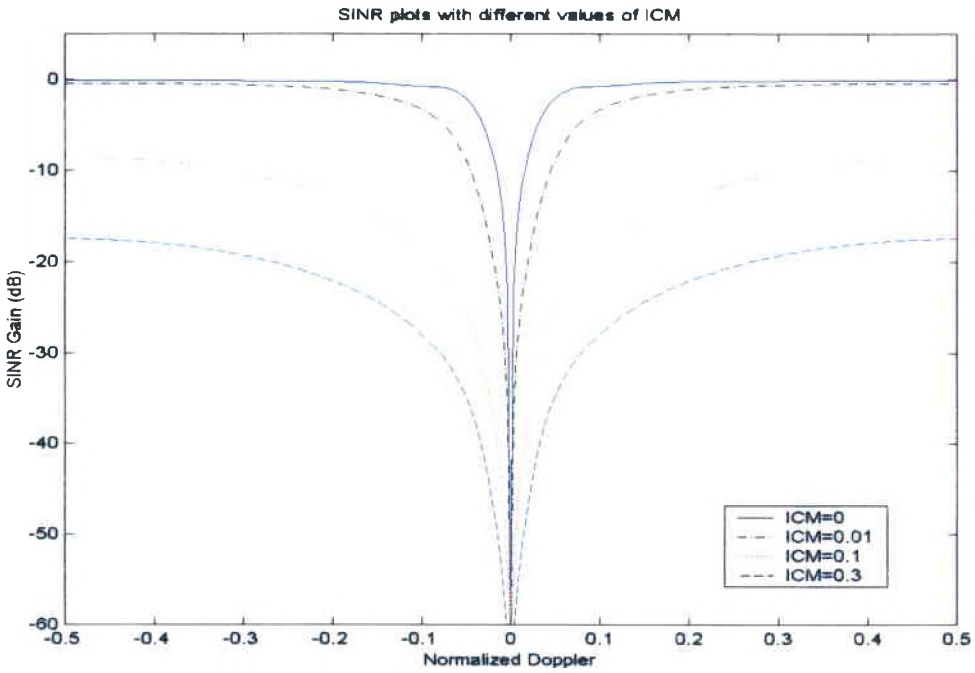

Figure16: SINR Plots with different values of ICM

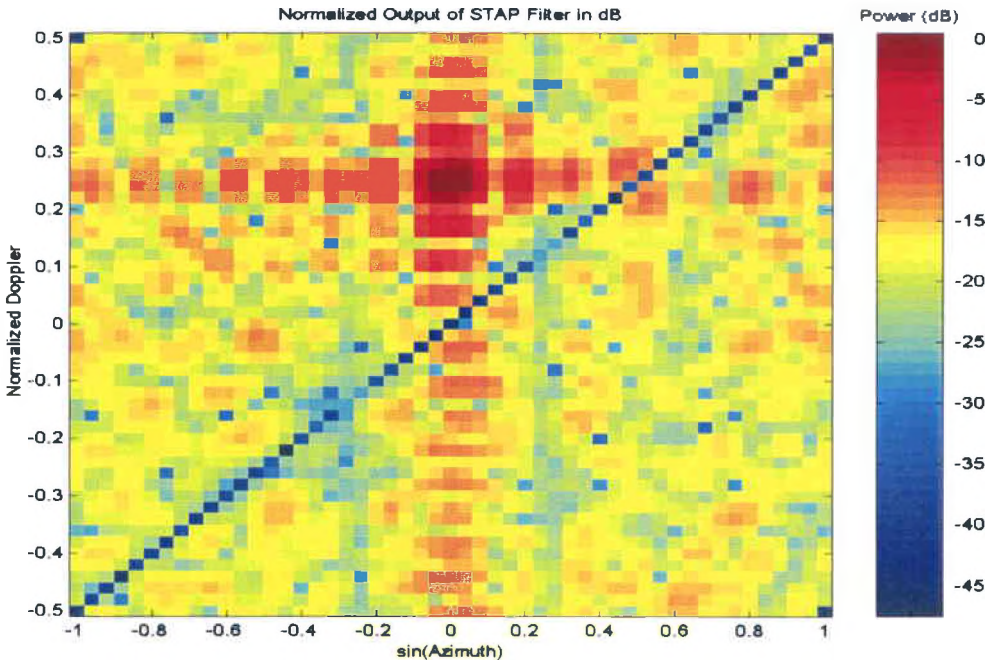

Figure 17a: Filter Output with ICM=0

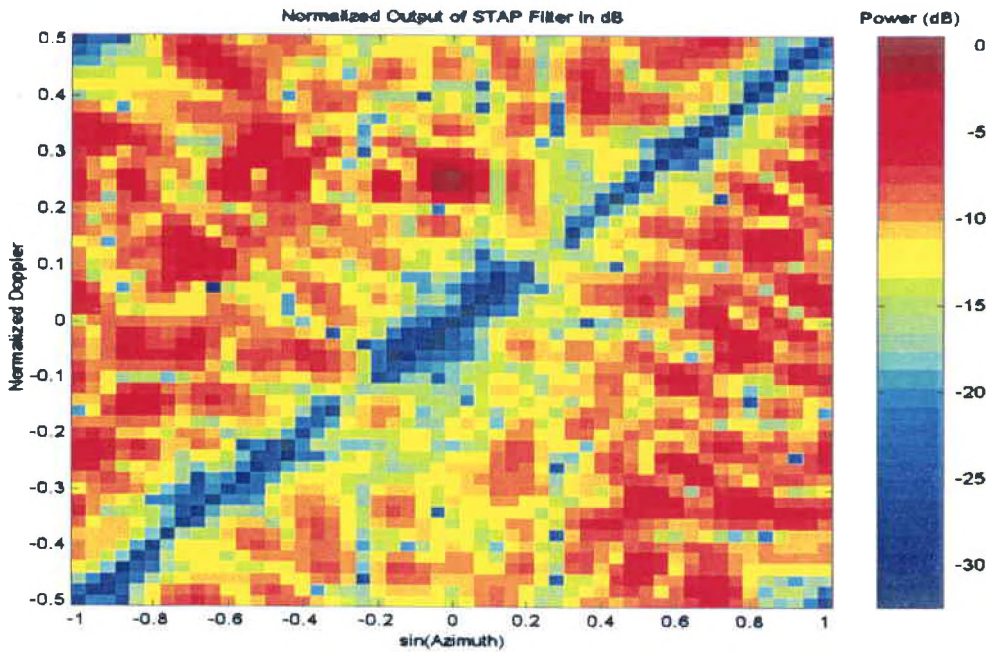

Figure 17b: Filter output with ICM=0.1

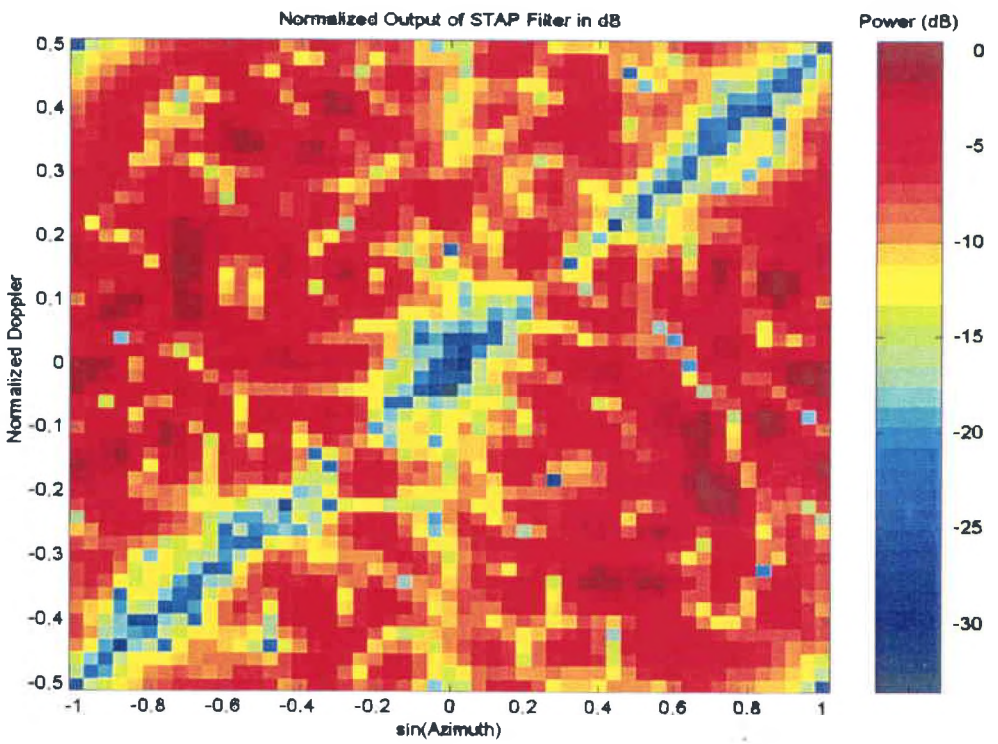

Figure 17c: Filter Output with ICM=0.3

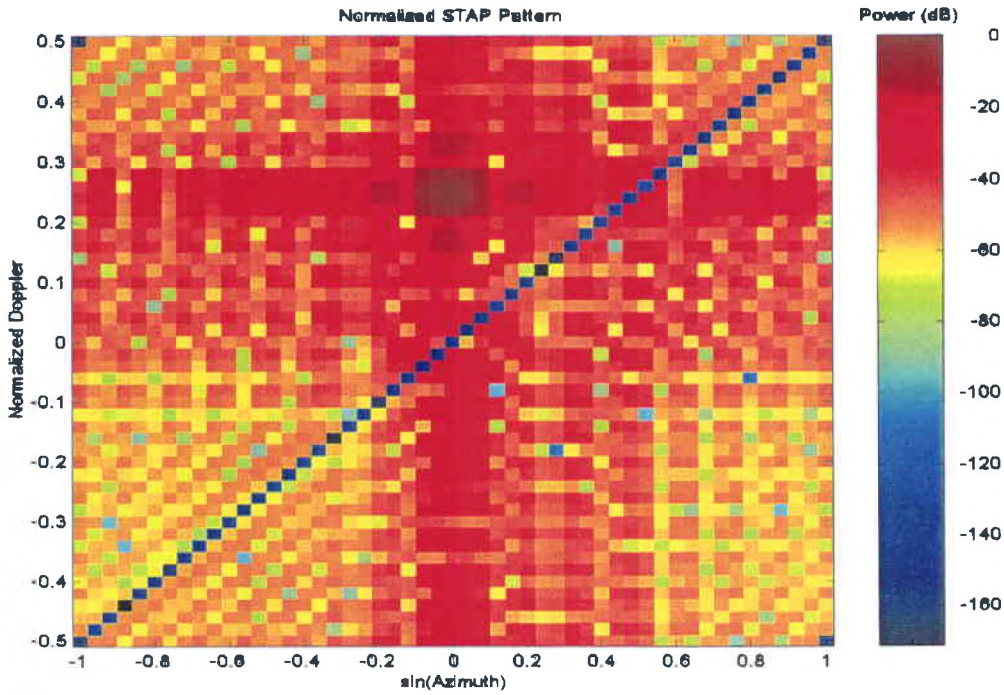

Figure 18a: Filter Pattern with ICM=0

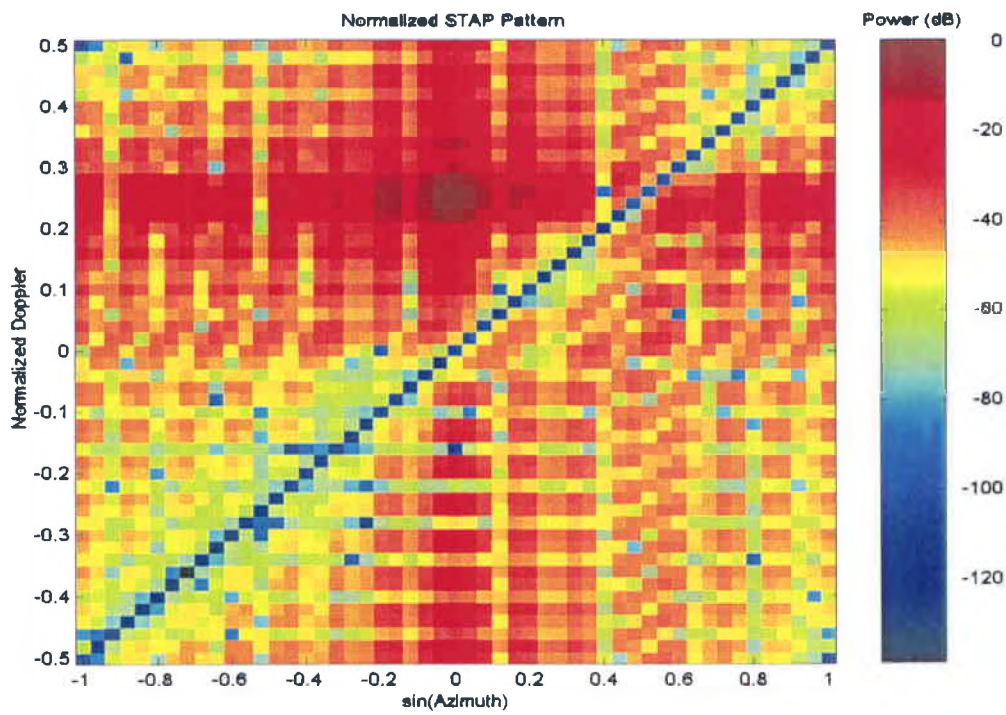

Figure 18b: Filter Pattern with ICM=0.1

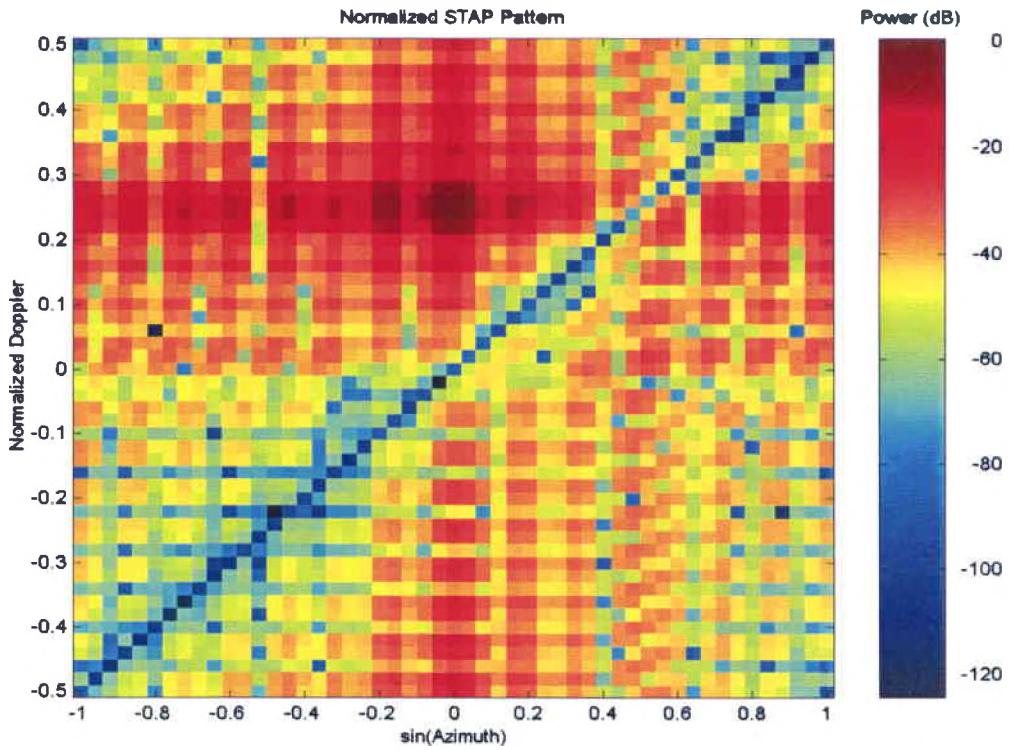

Figure 18c: Filter Pattern with ICM=0.3

3.3: Mover

The optimum weight vector is computed using the inverse of the interference covariance matrix. The secondary data vectors used to estimate the interference covariance matrix must not, therefore, contain any target signal or target signal like signal. When the target of interest is a ground-moving target it is likely that the secondary data vectors drawn from the adjacent range rings contain a moving target whose velocity is similar to that of the target. A weight vector computed using such a secondary data set leads to a STAP filter that not only cancels clutter, but in addition results in unwanted signal cancellation as well. The amount of cancellation depends upon the degree of coupling that exists between the target and the "mover" that is present in the secondary

data. The degree of coupling depends upon the Doppler and the azimuth of the target and the mover being close to each other. When there is strong coupling, significant loss in SINR takes place and filter and the radar become desensitized. The Stronger the echo from the mover, the greater is the loss in SINR. A simulation-based study of this phenomenon is presented here. A mover is modeled as a point target and is injected into a secondary clutter data vector at a given azimuth with specified Doppler. It is shown here that as the target Doppler approaches the mover Doppler, SINR degradation takes place. The extent of SINR degradation depends upon the azimuth of the mover in relation to that of the target Doppler.

3.3.1: Theory:

The mover can be modeled as a point scatterer in any of the clutter patches and behaves similar to the target. Let us consider a mover with the co-ordinates R_{mvr}, azimuth ϕ_{mvr}, and θ_{mvr} its elevation moving with a radial velocity v_{mvr}. Using an analysis similar to that of the target, the signal returned can be computed as,

$$\vec{\chi}_{mvr} = \begin{bmatrix} \vec{x}_0 \\ \vec{x}_1 \\ .. \\ . \\ \vec{x}_{M-1} \end{bmatrix} \tag{3.7}$$

where $\vec{x}_m$ is the spatial snapshot for the mth pulse.

$$\vec{x}_m = \begin{bmatrix} x_{0,m} \\ x_{1,m} \\ . \\ . \\ . \\ x_{N-1,m} \end{bmatrix} = \begin{bmatrix} \alpha_t e^{jm2\pi\varpi_{mvr}}.1 \\ \alpha_t e^{jm2\pi\varpi_{mvr}}.e^{j\pi 2\vartheta_{mvr}} \\ . \\ \alpha_t e^{jm2\pi\varpi_{mvr}}.e^{j\pi 2n\vartheta_{mvr}} \\ . \\ \alpha_t e^{jm2\pi\varpi_{mvr}}.e^{j\pi 2(N-1)\vartheta_{mvr}} \end{bmatrix}$$

$$\vec{x}_m = \alpha_t.e^{jm2\pi\varpi_{mvr}}.\vec{a}(\vartheta_{mvr})$$

Where $\vec{a}(\vartheta_{mvr}) = [1, e^{j\pi 2\vartheta_{mvr}}, ...e^{j\pi 2(N-1)\vartheta_{mvr}}]$ is the spatial steering vector Thus,

$$\begin{aligned}\vec{\chi}_{mvr} &= [\vec{x}_0; \vec{x}_1; .....; \vec{x}_{M-1}] \\ &= \alpha_{mvr}[\vec{a}(\vartheta_{mvr}); e^{j\pi 2\varpi_{mvr}}\vec{a}(\vartheta_{mvr}); .....; e^{j\pi 2(M-1)\varpi_{mvr}}\vec{a}(\vartheta_{mvr})] \\ &= \alpha_{mvr}[1; e^{j\pi 2\varpi_{mvr}}; e^{j\pi 2.2\varpi_{mvr}}; .....; e^{j\pi 2(M-1)\varpi_{mvr}}] \otimes [\vec{a}(\vartheta_{mvr})]\end{aligned}$$

By the definition of Kronecker product

$$A \otimes B = [a(m,n) \times B]$$

$$\vec{\chi}_{mvr} = \alpha_{mvr}\vec{b}(\varpi_{mvr}) \otimes \vec{a}(\vartheta_{mvr}) = \alpha_{mvr}\vec{v}_{mvr}$$

where

$$\vec{b}(\varpi_{mvr}) = [1; e^{j2\pi\varpi_{mvr}}; e^{j4\pi\varpi_{mvr}}; .....; e^{j2(M-1)\pi\varpi_{mvr}}]$$

and $\vec{v}_{mvr} = \vec{b}(\varpi_{mvr}) \otimes \vec{a}(\vartheta_{mvr})$ is the steering vector.

The signal vector from the clutter patch in which this mover is positioned using Equation 2.30, now becomes

$$\chi_{c,ik} = \alpha_{ik}\vec{v}_{ik}(\theta_i, \phi_{ik}) + \vec{\chi}_{mvr} \tag{3.8}$$

The total clutter is computed as before from Equation 2.32

$$\chi_c = \sum_{i=1}^{Nr}\sum_{k=1}^{Nc}\chi_{c,ik} \text{ and the clutter co-variance matrix is derived as} \tag{3.9}$$

$$R_c = E[\chi_c\chi_c^H] \tag{3.10}$$

3.3.2: Results

To carry out this simulation study, the following parameters are used: N=16 and M=18. The target is present at 0° azimuth and the normalized target Doppler is varied from –0.5 to 0.5. The normalized Doppler of the mover is taken to be 0.23. Two different mover azimuth locations at φ=0° and φ=2° are considered. Note that the null-to-null beam width for this configuration is about 4°. Figure 19 and 20 show that as the target Doppler approaches the mover Doppler there is a loss in SINR and also that the greater the mover strength, the greater the loss. Note that the SINR loss is more significant when the mover is at φ=0° than when the mover is at φ=2°. Indeed, when the mover is more than a beam width away from the target there is little coupling between the target and the mover and hence there is little effect on SINR.

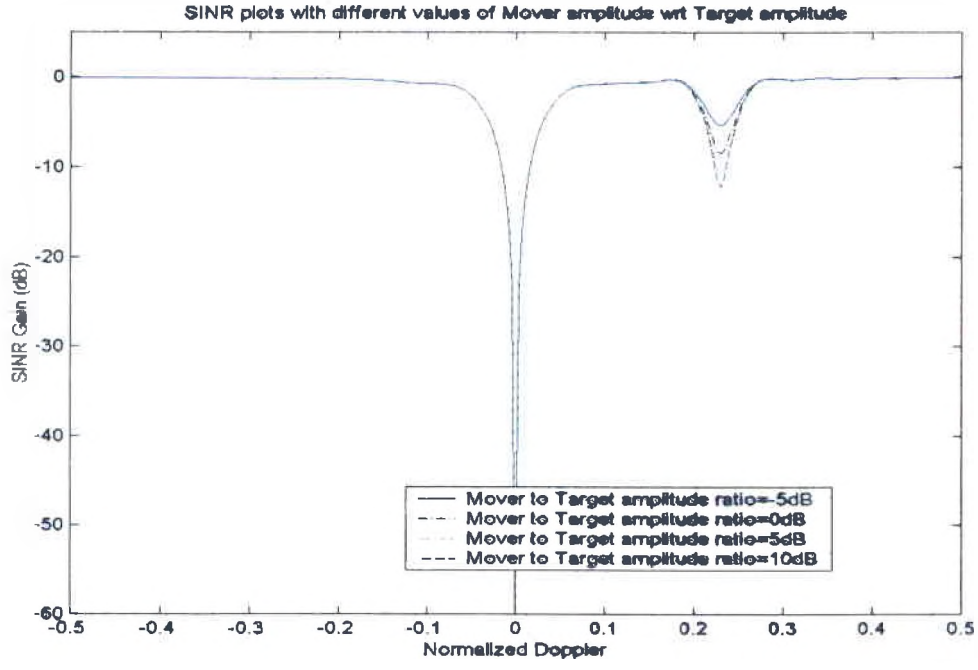

Figure 19: SINR plot with different Mover to Target amplitude ratio, Mover Doppler=0.23, Phi=0.

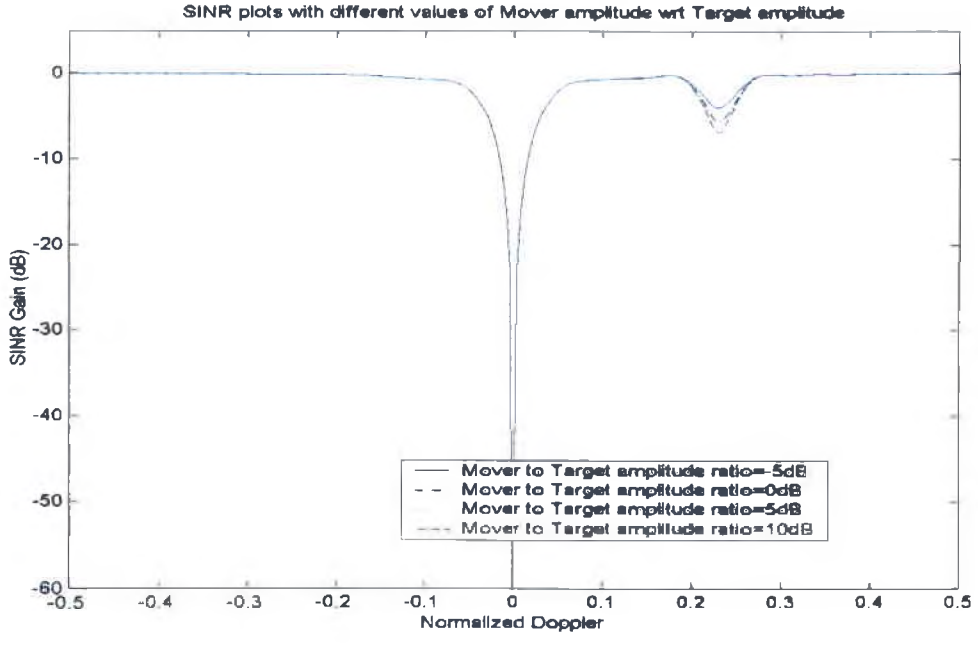

Figure 20: SINR with different Mover to Target amplitude ratio, Mover Doppler=0.23, Phi=2.

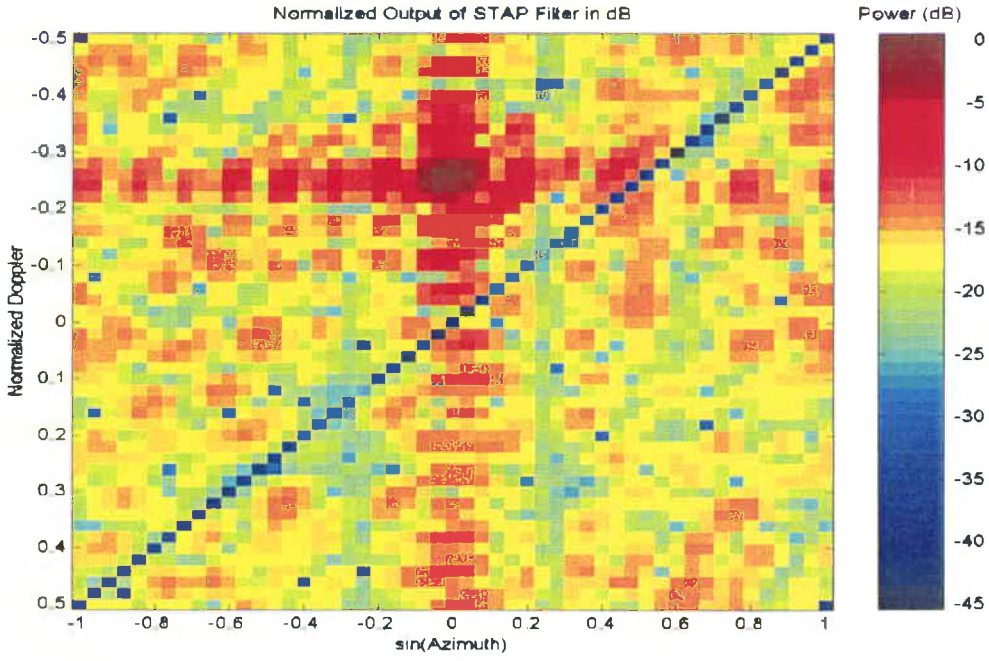

Figure 21a: Filter output, Mover to Target amplitude ratio =0dB

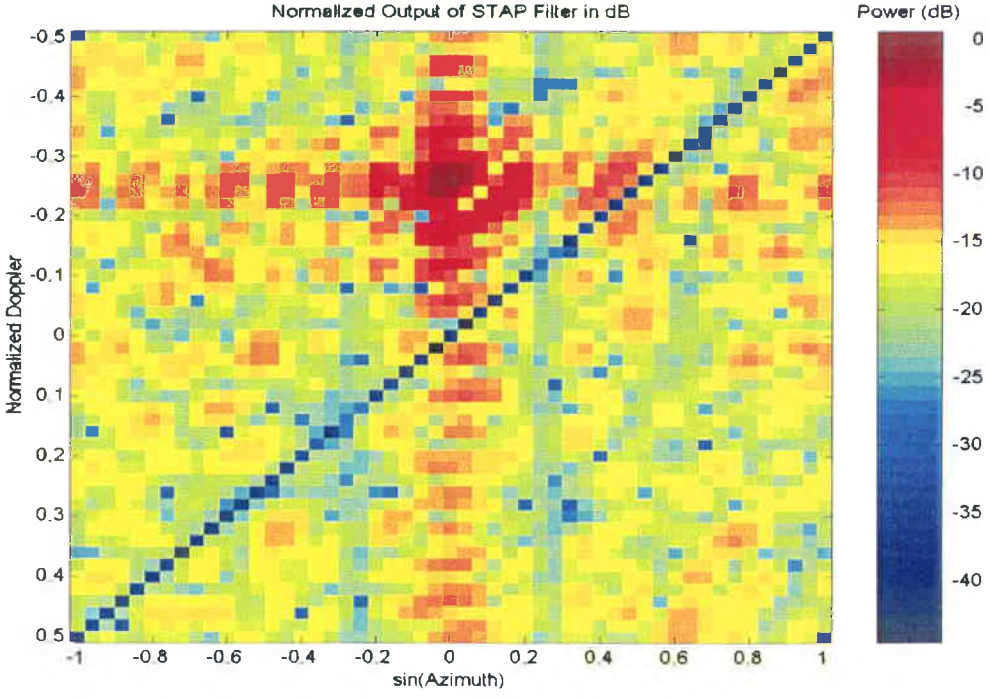

Figure 21b: Filter output, Mover to Target amplitude ratio =5dB

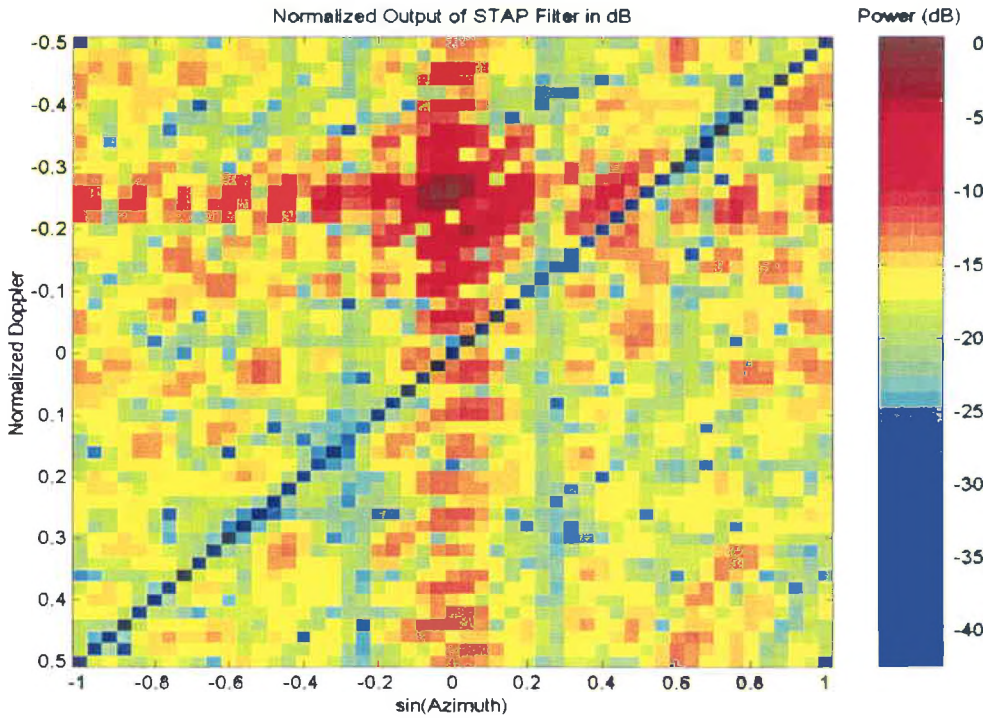

Figure 21c: Filter output, Mover to Target amplitude ratio =10dB

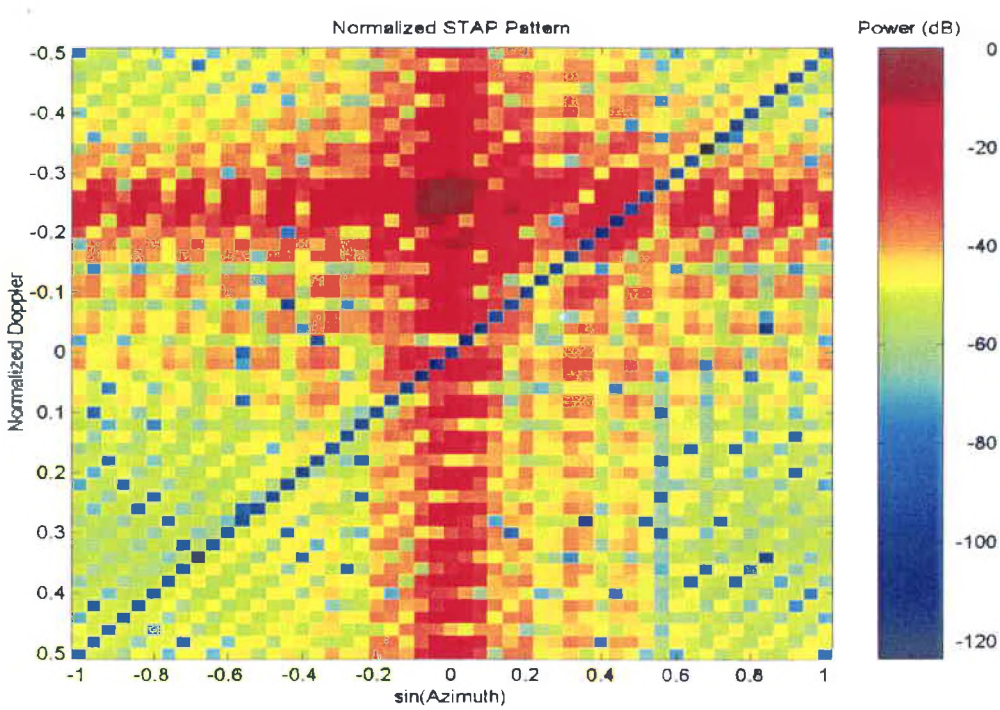

Figure 22a: Filter pattern, Mover to Target amplitude ratio=0dB

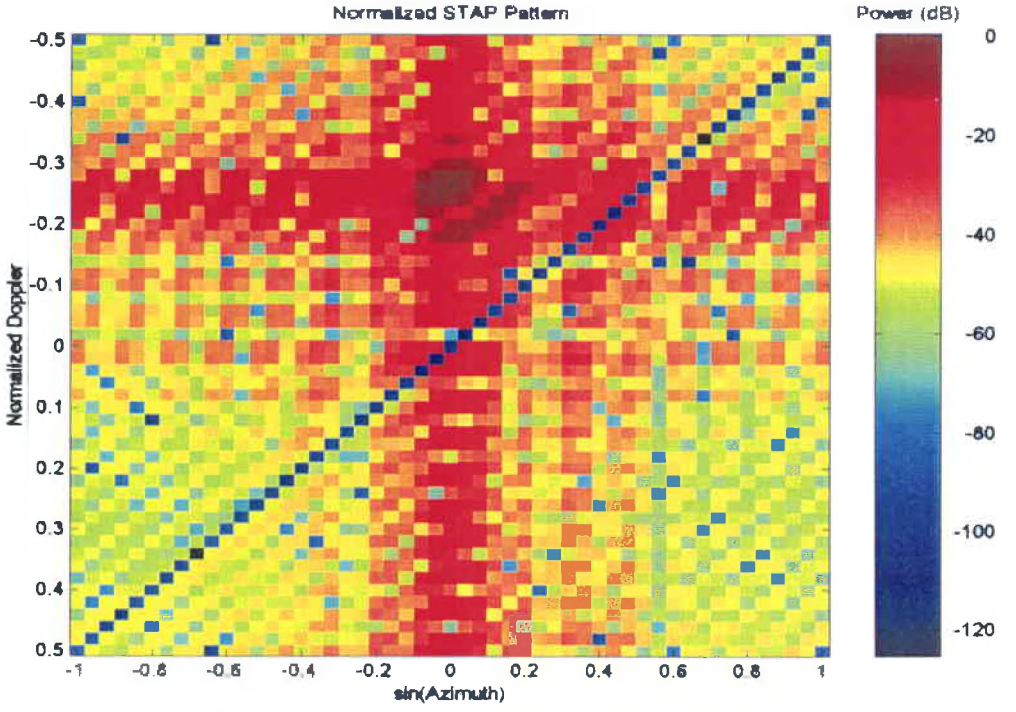

Figure 22b: Filter pattern, Mover to Target amplitude ratio=5dB

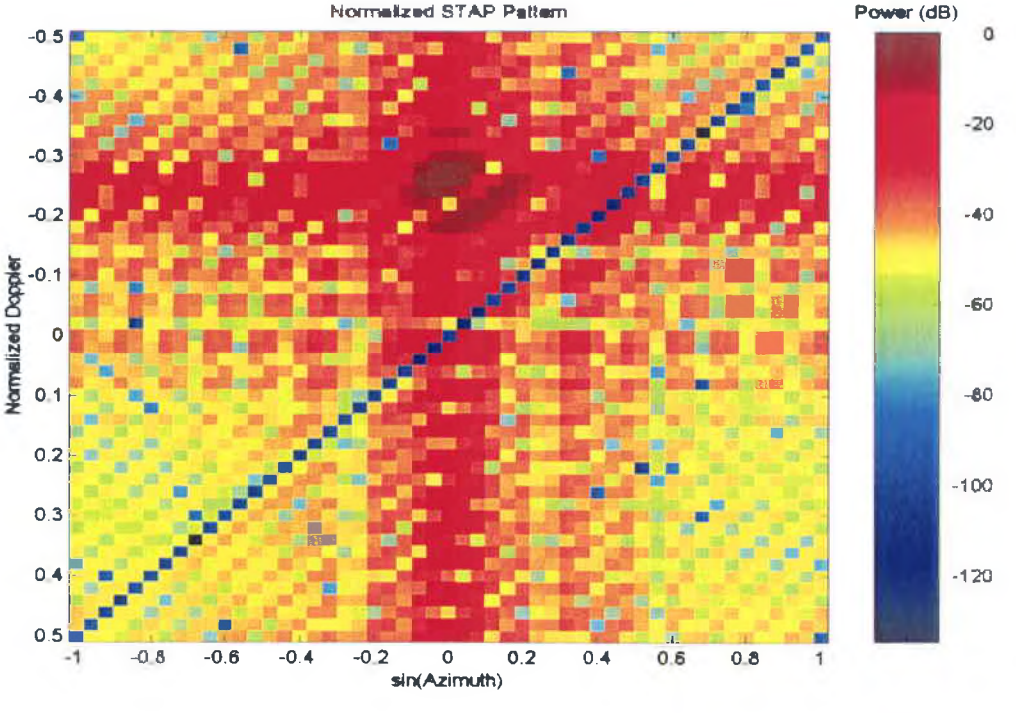

Figure 22c: Filter pattern, Mover to Target amplitude ratio=10dB

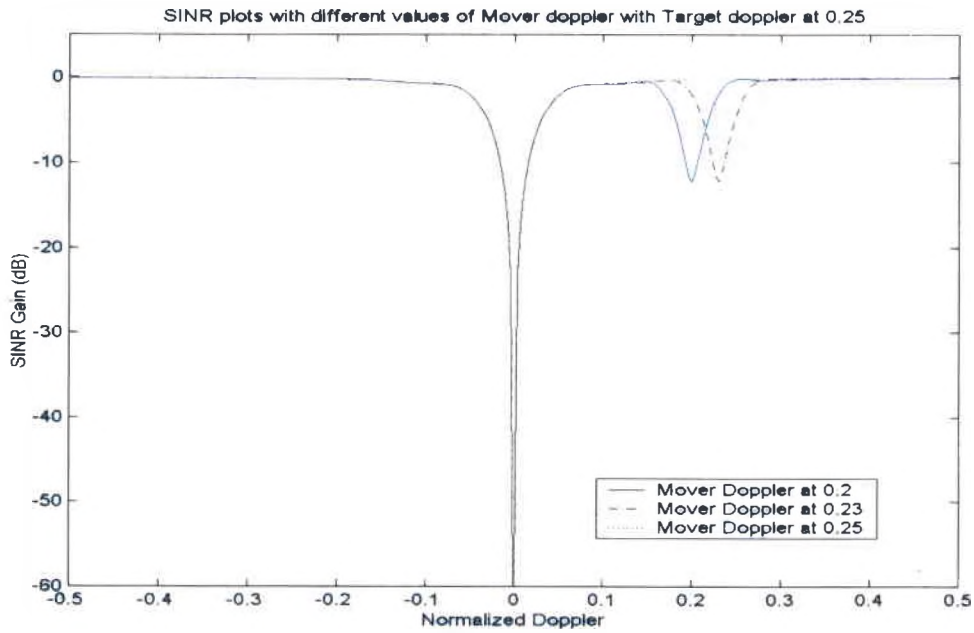

Figure 24: SINR with different Mover Doppler, with Mover to Target amplitude ratio=10dB,Phi=1

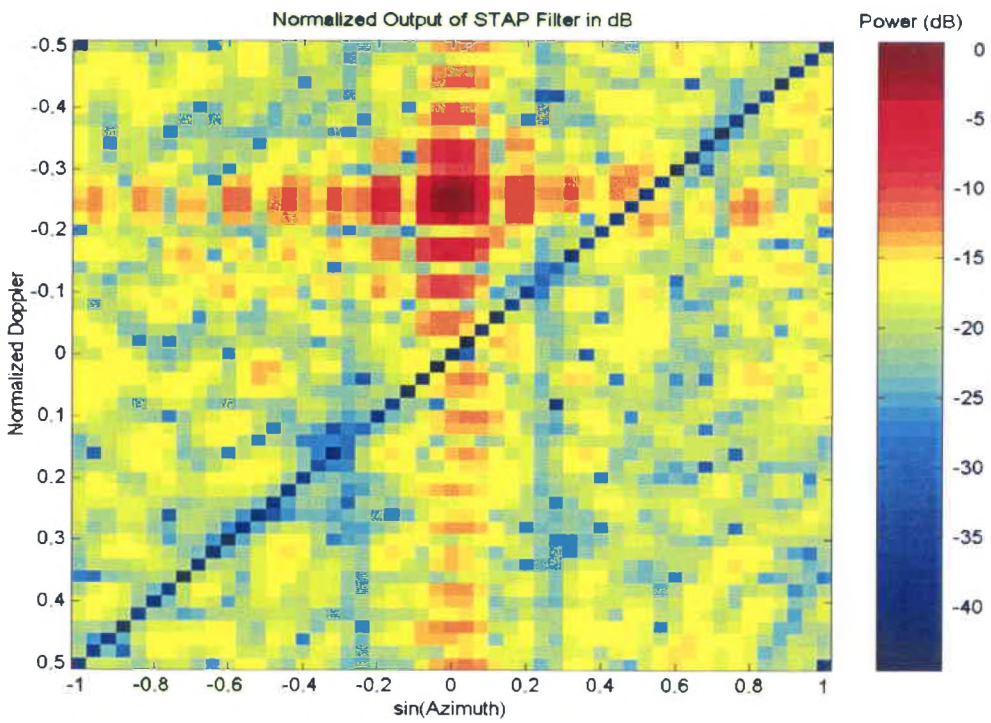

Figure 25a: Filter Output with Mover Doppler=0.2

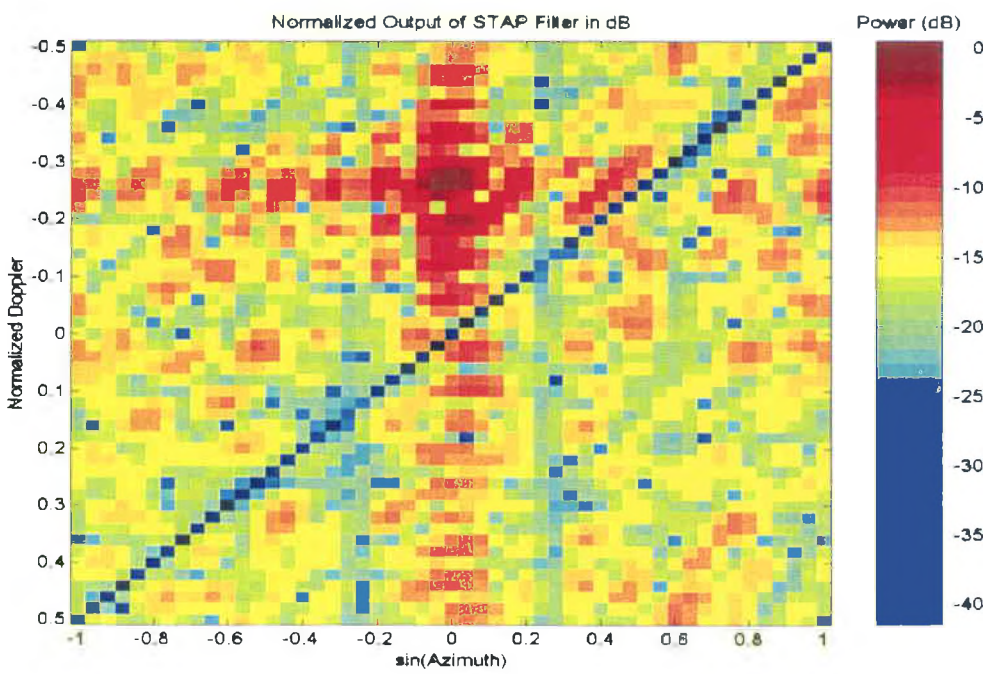

Figure 25b: Filter Output with Mover Doppler=0.23

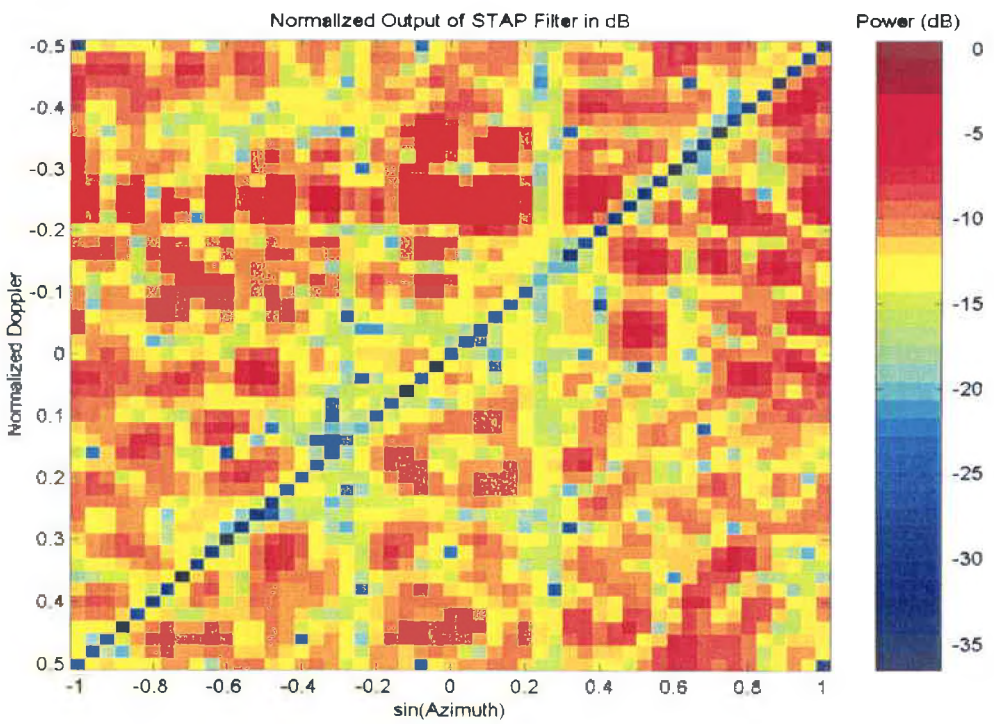

Figure 25c: Filter Output with Mover Doppler=0.25

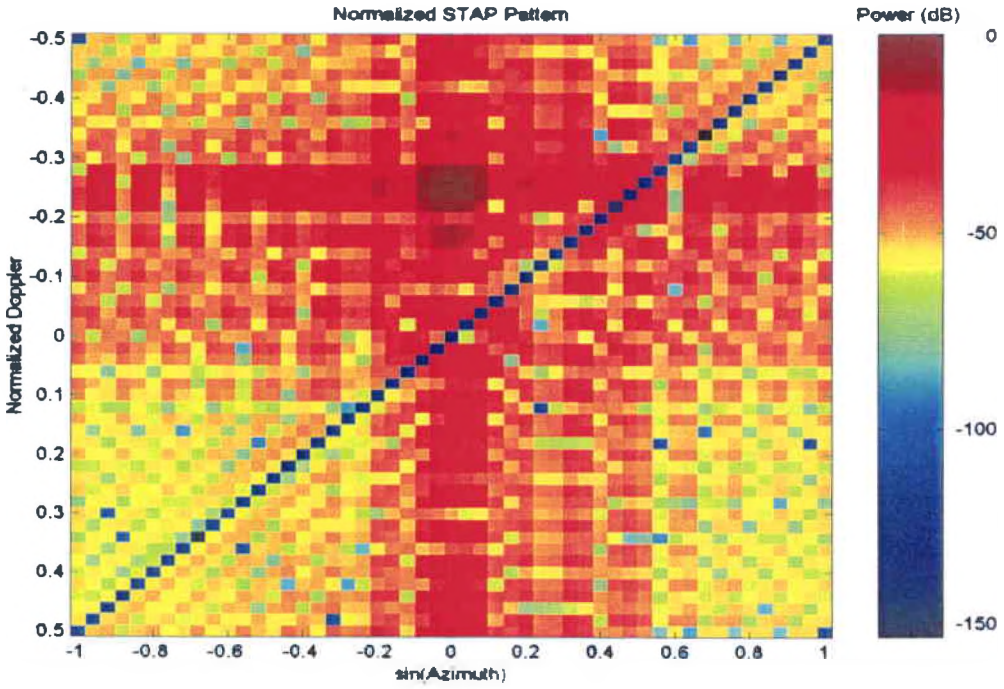

Figure 26a: Filter Pattern with Mover Doppler=0.2

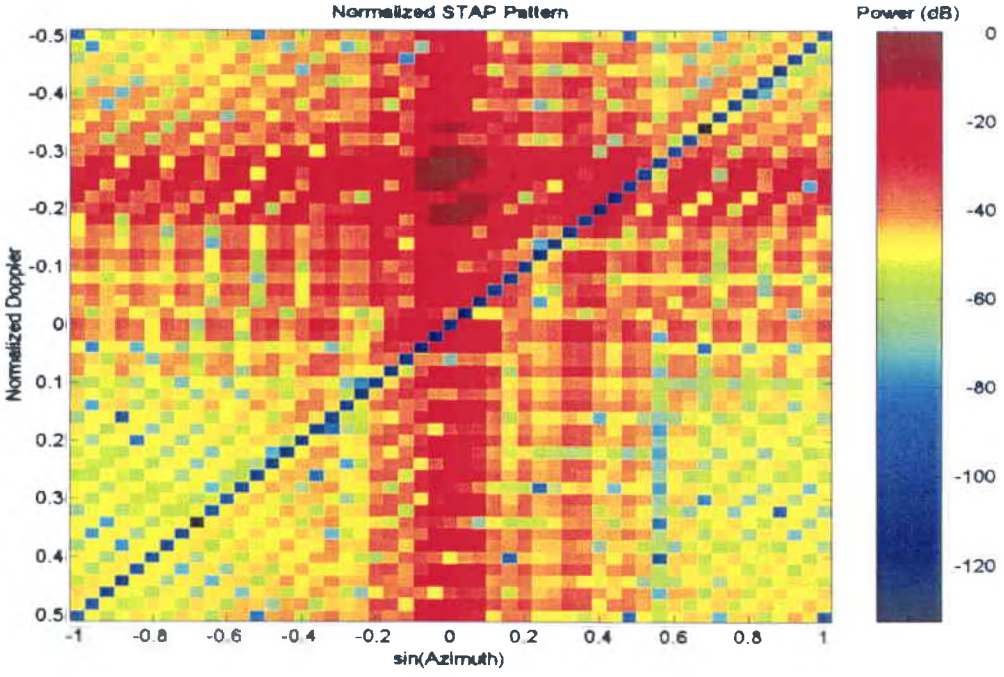

Figure 26b: Filter Pattern with Mover Doppler=0.23

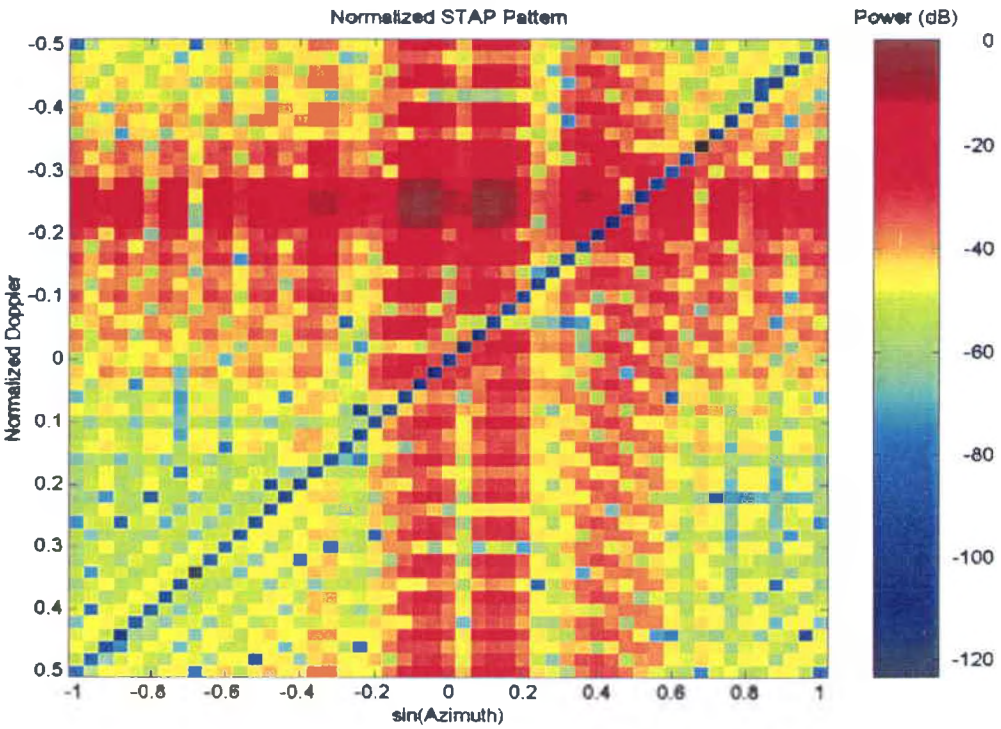

Figure 27c: Filter Pattern with Mover Doppler=0.25

CHAPTER IV

Broad-Band STAP

4.1 Introduction

Increasingly, radars are expected to provide more and more information about the target. The high range resolution radar (HRR) is one such example. It is expected to identify the target rather than simply detect the target. Such complex tasks require the radar to have wide bandwidth, on the order of 5% or so. Typical surveillance radars are usually considered to be narrowband with bandwidths on the order of 1% or less. The effect of bandwidth on the performance of adaptive antennas has been considered, for example by Compton[5]. The effect of bandwidth on STAP has received relatively little consideration but lately there is increasing interest in this direction [24]-[28]. We consider here the performance of STAP when signal bandwidth is taken into account.

It is demonstrated here that finite bandwidth has a significant and adverse effect on the ability of the STAP filter to suppress interference. Signal bandwidth gives rise to interference bandwidth as well and cancellation of the interference with non-zero bandwidth is a more challenging task. It is shown here that even for signal bandwidths less than 1% the SINR performance is adversely affected and in particular, the clutter ridge is widened. This widening of the clutter ridge results in the minimum detectable velocity to be higher than that predicted by the optimum STAP filter for the zero bandwidth case. It is shown that the rank of the clutter covariance matrix increases. Such

increase in the interference subspace size has implications in the design of partially adaptive algorithms and also in determining the minimum sample support requirements.

4.2. Theory:

The conventional signal modeling used in STAP does not take into account finite bandwidth of the signal. The principal effect of finite signal bandwidth is in increasing the bandwidth of the interference from the clutter as well. The covariance matrix of cutter R_c, is given by,

$$R_c = \sum_{i=1}^{N_r} \sum_{k=1}^{N_c} (\xi_{ik}\sigma^2)\vec{v}_{ik}\vec{v}_{ik}^{\,k} \tag{4.1}$$

Here N_r is the number of range ambiguities and N_c is the number of clutter patches in a range ring. $(\xi_{ik}\sigma^2)$ is the average power of clutter interference from the ik^{th} patch. $\vec{v}_{ik}$ is the Space-Time steering vector corresponding to the ik^{th} patch. The space-time steering vector is defined by,

$$\vec{v}(\vartheta,\varpi) = \vec{b}(\varpi) \otimes \vec{a}(\vartheta)$$
$$\vec{b}(\varpi) = \left[1, e^{j2\pi\varpi}; \ldots\ldots; e^{j(M-1)2\pi\varpi}\right]$$
$$\text{and} \quad \vec{a}(\vartheta) = \left[1; e^{j2\pi\vartheta}; \ldots\ldots; e^{j(N-1)2\pi\vartheta}\right]$$

The spatial frequency, ϑ, and the normalized Doppler are given by

$$\vartheta = \frac{d}{\lambda_0}\cos\theta\sin\phi \quad = \quad f_0\frac{d}{c}\cos\theta\sin\phi$$
$$\varpi = \frac{f_d}{f_r} = \frac{2v}{\lambda_0}.\frac{1}{f_r} = \frac{2v}{c}\frac{f_0}{f_r} \tag{4.2}$$

Here f_r is the pulse repetition frequency, v is the relative radial velocity and f_0 is the center frequency of the signal. To account for the effect of bandwidth, the definition of the clutter covariance matrix is defined as

$$R_{c,B} = \frac{1}{B}\int_{f_0-B/2}^{f_0+B/2} R_c\,df. \tag{4.3}$$

This is best implemented by carrying out the integration for each element of the matrix and the details of such a process are given below.

The $(p,q)^{th}$ element of the clutter covariance matrix, R_c for a narrow-band signal is given by

$$[R_c]_{p,q} = \sum_{i=1}^{Nr}\sum_{k=1}^{Nc}\sigma^2\xi_{ik}e^{j2\pi(n(p)-n(q)\vartheta_{ik}}e^{j2\pi[m(p)-m(q)]\varpi_{ik}} \tag{4.4}$$

Let

$$n(p)-n(q)=\bar{n};\qquad n(p)=\text{modulo}(p,N);\qquad n(q)=\text{modulo}(q,N)$$

$$m(p)-m(q)=\bar{m};\quad m(p)=floor(\frac{p}{N});\qquad m(q)=floor(\frac{q}{N})$$

Then

$$[R_c]_{p,q} = \sum_{i=1}^{Nr}\sum_{k=1}^{Nc}\sigma^2\xi_{ik}e^{j2\pi\bar{n}\vartheta_{ik}}e^{j2\pi\bar{m}\varpi_{ik}}. \tag{4.5}$$

For a signal with non-zero bandwidth, the definition for spatial frequency is modified to reflect its change with frequency and is given below.

$$\vartheta_{ik} = \frac{d}{\lambda_0}\cos\theta_c\sin\phi_{ik} = \frac{fd}{c}\cos\theta_c\sin\phi_{ik}$$
$$\varpi_{ik} = 2\frac{v_{ik}}{\lambda_0}.\frac{1}{f_r} \tag{4.6}$$

Note that ϑ_{ik} is now a function of frequency but the definition of normalized Doppler continues to be based on the center frequency.

$$[R_c]_{p,q} = \frac{1}{B}\int_{f_0-B/2}^{f_0+B/2}\sum_{i=1}^{Nr}\sum_{k=1}^{Nc}\sigma^2\xi_{ik}e^{j2\pi\bar{n}\bar{\vartheta}_{ik}}e^{j2\pi\bar{n}\varpi_{ik}}$$

$$= \sum_i\sum_k \sigma^2\xi_{ik}e^{j2\pi\bar{n}\varpi_{ik}}\frac{1}{B}\int_{f_0-B/2}^{f_0+B/2}e^{j2\pi\bar{n}\bar{\vartheta}_{ik}}df$$

$$= \sum_i\sum_k \sigma^2\xi_{ik}e^{j2\pi\bar{n}\varpi_{ik}}\frac{1}{B}\int_{f_0-B/2}^{f_0+B/2}e^{j2\pi\bar{n}\bar{\vartheta}_{ik}f}df; \quad \bar{\vartheta}_{ik} = \frac{d}{c}\cos\theta_c\sin\phi_{ik}$$

$$= \sum_i\sum_k \sigma^2\xi_{ik}e^{j2\pi\bar{n}\varpi_{ik}}\frac{1}{B}\left[\frac{e^{j2\pi\bar{n}\bar{\vartheta}_{ik}f}}{j2\pi\bar{n}\bar{\vartheta}_{ik}}\right]_{f_0-B/2}^{f_0+B/2}$$

$$= \sum_i\sum_k \sigma^2\xi_{ik}e^{j2\pi\bar{n}\varpi_{ik}}\frac{1}{B}\frac{1}{j2\pi\bar{n}\bar{\vartheta}_{ik}}[e^{j2\pi\bar{n}\bar{\vartheta}_{ik}(f_0+B/2)} - e^{j2\pi\bar{n}\bar{\vartheta}_{ik}(f_0-B/2)}]$$

$$= \sum_i\sum_k \sigma^2\xi_{ik}e^{j2\pi\bar{n}\varpi_{ik}}\frac{1}{B}e^{j2\pi\bar{n}\bar{\vartheta}_{ik}f_0}\frac{2j\sin(\pi\bar{n}\bar{\vartheta}_{ik}B)}{j2\pi\bar{n}\bar{\vartheta}_{ik}}$$

$$= \sum_i\sum_k \sigma^2\xi_{ik}e^{j2\pi\bar{n}\varpi_{ik}}e^{j2\pi\bar{n}\bar{\vartheta}_{ik}f_0}.\frac{\sin[\pi\bar{n}\bar{\vartheta}_{ik}B]}{\pi\bar{n}\bar{\vartheta}_{ik}B}$$

$$R_{c,B} = \sum_i\sum_k R_{c,ik}\Theta R_{B,ik} \tag{4.7}$$

where,

$$\begin{aligned}\left[R_{B,ik}\right]_{p,q} &= \frac{\sin[\pi\bar{n}\bar{\vartheta}_{ik}B]}{\pi\bar{n}\bar{\vartheta}_{ik}B}\\ \left[R_{c,ik}\right]_{p,q} &= \sigma^2\xi_{ik}e^{j2\pi\bar{n}\bar{\vartheta}_{ik}f_0}e^{j2\pi\bar{n}\varpi_{ik}}\end{aligned} \tag{4.8}$$

and Θ indicates the Hadamard matrix product.

4.3 Results:

With the covariance matrix for finite bandwidth, as defined in Section-4.2, the optimum weight vector is computed in the usual fashion and is given by

$$\vec{W}_{opt} = R_{c,B}^{-1}\vec{v}_t. \tag{4.9}$$

Note that the steering vector, $\bar{v}_t$, used here corresponds to the expected target Doppler and angle at the center frequency. Whether the steering vector should be modified or not to account for the finite bandwidth is an interesting question to be considered. The SINR is computed in the usual fashion for two different values of clutter to noise ratio and are shown below in Figure 27. For all the computations presented here, only the side looking radar configuration has been considered. The number of elements in the array is 16 and the number of pulses in the coherent processing interval is 18. The radar center frequency is 450 MHz.

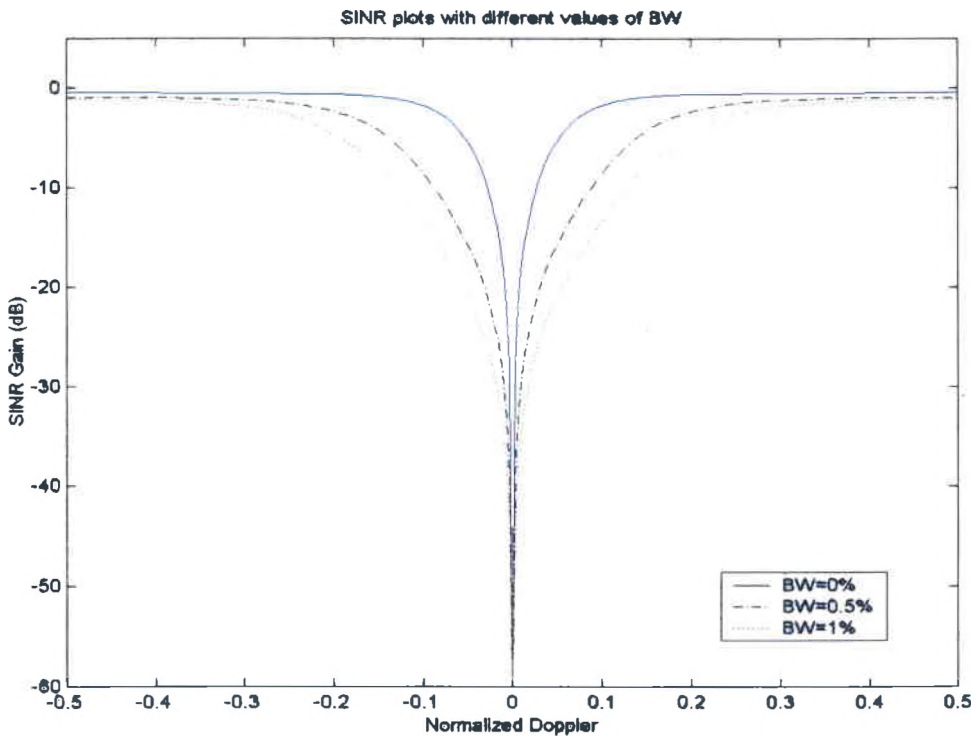

Figure 27a: Effect of bandwidth on SINR. SNR= 10 dB,CNR=47.

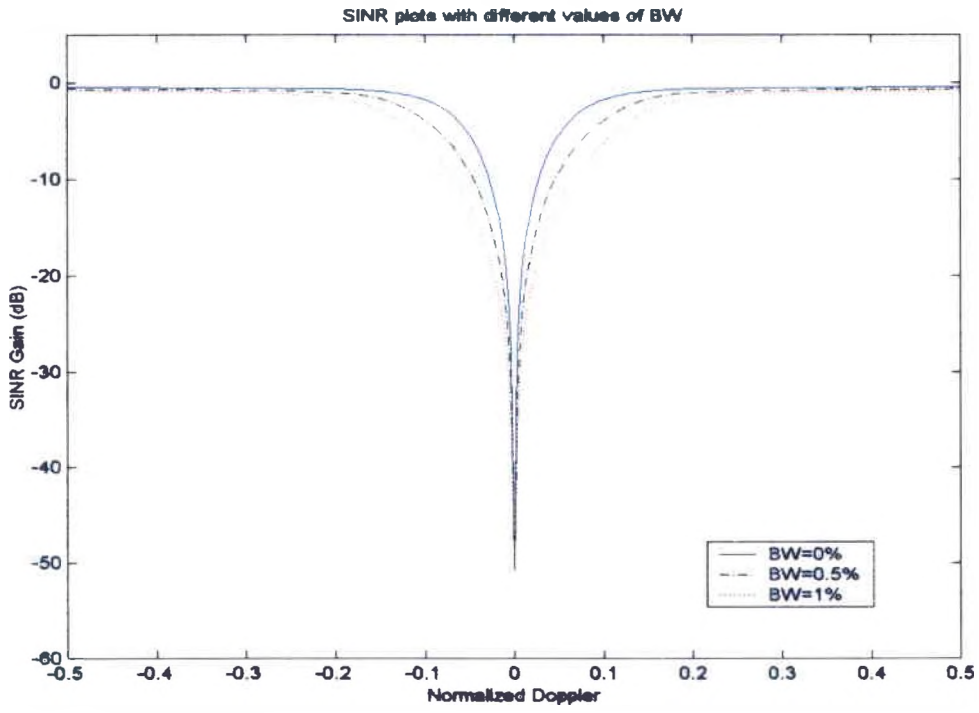

Figure 27b: Effect of bandwidth on SINR. SNR= 10 dB, CNR=37

These results clearly show that even relatively small bandwidths have an adverse impact on the clutter cancellation capability of the STAP filter. Also, it may be noted that the clutter to noise ratio also has an impact on the ability of the filter to cancel the clutter. The clutter notch is significantly widened resulting in a loss in the ability to detect slow moving targets; that is, the minimum detectable velocity is increased. The reason for the loss in performance lies in the increase in the clutter bandwidth when the signal bandwidth increases. The interference from each clutter patch, emanating from a given azimuth angle at the array, appears as an extended source because of non -zero bandwidth.

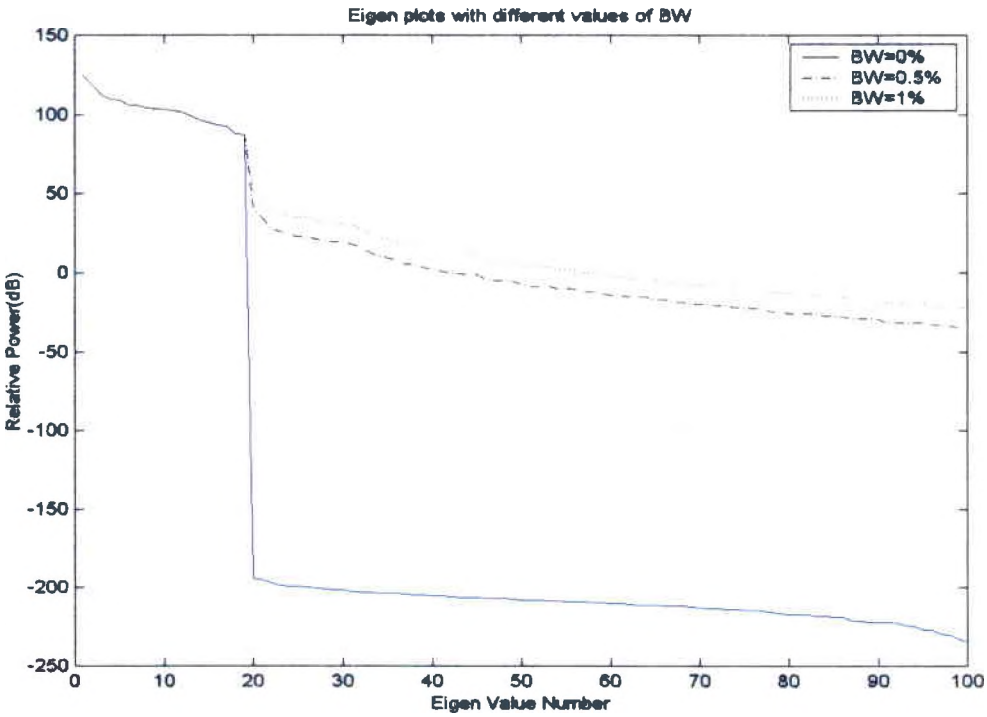

Figure 28: The effect of bandwidth on the clutter eigenspectrum

This effect serves to raise the rank of the clutter covariance matrix. Figures 28 shows the clutter eigenspectra for CNR=47 dB. The significant increase in the size of the interference subspace is quite evident and is responsible for the loss in the filter performance. It may be noted that the low rank nature of the clutter covariance matrix for the zero bandwidth case is taken advantage of to design a number of partially adaptive algorithms that require less degrees of freedom but at the same time yield a filter performance close to that of the fully adaptive case. It appears that the finite signal bandwidth makes it that much harder to attain good performance with the partially adaptive algorithms.

It is instructive to examine the STAP filter pattern and output to gain further insight into the loss in performance. Figure 29a, 29b and 29c show the filter output for

CNR=37 dB and a normalized target Doppler of 0.25 for three different bandwidths corresponding to 0%, 0.2% and 1%. It can be seen clearly that there is increasing amounts of interference in the filter output as the bandwidth is increased resulting in the SINR loss.

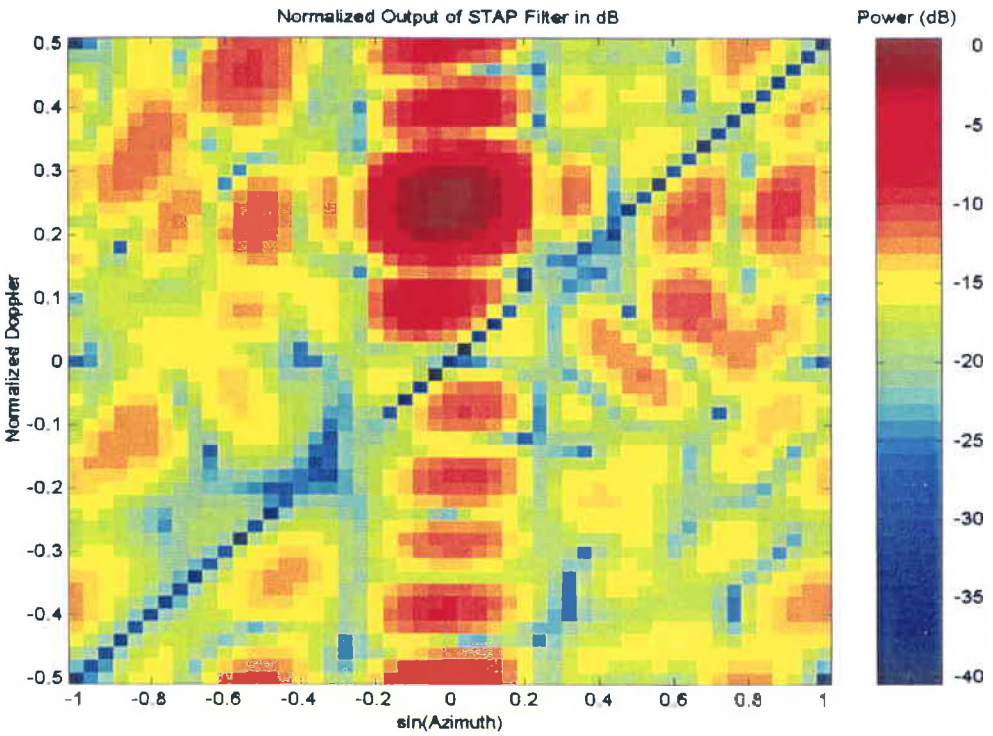

Figure 29a: Filter output. CNR=47 dB and SNR=10dB. Target Doppler=0.25. BW=0%

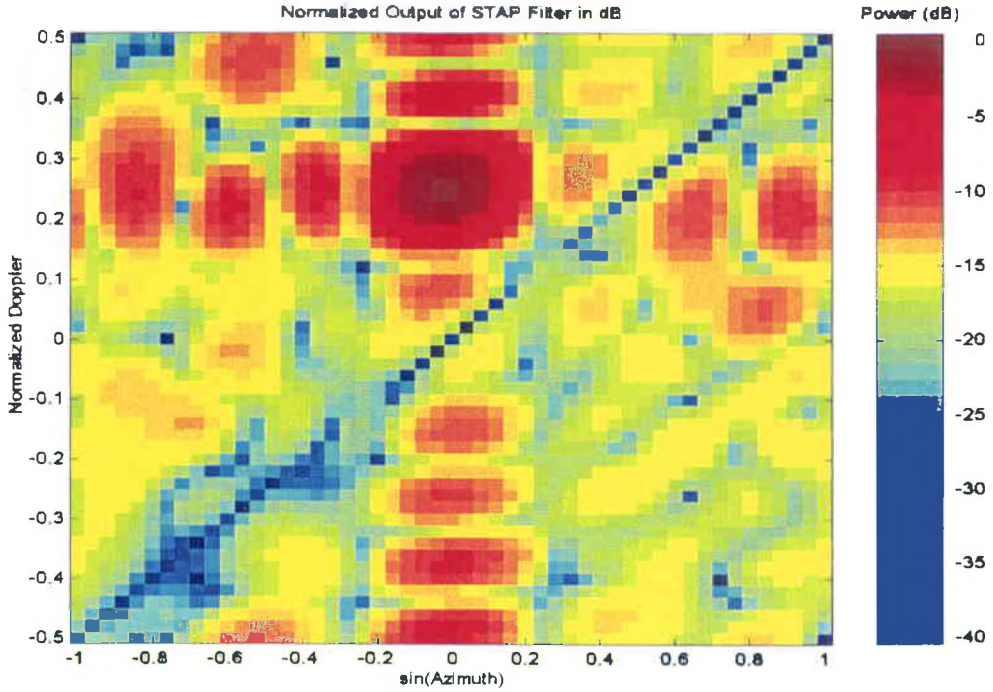

Figure 29b: Filter output. CNR=47 dB and SNR=10dB. Target Doppler=0.25. BW=0.5%

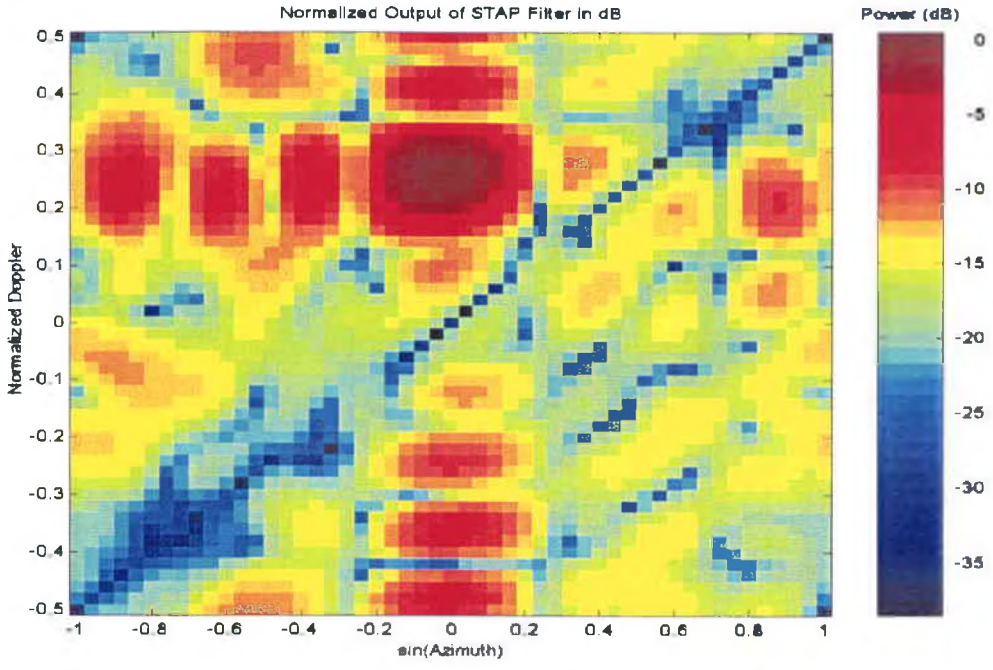

Figure 29c: Filter output. CNR=47 dB and SNR=10dB. Target Doppler=0.25. BW=1%

Figures 30a, 30b and 30c show the STAP patterns for the same case as considered for the filter output shown earlier. Deterioration of the patterns, in the form of increasing sidelobe levels, for increasing bandwidth is quite evident.

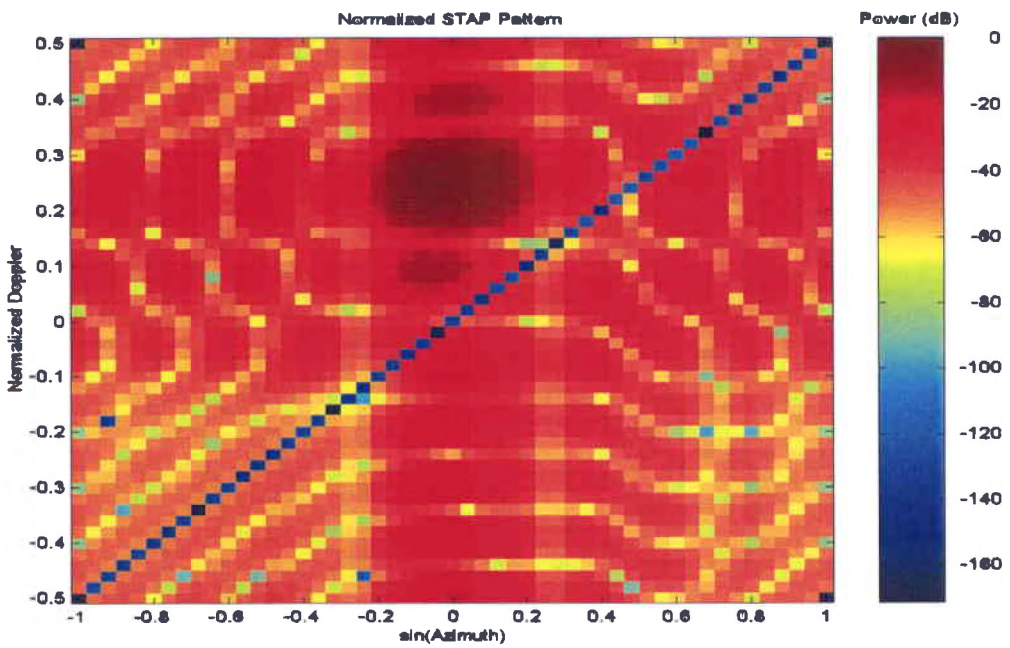

Figure 30a: Filter pattern. CNR=47 dB and SNR=10dB. Target Doppler=0.25. BW=0%

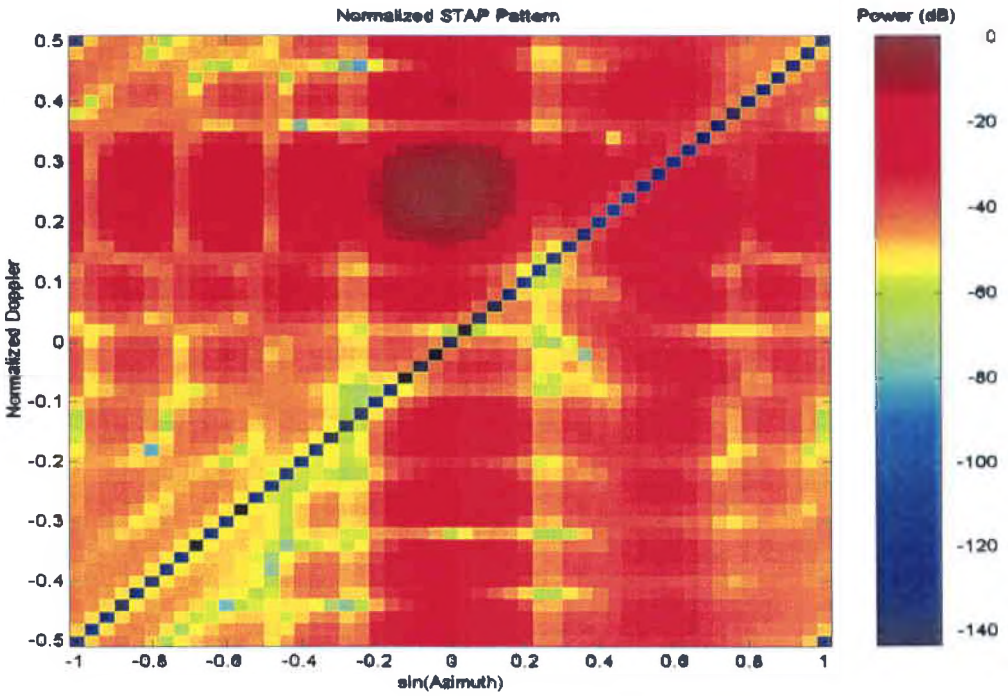

Figure 30b: Filter pattern. CNR=47 dB and SNR=10dB. Target Doppler=0.25. BW=0.5%

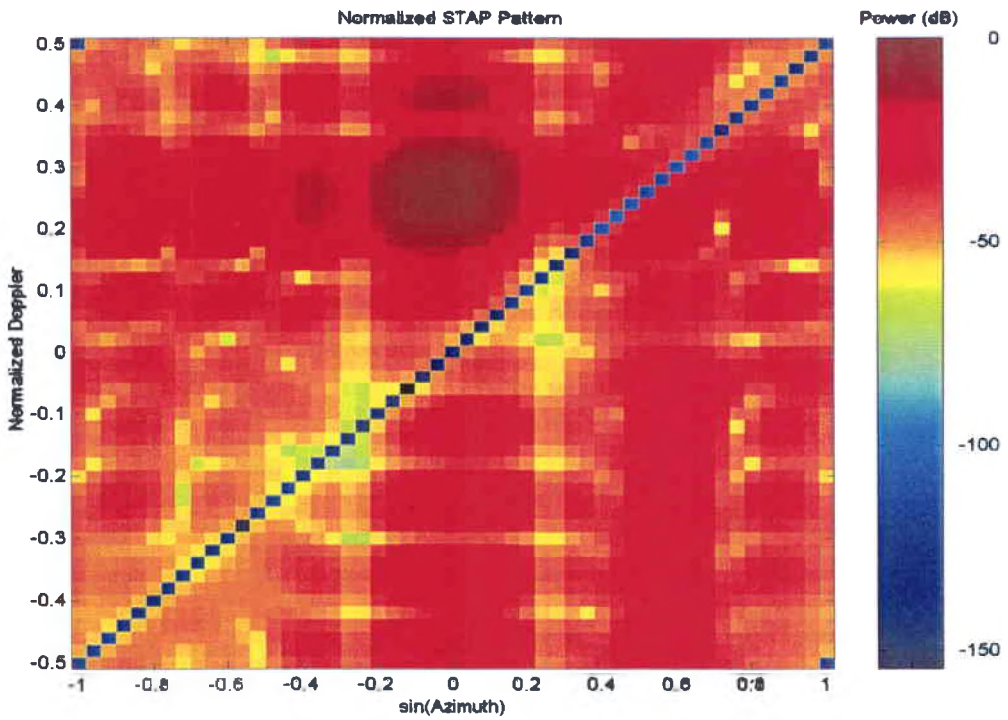

Figure 31c: Filter pattern. CNR=47 dB and SNR=10dB. Target Doppler=0.25. BW=1%

As the target Doppler gets closer to the clutter ridge, the ability of the filter to suppress interference is further compromised and can be seen clearly by examining the filter outputs and patterns for different bandwidths. For the sake of completeness, these outputs and patterns are given in figures 31 and 32 for a normalized target Doppler of 0.1.

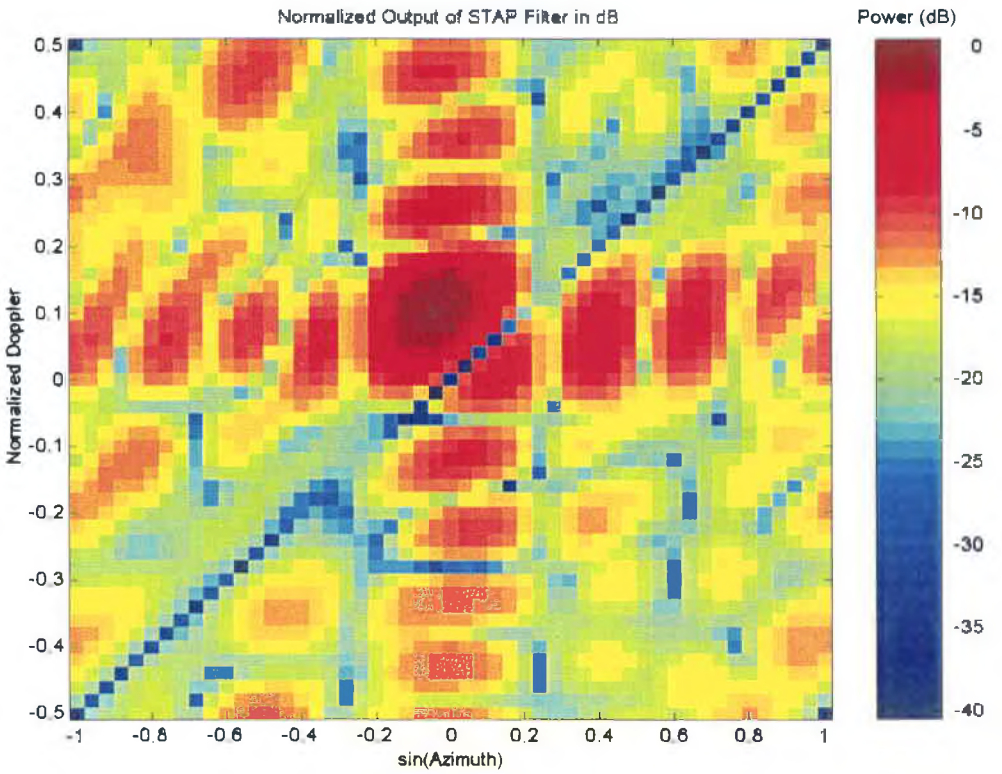

Figure 31a: Filter output. CNR=47 dB and SNR=10dB. Target Doppler=0.25. BW=0%

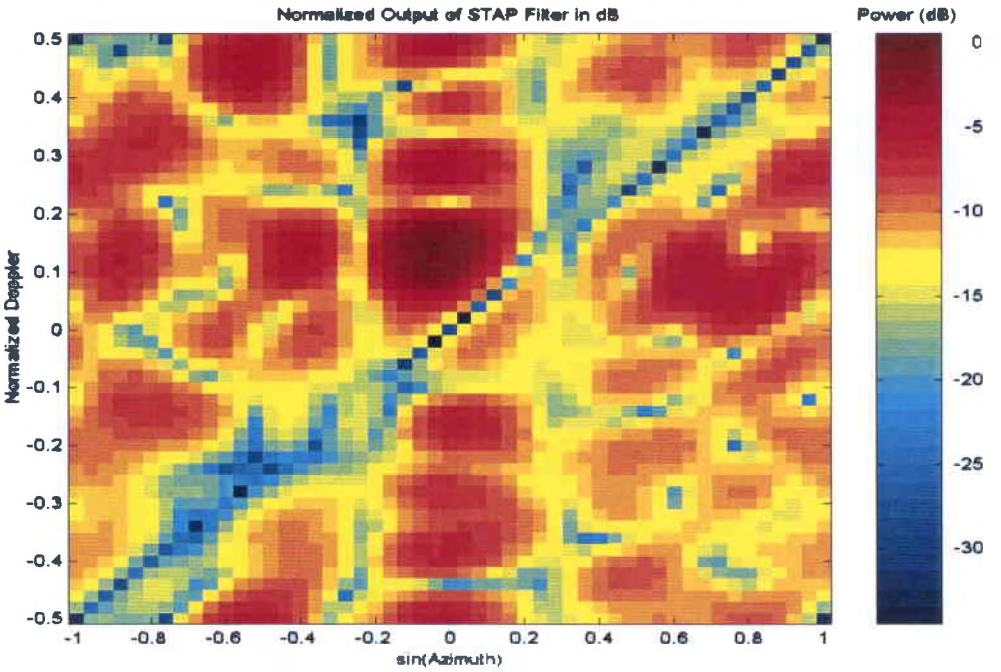

Figure 31b: Filter output. CNR=47 dB and SNR=10dB. Target Doppler=0.1. BW=0.5%

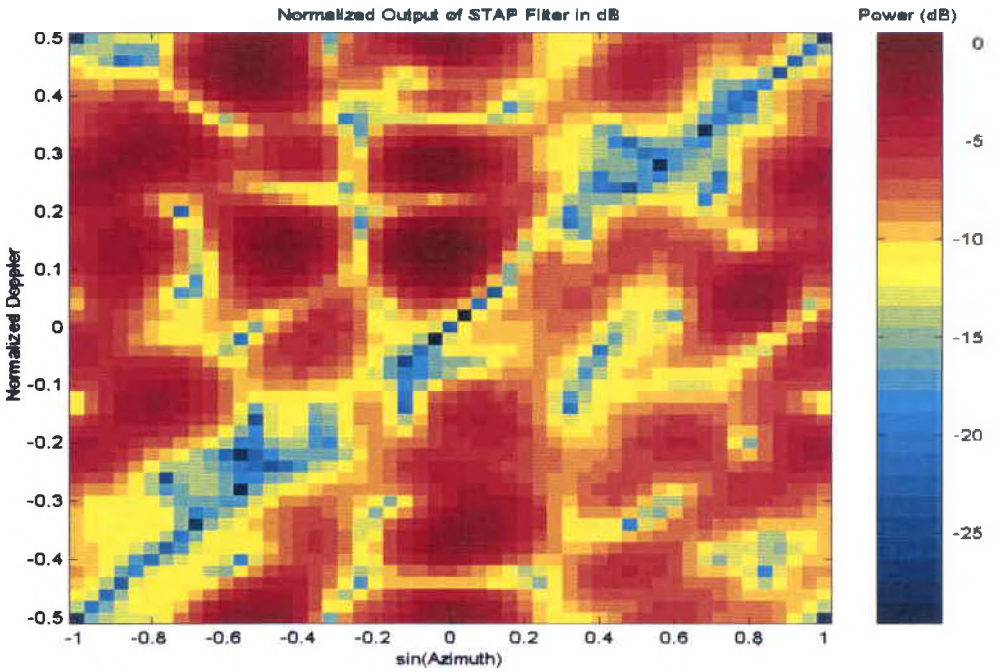

Figure 31c: Filter output. CNR=47 dB and SNR=10dB. Target Doppler=0.1. BW=1%

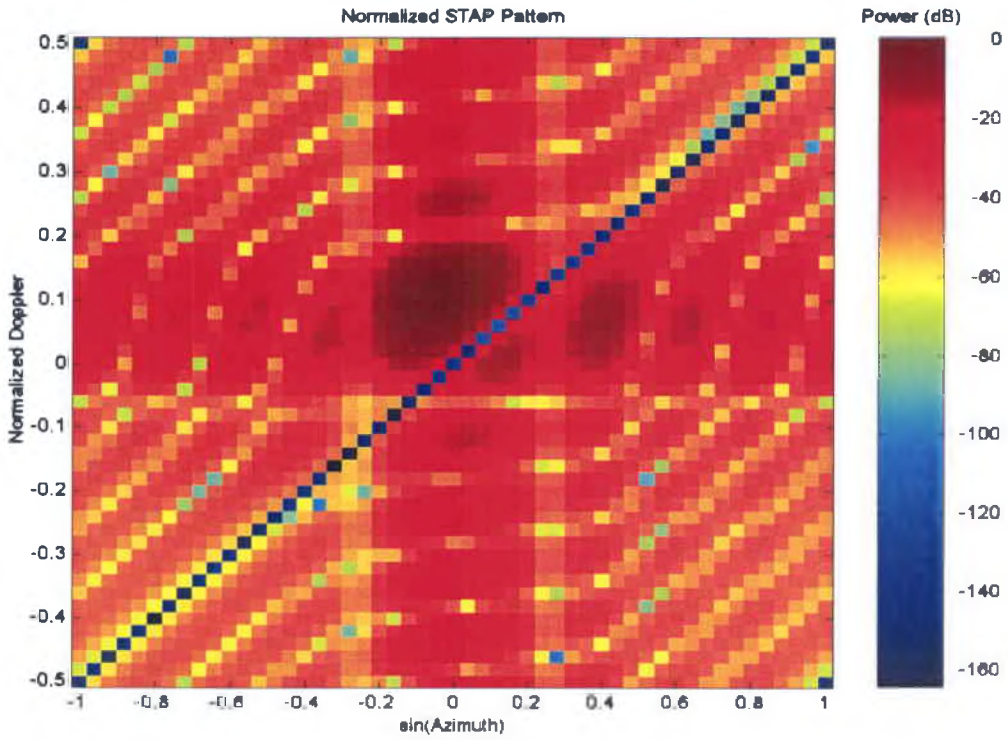

Figure 32a: Filter pattern. CNR=47 dB and SNR=10dB. Target Doppler=0 .1. BW=0%

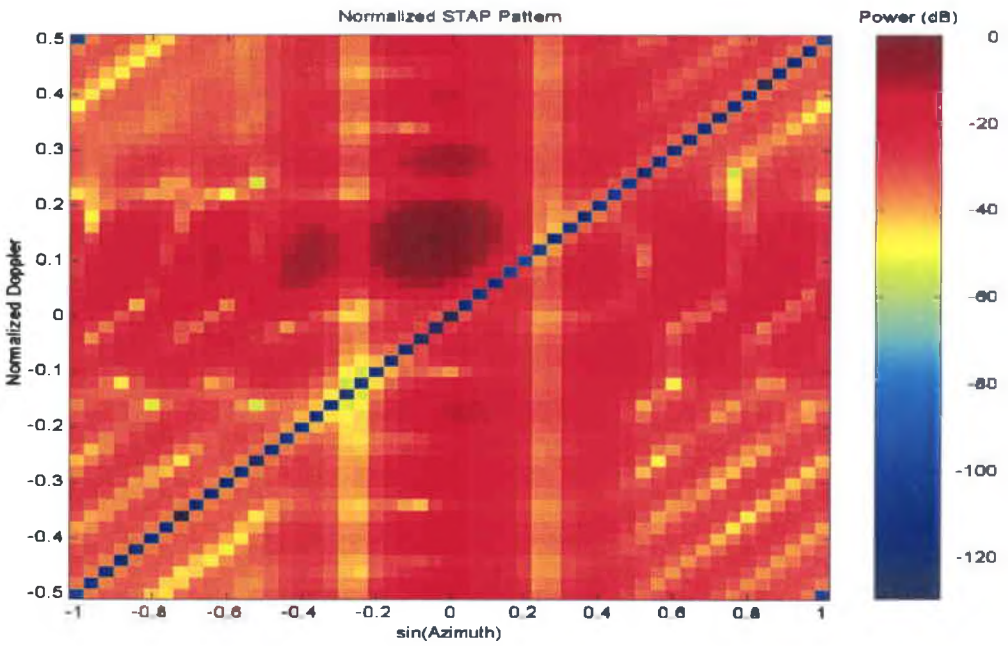

Figure 32b: Filter pattern. CNR=47 dB and SNR=10dB. Target Doppler=0.1. BW=0.5%

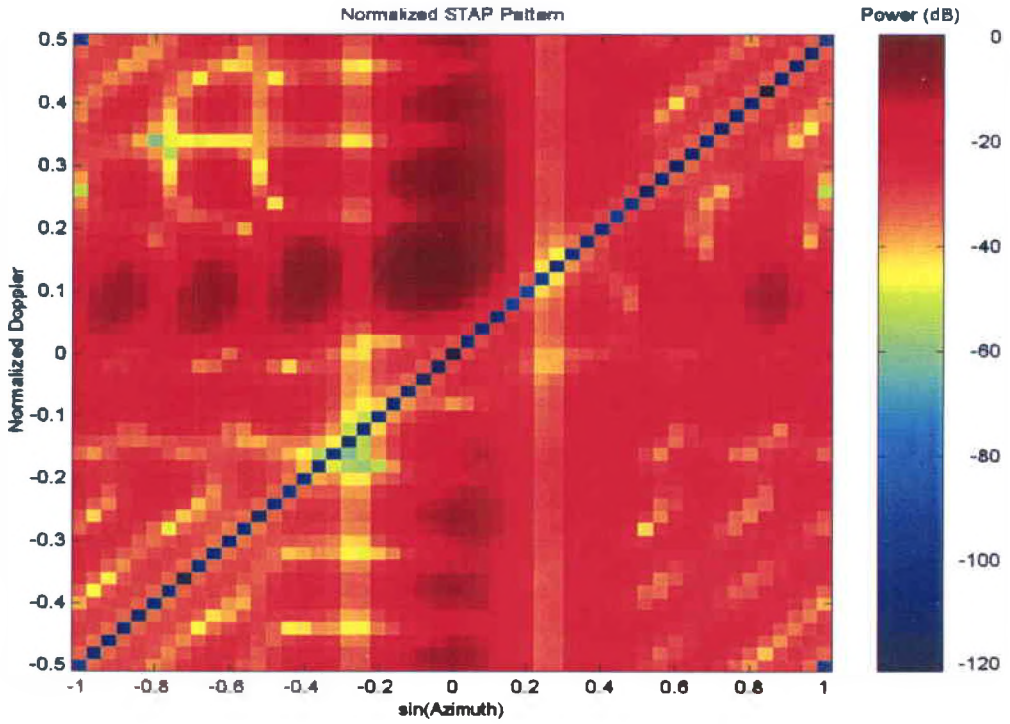

Figure 32c: Filter pattern. CNR=47 dB and SNR=10dB. Target Doppler=0.1. BW=1%

As a further exercise, the jammers used in the earlier simulations were removed and a similar set of results was obtained. The original configuration of a side looking radar was retained.

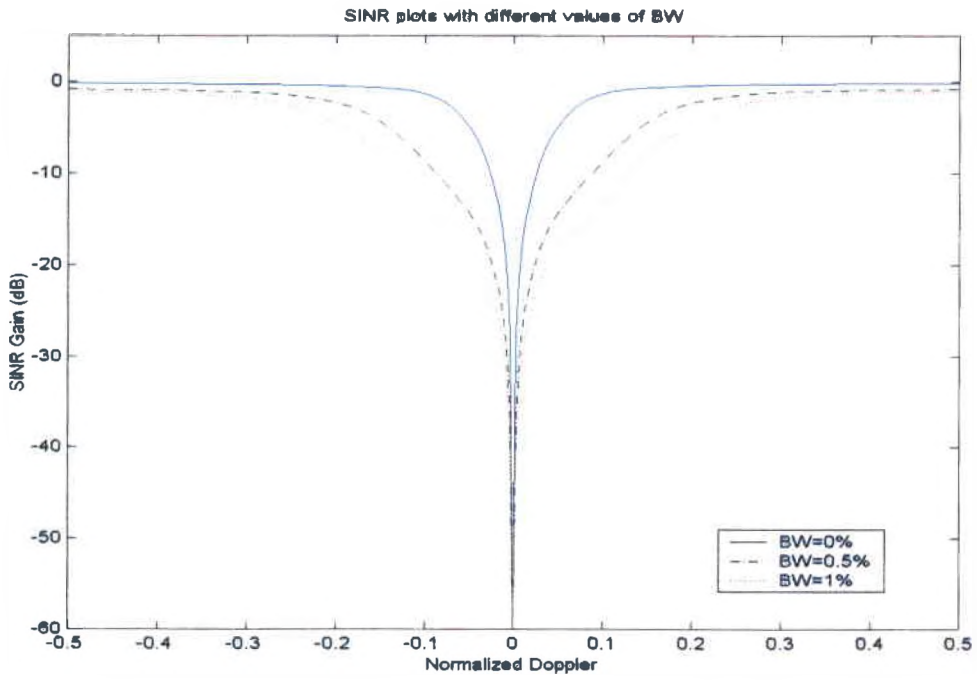

Figure 33: Effect of bandwidth on SINR, SNR=10dB, CNR=47,Without Jammers.

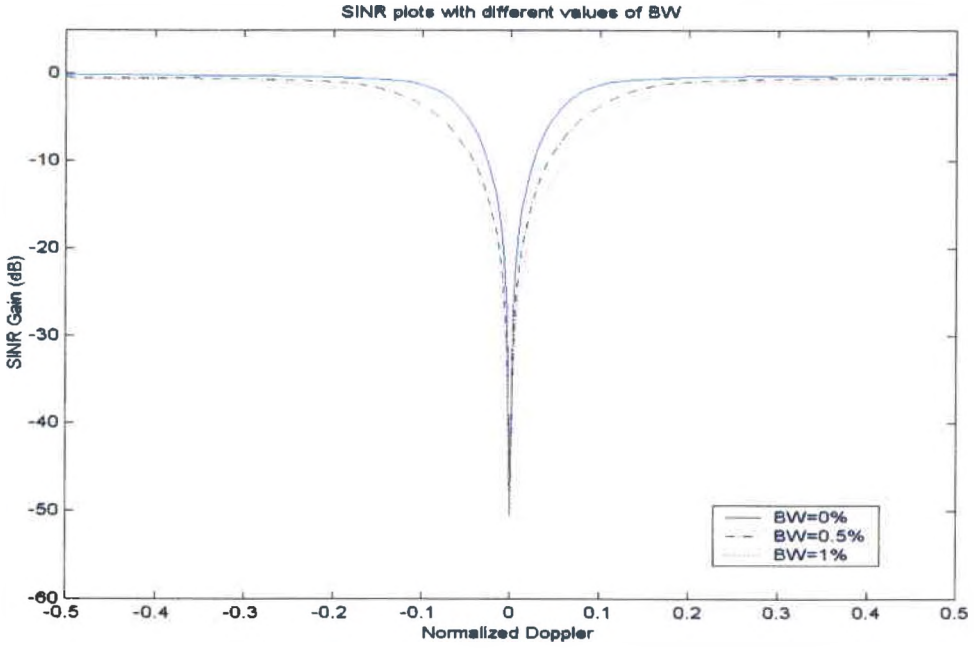

Figure 34: Effect of Bandwidth on SINR, SNR=10dB, CNR=37, Without Jammers.

We obtain similar results showing the adverse impact on the clutter cancellation capability of the filter. Figures 33 and 34 also show that the clutter to noise ratio has an impact on the filter capability. Figure 35 shows the clutter eigenspectra for CNR = 47 which depicts the increase in the size of the interference subspace.

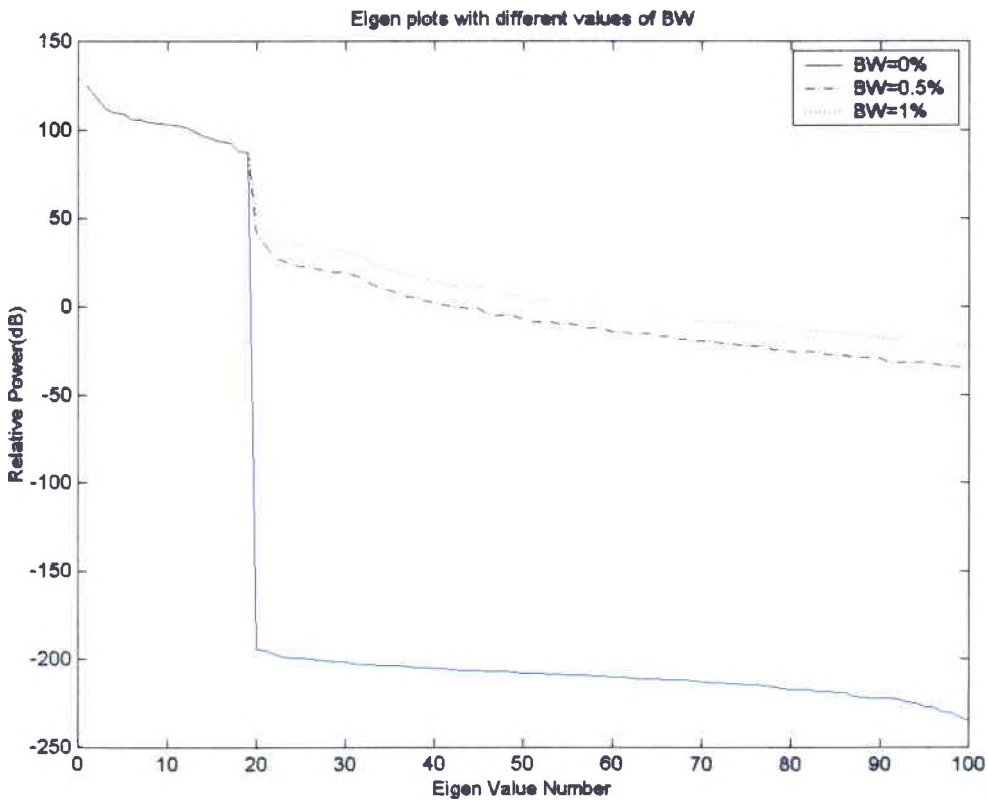

Figure 35: Effect of bandwidth on clutter eigenspectrum. No Jammer scenario.

The STAP filter output and patterns are next shown. As is evident from the figures, as we increase the bandwidth, the interference is of a greater degree as compared to a similar scenario with Jammers included. The STAP patterns also show a similar deterioration for increasing bandwidth.

Figures 36a, 36b and 36c show the filter output for CNR = 47dB and a target Doppler of 0.25 for three different bandwidths corresponding to 0%, 0.5% and 1%. Figures 37a, 37b and 37c show the STAP patterns for the same case.

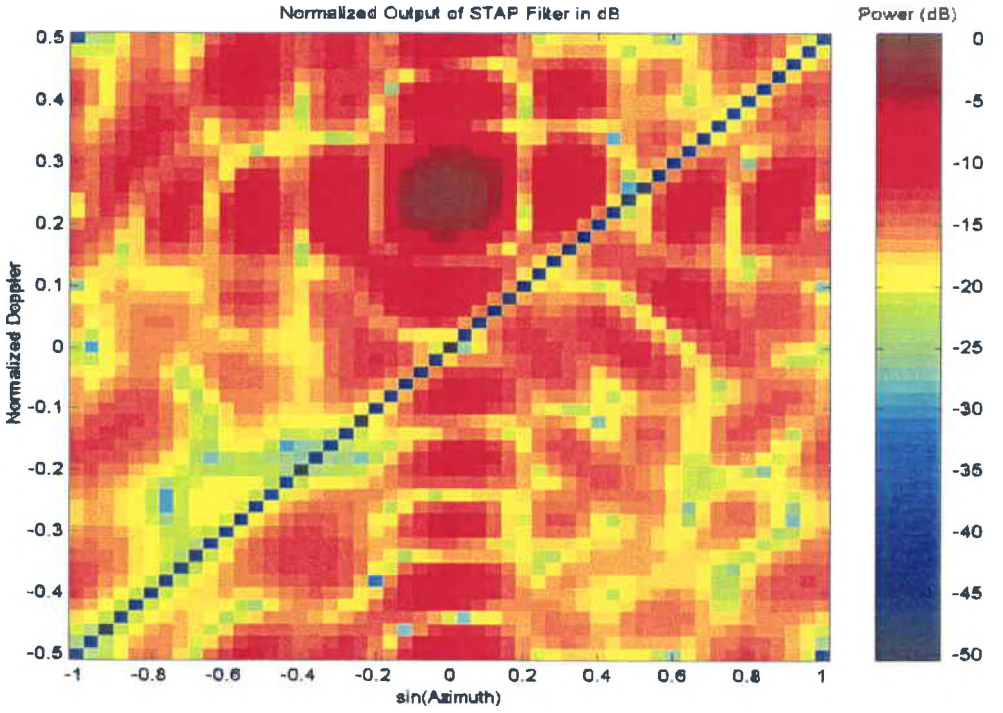

Figure 36a: Filter output. CNR=47 dB and SNR=10dB. Target Doppler=0.25. BW=0%

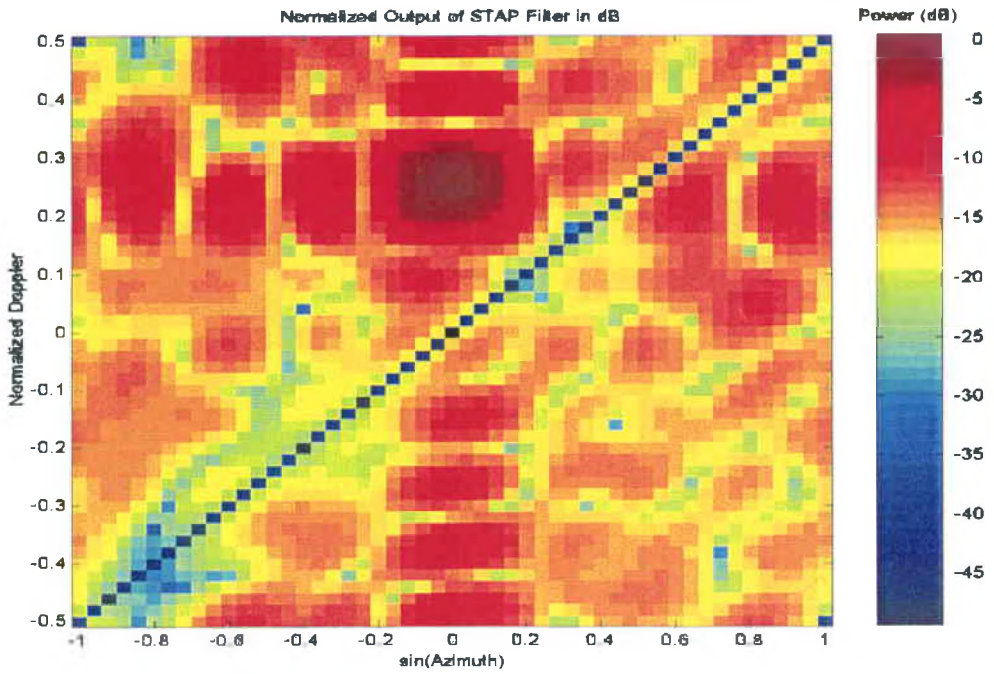

Figure 36b: Filter output. CNR=47 dB and SNR=10dB. Target Doppler=0.25. BW=0.5%

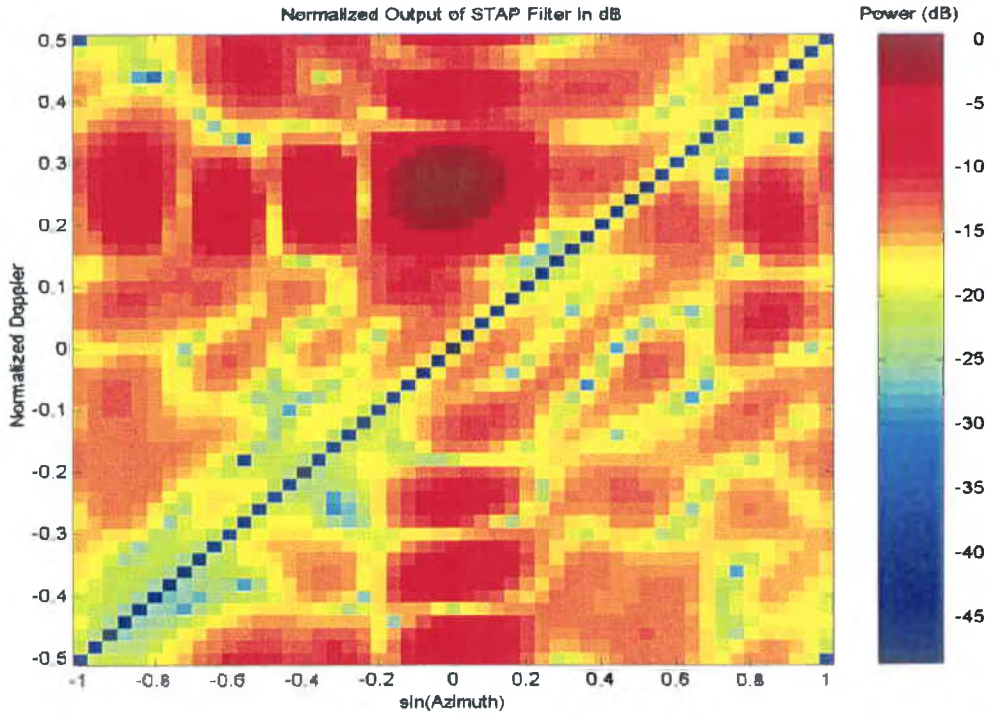

Figure 36c: Filter output. CNR=47 dB and SNR=10dB. Target Doppler=0.25. BW=1%

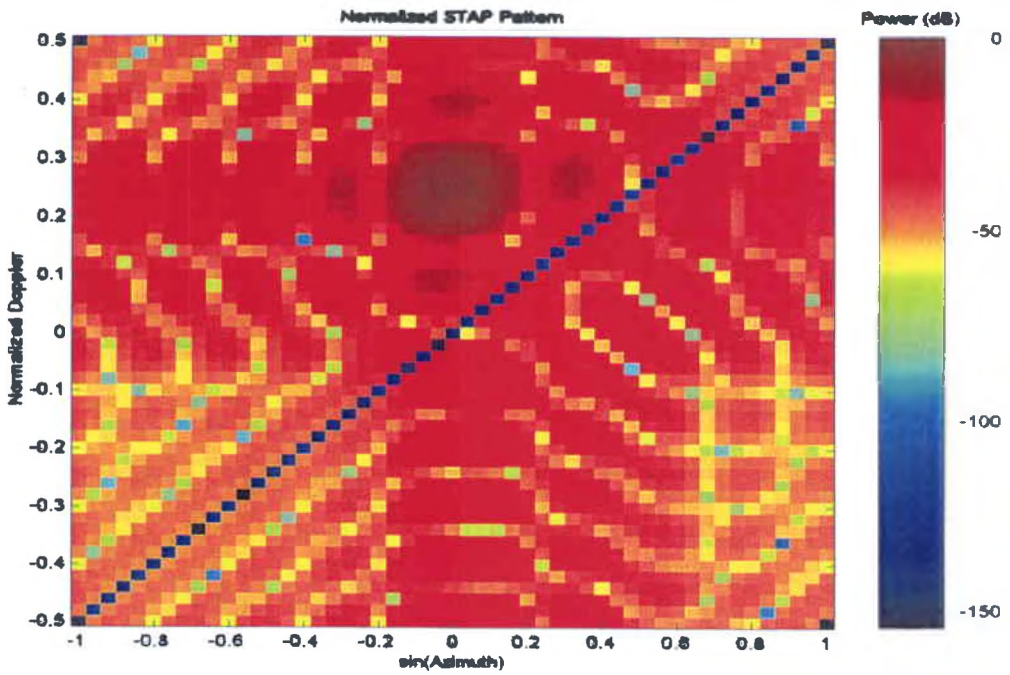

Figure 37a: Filter pattern. CNR=47 dB and SNR=10dB. Target Doppler=0.25. BW=0%

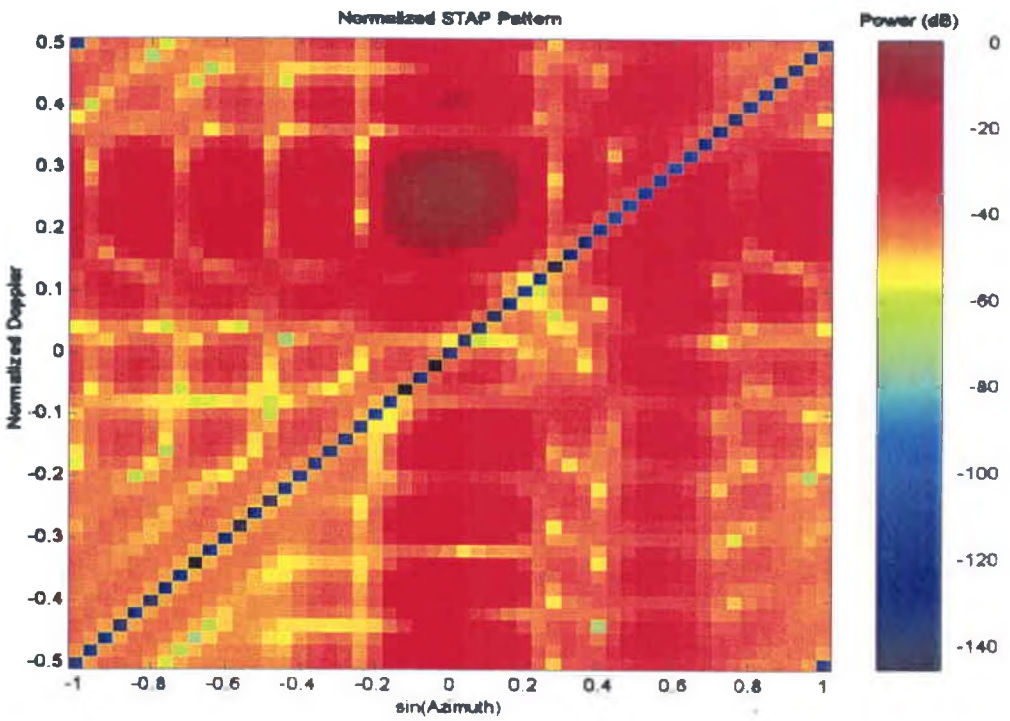

Figure 37b: Filter pattern. CNR=47 dB and SNR=10dB. Target Doppler=0.25. BW=0.5%

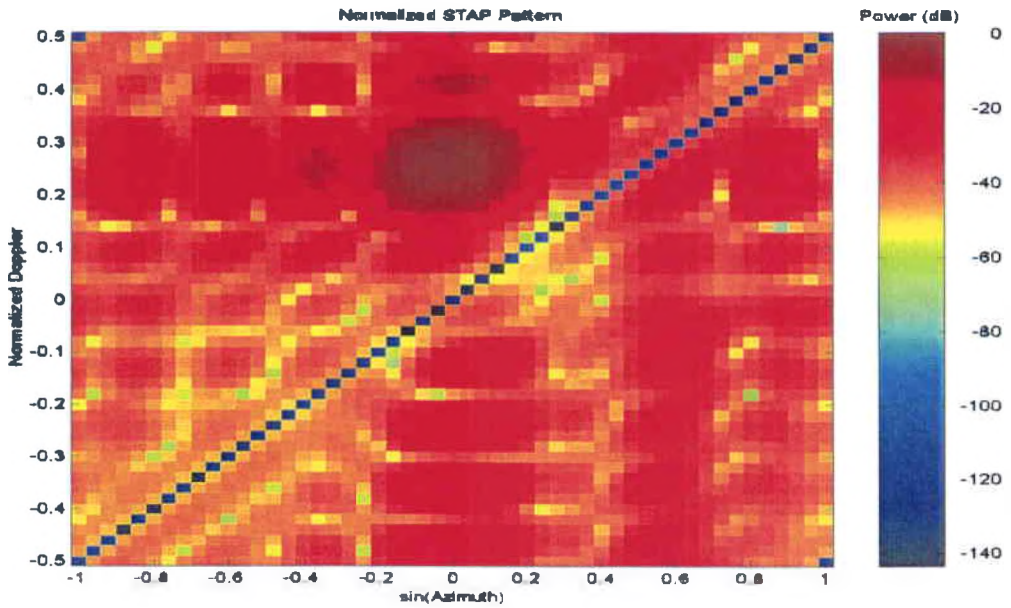

Figure 37c: Filter pattern. CNR=47 dB and SNR=10dB. Target Doppler=0.25. BW=1%

The same set of figures with CNR = 47dB, target Doppler of 0.1 is shown in Figures 38 and 39.

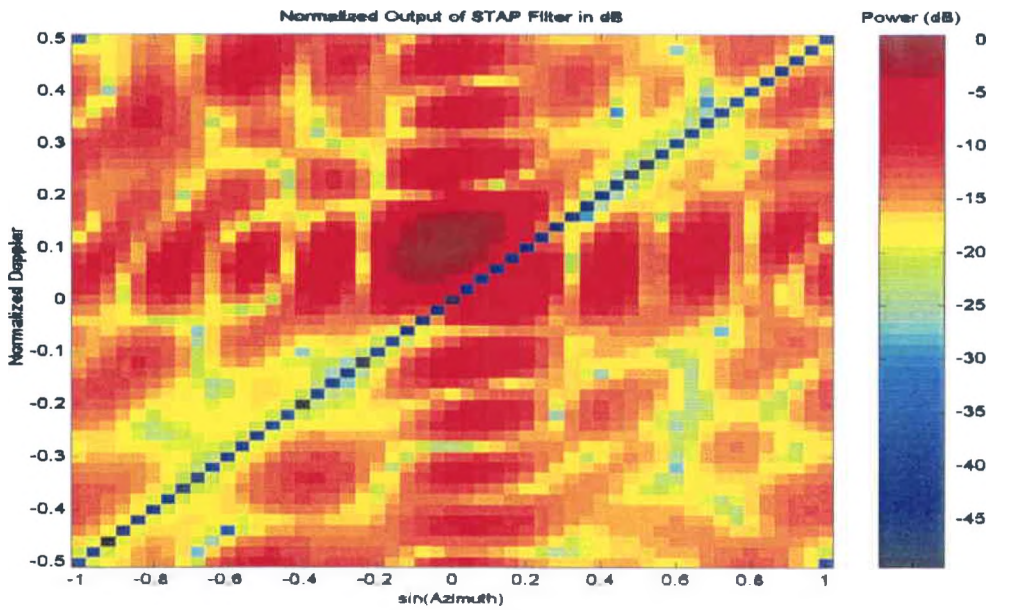

Figure 38a: Filter pattern. CNR=47 dB and SNR=10dB. Target Doppler=0.1. BW=0%

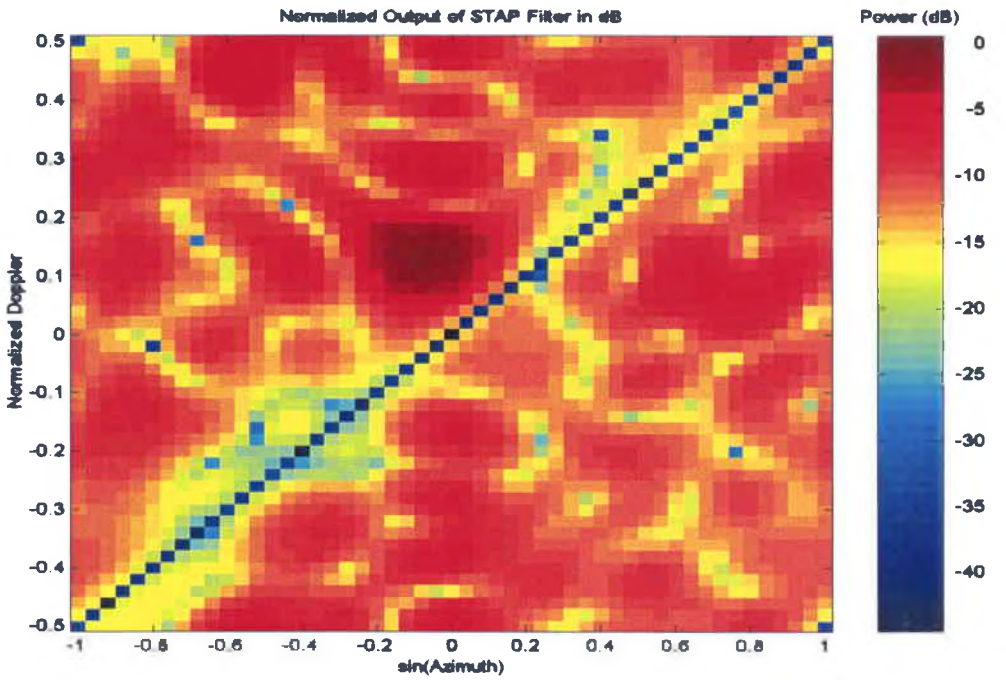

Figure 38b: Filter pattern. CNR=47 dB and SNR=10dB. Target Doppler=0.1. BW=0.5%

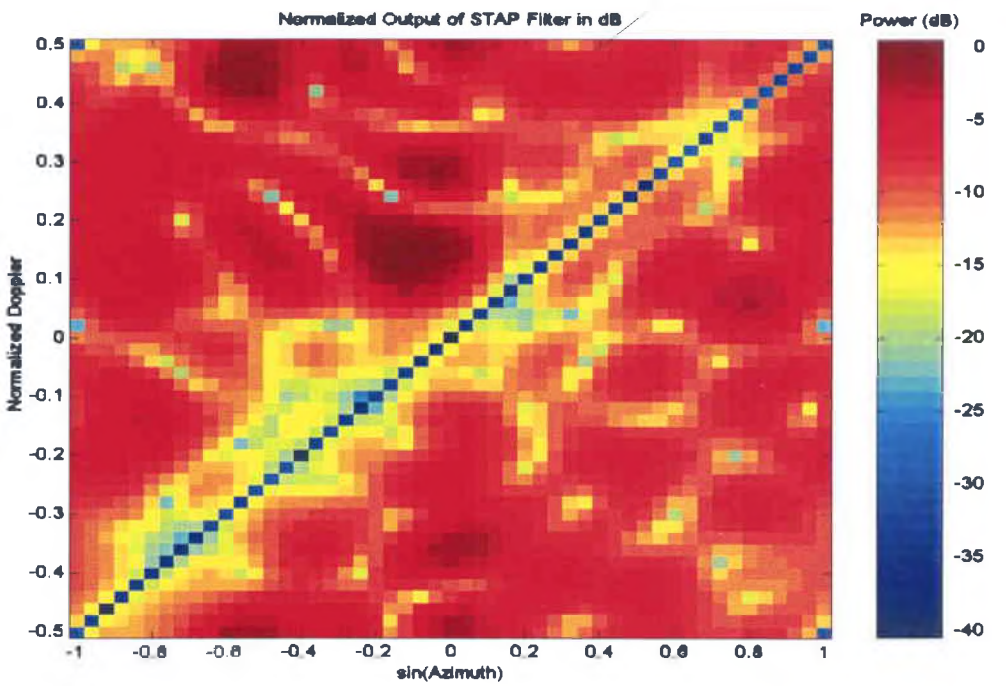

Figure 38c: Filter pattern. CNR=47 dB and SNR=10dB. Target Doppler=0.1. BW=1%

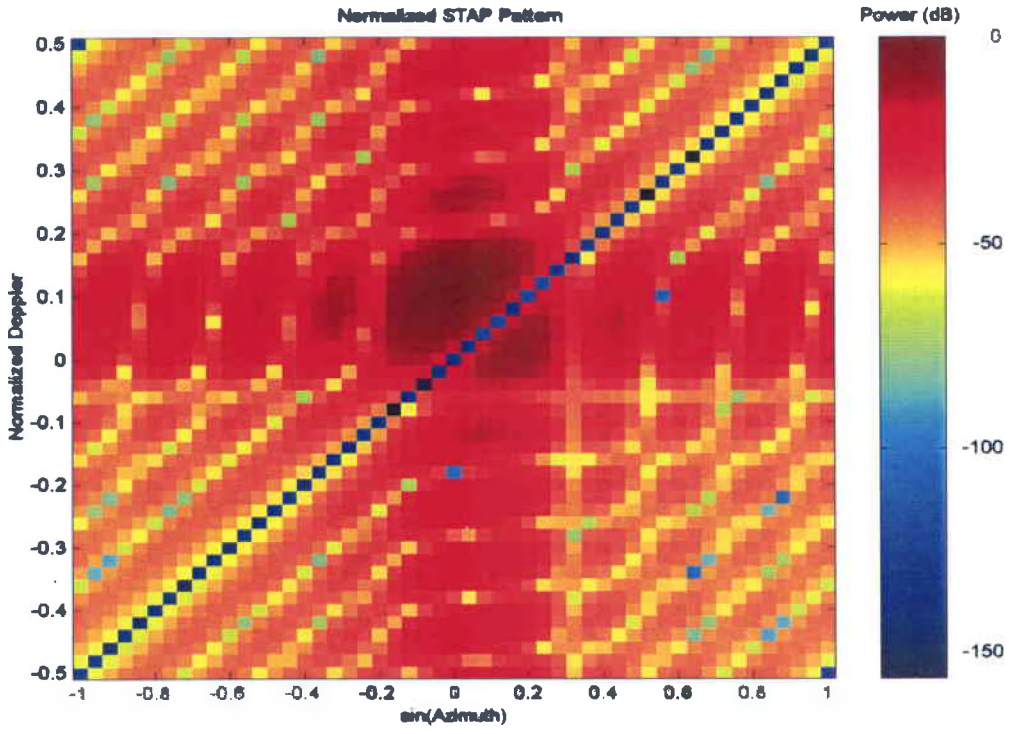

Figure 39a: Filter pattern. CNR=47 dB and SNR=10dB. Target Doppler=0.1. BW=0%

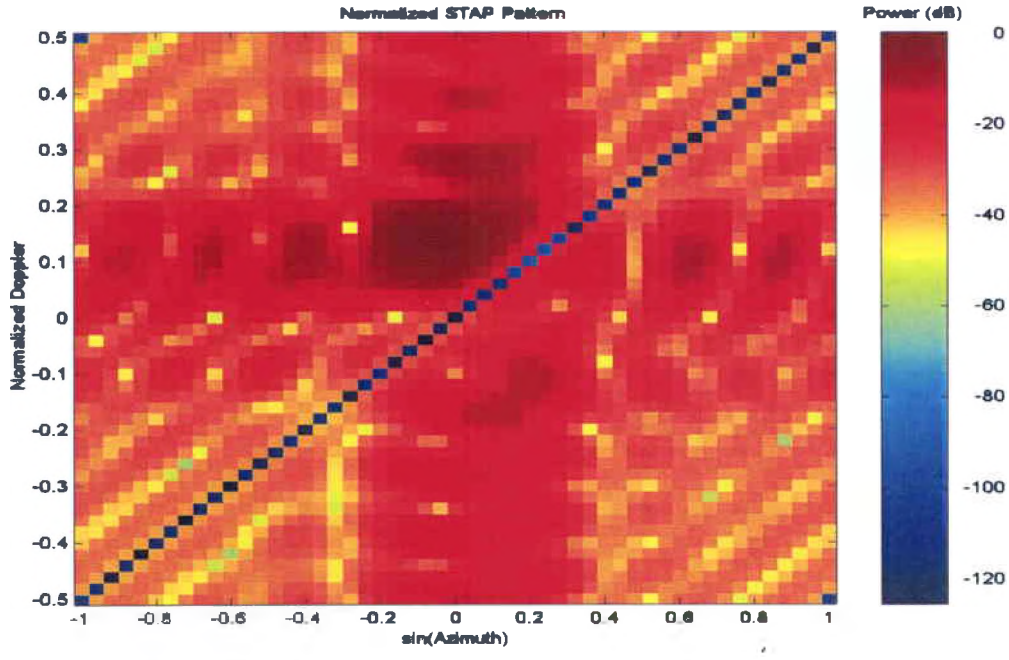

Figure 39b: Filter pattern. CNR=47 dB and SNR=10dB. Target Doppler=0.1. BW=0.5%

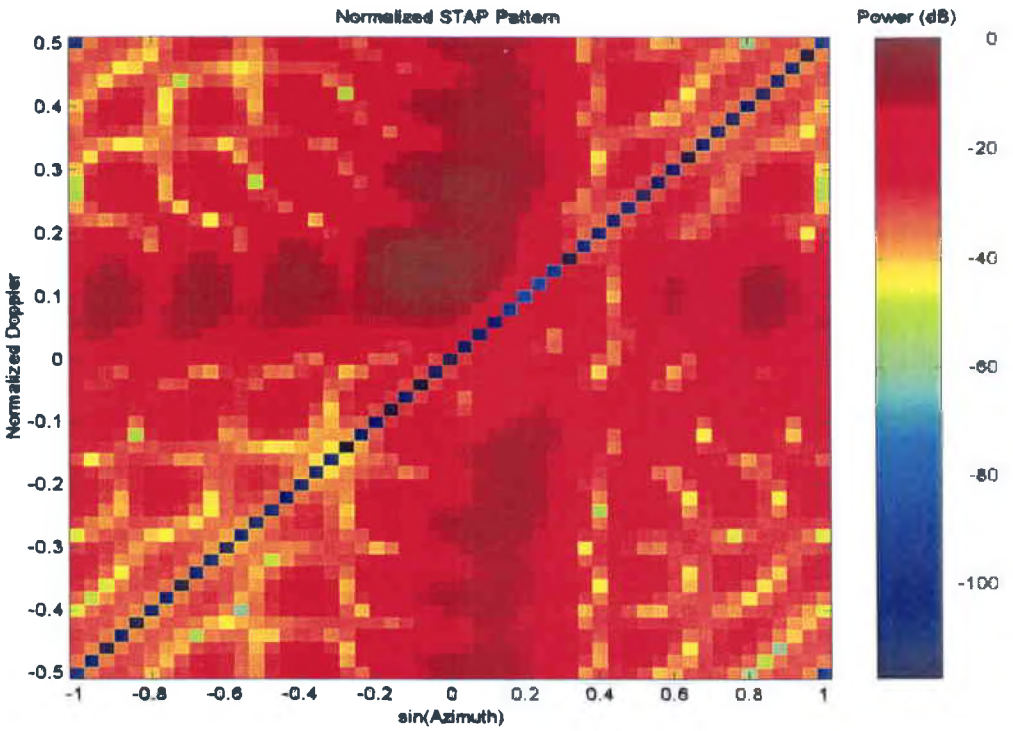

Figure 39c: Filter pattern. CNR=47 dB and SNR=10dB. Target Doppler=0.1. BW=1%

CHAPTER V

CONCLUDING REMARKS

The theoretical development of STAP to suppress interference is now well established. The challenges lie in making STAP a practical reality. Designing a processor that is fast enough that it has the computational throughput necessary to implement the complex computations of STAP in real time is one such important challenge. In addition, a practical implementation of STAP requires an estimate of the interference covariance matrix. This requires the existence of a sufficient sample support that is homogeneous. In practice, the sample support may neither be sufficient nor homogenous. We have examined here two specific ways the sample support is heterogeneous and their consequences. Both ICM and "movers" in their own different ways adversely impact the STAP performance. The heterogeneity forces the designer to come up with algorithms that require fewer degrees of freedom and/or more efficient methods of covariance matrix estimation.

We also considered here the effect of finite non-zero bandwidth on the performance of STAP filters. Conventional STAP analyses, for instance, as in [9], in effect consider the bandwidth to be essentially zero. Usually, signal bandwidths less than 1% are taken to be "narrow band". It is shown here that finite bandwidth has a significant and adverse effect on the ability of the STAP filter to suppress interference. Signal

bandwidth gives rise to interference bandwidth as well and cancellation of the broadband interference is a more challenging task than interference of zero bandwidth. It is shown here that even for signal bandwidths less than 1% the SINR performance is adversely affected and in particular, the clutter ridge is widened. This widening of the clutter ridge results in the minimum detectable velocity to be higher than that predicted by the optimum STAP filter for the zero bandwidth case. The interference arriving from each clutter patch appears to the adaptive array as an extended source (in angle) and as a result the rank of the clutter covariance matrix increases. Such increase in the interference subspace size has implications in the design of partially adaptive algorithms and also in determining the minimum sample support requirements. Two possible approaches come to mind to mitigate the effect of non-zero bandwidth. It would be interesting to consider incorporating true time delay line beam forming into the STAP architecture to overcome the dispersive effects of bandwidth across the array. A second approach might be the use of fast time taps in addition to the slow time taps that are normal part of the STAP architecture. Yet another approach is sub-band based architecture for STAP.

BIBLIOGRAPHY

1. M. Skolnik, "Radar handbook", (McGraw-Hill, New York, 2nd Edn. 1990).
2. Bernard Widrow and Samuel D. Stearns, "Adaptive signal processing", (Prentice-Hall, Englewood Cliffs, N.J, 1985)
3. R. A. Monzingo and T. W. Miller, "Introduction to adaptive arrays", (John Wiley &Sons, 1980)
4. J. E. Hudson, "Adaptive array principles" (Peter Peregrinus Ltd, 1981)
5. R.T. Compton, Jr, "Adaptive Antennas – Concepts and Performance", (Englewood cliffs, NJ: Prentice Hall, 1980)
6. T. W. Anderson, "An introduction to multivariate statistical analaysis", (John Wiley, New York, 1957)
7. L. E. Brennen and I. S. Reed, "Theory of adaptive radar", IEEE Transactions on Aerospace and Electronic Systems, Vol. AES-9, March 1973, pp.237-252.
8. R. Klemm, "Adaptive clutter suppression for airborne phased array radars", IEEE Proceedings, Vol.130, Pts F and H, No-1, February 1983, pp 125-131.
9. R. Klemm, "Adaptive clutter suppression in step scan radars", IEEE Transactions on Aerospace and Electronic Systems, 14,(4), pp.210-212.
10. R. Klemm, "Effect of time-space clutter filtering on SAR resolution", Proceedings, ISSSE 92, Paris, September, pp.462-465.

11. R. Klemm, "Adaptive airborne MTI with two-dimensional motion compensation", IEE Proceedings. F Radar Signal Processing., 138, December, pp. 551-558.

12. R. Klemm, "Space-Time Adaptive Processing: Principles and Applications", (IEE Radar, Sonar, Navigation and Avionics Series 9), Exeter, U. K: Short Run Press Ltd., 1998.

13. I. S. Reed, J. D. Mallet and L. E. Brennen, "Rapid Convergence rate in adaptive arrays," IEEE Transactions on Aerospace and Electronic systems, AES-10, No.6, November 1974

14. H. Wang and L. Cai, "On adaptive spatial-temporal processing for airborne surveillance radar systems," IEEE Transactions on Aerospace and Electronic systems, Vol.AES-30, No. 3, July 1994, pp.1015-1032.

15. A. Haimovich, "The Eigen Canceller: Adaptive radar by Eigenanalysis methods," IEEE Transactions on Aerospace and Electronic systems, Vol-32, No.2, July 1996.

16. W. L. Melvin, "Space-Time Adaptive Processing and Adaptive Arrays: Special Collection of papers," IEEE Transactions on Aerospace and Electronic Systems, Vol. 36, No. 2, April 2000, pp.508-509.

17. Y. Wang and Y. Peng, "Space-time joint processing method for simultaneous clutter and jammer rejection in airborne radar", Electron. Lett., 32(3), pp. 258-259 (1996a)

18. M. Wicks, H. Wang and L. Cai, "Adaptive array processing for airborne radar", IEE Radar 92, Brighton, UK, pp. 159-162.

19. J. Ward, "Space-Time Adaptive Processing for Airborne Radar," Technical Report 1015, M.I.T Lincoln Laboratory, December 1994.

20. E. C. Barile, R. L. Fante, and J. A. Torres, "Some limitations on the effectiveness of airborne adaptive radar," IEEE Transactions on Aerospace and Electronic systems, Vol.AES-28, October 1992, pp.1015-1032.

21. S. U. Pillai, Y. L. Kim and J. R. Guerci, "Generalized Forward/Backward Subaperture Smoothing Techniques for Sample starved STAP," IEEE Transactions on Signal Processing, Vol.48, No.12, December 2000.

22. W. L. Melvin, " Space-Time Adaptive Radar Performance in Heterogeneous Clutter," IEEE Transactions on Aerospace and Electronic Systems, Vol.36, No.2, pp.621-633, April 2000.

23. E. M. Friel and K. M. Pasala, "Effects of Mutual Coupling on Performance of STAP Antenna Arrays," IEEE Transactions on Aerospace and Electronic Systems, Vol.36, No.2, pp.518-527, April 2000.

24. M. Zatman and E. Baranoski, "Time delay steering architectures for space-time adaptive processing," IEEE Antennas and Propagation Society International Symposium Digest, part vol.4, pp. 246-249, 1997.

25. A. Hoffman and S. M. Kogon, "Subband STAP in wideband radar systems," Proceedings of the 2000 IEEE sensor array and multi-channel signal processing workshop, pp. 256-260

26. A. O. Steinhardt and N. B. Pulsone, "Subband STAP processing, the fifth generation, Proceedings of the 2000 IEEE sensor array and multi-channel signal processing workshop, pp. 1-6.

27. G. M. Herbert, Space-time adaptive processing for airborne radar, "Record of the IEEE 2000 International Radar Conference," pp. 620-625

28. M. Zatman, "How narrow is narrowband," IEE. Proceedings, Radar, Sonar, Navig, Vol. 145, No. 2, April 1998.